PERFORMANCE AND RELIABILITY COMPARISON OF GRID CONNECTED SMALL WIND TURBINE SYSTEMS

MD. ARIFUJJAMAN

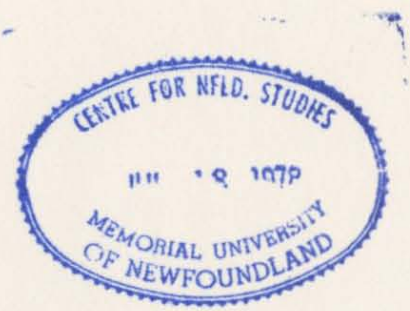
CENTRE FOR NFLD. STUDIES
MEMORIAL UNIVERSITY
OF NEWFOUNDLAND

PERFORMANCE AND RELIABILITY COMPARISON OF GRID CONNECTED SMALL WIND TURBINE SYSTEMS

BY

MD. ARIFUJJAMAN, B.Sc., M.Eng.

A thesis

submitted to the school of Graduate Studies

in partial fulfillment of the requirements for the degree of

DOCTOR OF PHILOSOPHY

FACULTY OF ENGINEERING AND APPLIED SCIENCE
MEMORIAL UNIVERSITY OF NEWFOUNDLAND

St. John's, Newfoundland, Canada
August, 2010

Abstract

Small wind energy conversion systems are electromechanical devices that generate electricity from wind power for use in commercial as well as residential applications. System level comparison pertaining to such conversion systems is an important and challenging problem and in-depth analysis is essential for high penetration of wind power. A set of unique problems associated with this technology requires that the maximum power point tracking control be achieved through a simple, efficient, and most importantly, highly reliable manner. This research identifies these challenges and subsequently presents a comparison in terms of the performance and reliability of a furling control grid connected Permanent Magnet Generator (PMG) and Wound Rotor Induction Generator (WRIG)-based small wind turbine system. The power conditioning system for grid connection of the PMG-based system requires a rectifier, boost converter and a grid-tie inverter, while the WRIG-based system employs a rectifier, a switch and an external resistance in the rotor side with the stator directly connected to the grid. The proposed research develops the system level mathematical model for the power conditioning system losses that fluctuates with the wind speed. It is found by the simulation that compared to the PMG-based system, the WRIG-based system can provide low power losses at low wind speeds, thus resolving the typical obstacle of variable speed operation. The comparison is further enhanced by investigating the annual energy capture, annual energy loss and efficiency for the wind speed information of eight test sites in Newfoundland and Labrador, Canada: Battle Harbour (BH); Cartwright (CW);

Little Bay Island (LB); Mary's Harbour (MH); Nain (NA), Ramea (RA); St. Brendan's (SB); and St. John's (SJ). It is demonstrated that the WRIG-based system yields lower energy loss which results in a system of higher efficiency for a wind speed of 2 m/s (cut-in) to 17 m/s (cut-out). Furthermore, experimental test benches are developed for both systems based on a wind turbine emulator that incorporates furling control and associated dynamics, as well as power conditioning systems required for variable speed operation. The maximum power extraction to the grid for both systems is ensured by tracking the optimum tip speed ratio. The experimental energy production is calculated for the regions considered during simulation. It is found that the WRIG-based system provides 2% more efficiency than the PMG-based system and corresponds well with the simulated conclusion.

Additionally, the reliability of the power conditioning system for the systems is analyzed at a predetermined wind speed. The analysis reveals that the Mean Time Between Failures (MTBF) of the power conditioning system of the WRIG-based system is much longer than the MTBF of the power conditioning system of the PMG-based system. The investigation is extended to identify the least reliable component within the power conditioning system for both systems. It is shown that the inverter has the dominant effect on the system reliability for the PMG-based system, while the rectifier is the least reliable component for the WRIG-based system. This research finally concludes that the WRIG-based small wind turbine system with a simple power conditioning system is a much better option for a small wind energy conversion system.

Acknowledgements

This research project has been carried out at the Faculty of Engineering and Applied Science at Memorial University of Newfoundland (MUN), Canada. The financial support provided by the National Science and Engineering Research Council (NSERC), Canada is gratefully acknowledged.

My gratitude goes towards my supervisors, Dr. M.Tariq Iqbal and Dr. John E. Quaicoe, without whom this thesis would have never been completed. There overwhelming enthusiasm has kept me going when things felt tough. During my study at MUN, their extensive knowledge and experience have guided me through difficulties and encouraged me toward accomplishments. Working with Dr. Iqbal and Dr. Quaicoe has been a great pleasure and lots of fun! Also I would like to thank Dr. Glyn George, for the interest and feedback in this very 'windy' thesis.

I would also like to thank my external examiner Dr. Liuchen Chang, Department of Electrical and Computer Engineering, University of New Brunswick, Canada for his valuable comments and encouragement. It was an honor for me while I knew that he is my external examiner and reviewed my four years of research work.

I thank my family and wife, Morsheda Mamataz, for supporting and for giving me so many good reasons not to work hard! Most of all, thanks to my parents, Md. Abul Bashar and Rokeya Begum, their love and encouragement is a deep and strong force in my life; without that, I could not have pursued my goals.

Finally, my thanks go to my two months old baby girl, Toor Binte Jaman, and I wish, when she will grow up, she will read this acknowledgement and will find that I have dedicated my work to her.

Dedication

This thesis is dedicated to my daughter, **Toor Binte Jaman.**

Table of Contents

List of Figures

List of Tables

List of Symbols

ρ	Air density
θ	Furling angle
λ	Tip speed ratio
τ	Carrier period
α	Inverter output current angle
φ	Angle between inverter output current and voltage
$\overline{\beta}$	Vector regression coefficient
η	Efficiency of a system
η_{rec}	Experimental rectifier efficiency
η_{exp,BCI_unit}	Experimental BCI unit efficiency
η_{com,BCI_unit}	Commercial BCI unit efficiency
$\eta_{exp,composite}$	Experimental composite efficiency
$\eta_{com,composite}$	Commercial composite efficiency
ω	Rotor angular velocity of the generator in rpm
ω_s	Angular velocity of the wind turbine rotor
δ	On time for the IGBT of the boost converter
δ_0	Base line failure rate
$\delta(t,z)$	Variation of failure rate of a system with covariate and time

γ	Failure rate
γ_b	Base failure rate
γ_R	Resistance failure rate
π_R	Resistance factor
π_E	Environmental factor
π_Q	Quality factor
ΔT_J	Variation in junction temperature
a	Turn ratio of the rotor to stator
A	Model parameter
B	Constant
C	Model parameter
C_p	Power coefficient
$C_{p,OPT}$	Optimum value of power coefficient
d	Duty cycle
$e(t)$	Error value
E_2	Voltage at the rotor terminal of the WRIG
E_A	Activation energy
E_g	Annual energy capture
E_l	Annual energy loss
$E_{g,i}(w_i)$	Energy capture for a specific wind speed

$E_{l,i}(w_i)$	Energy loss for a specific wind speed
E_{SR}	Rated switching loss energy for a diode
E_{ON}	Rated on-state switching loss energy for the IGBT
E_{OFF}	Rated off-state switching loss energy for the IGBT
$E_{cd\backslash,IGBT}^{INV}$	Energy loss of an IGBT
f_{sw}	Switching frequency of the diode and IGBT
f_{WT}	Frequency of rotation of the wind turbine
$f_{dis}(w_i)$	Number of hours for a specific wind sped within a year
$H(s)$	Continuous furl dynamics
$H(z)$	Discrete furl dynamics
i	A wind speed within cut-in to cut-out
i_o	Sinusoidal current at the output of the inverter
i_a	Instantaneous output current at line *a* of the PMG
i_b	Instantaneous output current at line *b* of the PMG
i_c	Instantaneous output current at line *c* of the PMG
I_1	Stator current of the WRIG
I_2	Rotor current of the WRIG
I_a	RMS output current at line *a* of the PMG
I_b	RMS output current at line *b* of the PMG

I_c	RMS output current at line *c* of the PMG
I_{a3}	RMS stator output current at line *a* of the WRIG
I_{b3}	RMS stator output current at line *b* of the WRIG
I_{a4}	RMS rotor output current at line *a* of the WRIG
I_{on}	On state current of the diode or IGBT
I_{om}	Maximum current of the inverter
I_{dc}	Output current at the rectifier of the PMG-based system
I_{dc1}	Current through a diode of the rectifier of the PMG-based system
I_{dc2}	Inverter input current
I_{dc3}	Experimental rectified DC current of the PMG-based system
I_R	Experimental rectified DC current of the WRIG-based system
I_{DC}	Simulated rectified rotor current of the WRIG-based system
I_{DC3}	Experimental rectified rotor current of the WRIG-based system
$I_{ref,d}$	Reference commutation current of the diode of the PMG-based system
I_{ref1}	Reference commutation current of the diode of the WRIG-based system
$I_{ref,IGBT}$	Reference commutation current of the IGBT
K	Boltzmann's constant
K_ω	Slip ring electrical coefficient
K_δ	Slip ring frictional coefficient

K_p	Proportional gain
L_0	Base lifetime of a semiconductor
$L(V)$	Quantitative life measurement in hours
$L(T_J)$	Lifetime of a semiconductor
M	Modulation index
n	Number of sample
N_1	Number of turns of the stator
N_2	Number of turns of the rotor
p	Differential operator
P_{aero}	Aerodynamic power
P_{max}	Maximum aerodynamic power
P_s	Stator power of the WRIG
$P_{g,i}(w_i)$	Maximum power for a specific wind speed
$P(t)$	Instantaneous power of the output of the PMG
P_{loss}	Conduction and switching power loss of a semiconductor
$P_{cd1,d}^{DB}$	Conduction loss for a diode of the rectifier of the PMG-based system
$P_{sw1,d}^{DB}$	Switching loss for a diode of the PMG-based system
$P_{cdt,d}^{DB}$	Total conduction loss for the bridge rectifier of the PMG-based system
$P_{swt,DB}^{DB}$	Total switching loss for the bridge rectifier of the PMG-based system

$P_{t,d}^{DB}$	Total loss of the bridge rectifier for the PMG-based system
$P_{cd,d}^{BC}$	Conduction loss for the diode of the boost converter of the PMG-based system
$P_{cd,IGBT}^{BC}$	Conduction loss for the IGBT of the boost converter of the PMG-based system
$P_{sw,d}^{BC}$	Switching loss for the diode of the boost converter of the PMG-based system
$P_{sw,IGBT}^{BC}$	Switching loss for the IGBT of the boost converter of the PMG-based system
$P_{t,(d+IGBT)}^{BC}$	Total loss of the boost converter for the PMG-based system
$P_{cd1,d}^{INV}$	Conduction loss for the diode of the inverter of the PMG-based system
$P_{cd1,IGBT}^{INV}$	Conduction loss for the IGBT of the inverter of the PMG-based system
$P_{sw1,d}^{INV}$	Switching loss for the diode of the inverter of the PMG-based system
$P_{sw1,IGBT}^{INV}$	Switching loss for the IGBT of the inverter of the PMG-based system
$P_{cd,d}^{INV}$	Total conduction loss for the diodes of the inverter
$P_{cd,IGBT}^{INV}$	Total conduction loss for the IGBTs of the inverter
$P_{sw,d}^{INV}$	Total switching loss for the diodes of the inverter
$P_{sw,IGBT}^{INV}$	Total switching loss for the IGBTs of the inverter
$P_{t,(d+IGBT)}^{INV}$	Total loss of the inverter

$P_{t,slip}$	Slip power of the WRIG
$P_{l,ex}^{R}$	External rotor resistance and switch power loss
$P_{cd2,d}^{DB}$	Conduction loss of the rectifier of the WRIG-based system
$P_{sw2,d}^{DB}$	Switching loss of the rectifier of the WRIG-based system
$P_{l,rec}^{DB}$	Total loss of the rectifier of the WRIG-based system
$P_{l,elec}^{SR}$	Slip ring electrical power loss
$P_{l,fric}^{SR}$	Slip ring frictional power loss
$P_{l,sring}^{SR}$	Slip ring total power loss
P_t^{WRIG}	Total power loss of the WRIG-based system
P_t^{PMG}	Total power loss of the PMG-based system
$P_{out,gen}^{PMG}$	PMG output power
$P_{out,rec}^{PMG}$	The experimental output DC power from the rectifier of the PMG-based system
$P_{t,rec}^{PMG}$	The experimental power loss for the rectifier of the PMG-based system
$P_{out\_exp,grid}^{PMG}$	The experimental output power to the grid of the PMG-based system
$P_{out\_com,grid}^{PMG}$	The commercial output power to the grid of the PMG-based system
P_{t_exp,BCI_unit}^{PMG}	The experimental BCI unit power loss of the PMG-based system
P_{t_com,BCI_unit}^{PMG}	The commercial BCI unit power loss of the PMG-based system
$P_{t\_exp}^{PMG}$	The experimental total power loss of the PMG-based system

$P_{t\_com}^{PMG}$	The commercial total power loss of the PMG-based system
$P_{out\_ac,grid}^{WRIG}$	Line–to–line power input to the grid of the WRIG-based system
$P_{out\_bc,grid}^{WRIG}$	Line–to–line power input to the grid of the WRIG-based system
$P_{out\_exp,grid}^{WRIG}$	Total power at the grid of the WRIG-based system
$P_{t,rotor}^{WRIG}$	Total rotor output power of the WRIG-based system
$P_{t,ext}^{WRIG}$	Experimental external rotor resistance loss of the WRIG-based system
$P_{t,rec}^{WRIG}$	Experimental rectifier power loss of the WRIG-based system
$P_{elec\_slipring}^{WRIG}$	Experimental slip ring electrical power loss of the WRIG-based system
$P_{fric\_slipring}^{WRIG}$	Experimental slip ring frictional power loss of the WRIG-based system
$P_{t,slipring}^{WRIG}$	Experimental total slip ring power loss of the WRIG-based system
$P_{t,exp}^{WRIG}$	Experimental total power loss of the WRIG-based system
r_1	Stator resistance of the WRIG-based system
r_2	Rotor resistance of the WRIG-based system
r_d	On state resistance of the diode
r_{on}	On state resistance of the diode or IGBT
r_{ce}	On state resistance of the IGBT
R	Actual resistance of the rotor
R_0	Base reliability
R_e	Effective resistance of the rotor

R_w	Radius of wind turbine rotor
R_{system}	Reliability of system
R_{JA}	Junction resistance of a semiconductor
$R(t,z)$	Variation of reliability of a system with covariate and time
$R(T_r)$	Speed of reaction rate
s	Slip
S	Stress factor
T	Time period of the PWM wave
T_A	Ambient temperature
T_d	Derivative time
T_i	Integral time
T_J	Junction temperature
T_{ON}	ON time of the PWM wave
T_{OFF}	OFF time of the PWM wave
T_r	Temperature in Kelvin
T_s	Sampling time
T_v	Temperature in Centigrade
T_w	Wind turbine torque
u_0	Base value of the control signal
u_c	Controller output voltage

$u(t)$	Output of the PID controller
v_a	Instantaneous output voltage at phase *a* of the PMG
v_b	Instantaneous output voltage at phase *b* of the PMG
v_c	Instantaneous output voltage at phase *c* of the PMG
V_1	Stator voltage referred to the rotor of the WRIG
V_2	Rotor voltage referred to the rotor of the WRIG
V_a	RMS output voltage at phase *a* of the PMG
V_b	RMS output voltage at phase *b* of the PMG
V_c	RMS output voltage at phase *c* of the PMG
V_f	Forward voltage drop for the diode of the rectifier of the PMG-based system
V_{ac}	Line-to-line RMS output voltage of the PMG
V_{a1b1}	Line-to-line RMS grid voltage of the PMG-based system
V_{a4c4}	Line-to-line RMS rotor output voltage of the WRIG-based system
V_{a3c3}	Line-to-line RMS stator output voltage of the WRIG-based system
V_{b3c3}	Line-to-line RMS stator output voltage of the WRIG-based system
V_{ce}	Forward voltage drop for the IGBT of the PMG-based system
V_{ce0}	Threshold voltage drop of the IGBT
V_{dc}	Actual commutation voltage of the bridge rectifier for the PMG-based system

V_{dc2}	Inverter input voltage
V_{dc3}	Experimental rectified DC voltage at the rectifier output for the PMG-based system
V_{fo}	Threshold voltage drop of the diode
V_{f1}	Forward voltage drop for the diode of the boost converter of the PMG-based system
V_{for}	Forward voltage drop of the diode or IGBT
V_{thr}	Threshold voltage drop of the diode or IGBT
V_D	Simulated DC voltage at the external resistance output of the WRIG-based system when the switch is OFF
V_R	Rectifier voltage
V_{DC}	Simulated rectified output voltage at the rotor of the WRIG
V_{DC3}	Experimental rectified output voltage at the rotor of the WRIG
V_{ref1}	Reference commutation voltage of the diode for the WRIG-based system
$V_{ref,d}$	Reference commutation voltage of the diode of the PMG-based system
$V_{ref,IGBT}$	Reference commutation voltage of the IGBT
w	Wind speed
w_C	Cut-in wind speed
w_F	Cut-out wind speed
w_R	Rated wind speed

x_1	Stator reactance of the WRIG
x_2	Rotor reactance of the WRIG
z	Covariate vector

List of Abbreviations

AC	Alternating Current
A/D	Analogue to Digital
AEC	Annual Energy Capture
AEL	Annual Energy Loss
BC	Boost Converter
BCI	Boost Converter and Inverter
BH	Battle Harbour
CW	Cartwright
D/A	Digital to Analogue
DC	Direct Current
DSP	Digital Signal Processor
GW	Giga Watt
HALT	Highly Accelerated Life Testing
HP	Horse Power
IG	Induction Generator
IGBT	Insulated Gate Bipolar Transistor
IM	Induction Motor
kW	Kilo Watt
KHz	Kilo Hertz
LB	Little Bay Island

MH	Mary's Harbour
MPPT	Maximum Power Point Tracking
MTBF	Mean Time Between Failures
MW	Mega watt
NA	Nain
NREL	National Renewable Energy Laboratory
P	Proportional
PC	Personal Computer
PCS	Power Conditioning System
PI	Proportional Integral
PID	Proportional Integral Derivative
PMG	Permanent Magnet Generator
PV	Photovoltaic
PWM	Pulse Width Modulation
QBASIC	Quick Beginner's All-purpose Symbolic Instruction Code
RA	Ramea
RPM	Rotation per Minute
RMS	Root Mean Square
SB	St. Brendan's
SCIG	Squirrel Cage Induction Generator
SG	Synchronous Generator
SJ	St. John's
SWT	Small Wind Turbine

SWTE	Small Wind Turbine Emulator
THD	Total Harmonic Distortion
TSR	Tip-Speed-Ratio
WRIG	Wound Rotor Induction Generator
WT	Wind turbine
WTE	Wind Turbine Emulator

Chapter 1

Introduction

Generation of electricity from renewable sources has the advantage of being, to a certain extent relatively environmentally clean compared to non-renewable sources [1]. Most importantly, these sources can assist to gain energy independence, reduce liability to unstable grid prices and above all, be easily accessible from remote locations that are not connected to utility power grids. Among several identified renewable sources such as hydro, solar, tidal and wave, the electricity generation using wind is expected to be the second largest source of renewable energy by 2010 [2]. Wind power is presently considered to be an optimal renewable technology as it provides a continuously growing contribution to energy diversity and security. Reliable control strategies, custom designed generators, low maintenance and cost competitiveness promote large penetration of wind energy into the electrical power systems. The annual wind power development indicates

that between the years 2000 to 2006, there was a substantial growth in wind power, while it is expected that the use of wind power will double between the years 2006 to 2011 [3]. The expected saturation level of 1900 GW of wind turbine capacity installed world-wide will be reached in the years 2030-2035 [4]. Under international agreements, the penetration is expected to be faster, and 10% of the saturation level is expected to be achieved by the year 2016.

Along with the success of large and medium sized wind turbines, Small Wind Turbines (SWT) have found their role expanding as well. Depending on the local wind resource and utility rates, a small wind energy system can reduce the electricity bill by 50% to 90% [5]. It can be installed as a stand-alone system, eliminating the high cost of extending utility power lines to a remote location, or it can be connected to the power grid, enabling the customer to sell excess power to the utility or buy additional power as needed. While the contribution of the small wind turbine may be small in absolute terms, small wind turbines make a big difference in the daily lives of people around the globe. However, despite the enormous potential of the small wind turbine, the worldwide picture of small wind turbines is much less clear. The reasons for the shadowy existence are manifold: high cost; lack of technological maturity; insufficient testing; complex market with a large number of manufacturers; and lack of proper standards for the SWT. Nevertheless, it is expected that the inclusion of innovative system level design, novel design of airfoil, smart power electronics, increase in funding and research activities could lead to a reduction in the cost and help to increase the penetration of small wind turbine technology [5 – 9].

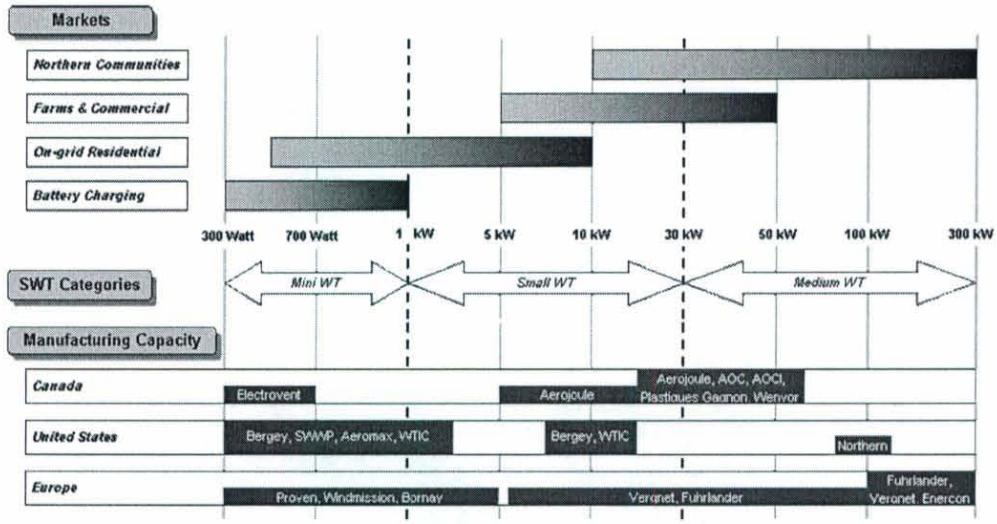

Fig. 1.1 Overview of Canadian Market Demand and International SWT Manufacturing Capacity

The prospect of SWT in Canadian market is relatively intermittent. The current total rated output of SWTs is in the range of 800 kW -1,000 kW which corresponds to 600 to 800 million for mini wind turbines (300W to 1 kW), $1.2 million for small wind turbines (1kW to 30 kW) and $0.7 million for medium wind turbines (30kW to 300 kW) [6]. Battery charging, grid connected residential systems, farms, commercial, and northern and remote communities are the main areas of application of the SWT in the market these days. There are 130 distributors and six manufacturers of commercial SWTs available in the Canadian market and most of them are concentrated in Ontario (55%), Quebec (15%), Alberta and British Columbia (8% each) [5]. Fig 1.1 presents an overview of Canadian Market Demand and International SWT Manufacturing Capacity. It is evident that the Canadian SWT manufacturing capacity is well-suited to the upper end of the farm and commercial markets, and to the lower end of the northern communities market. However, there is almost no manufacturing capacity in the grid connected residential market and

could be a potential focal point for research and development activities for grid connected small wind turbines in Canada.

1.1 Objectives

The main purpose of this research is to compare the performances of the grid connected SWT systems for low and high wind speed regimes. In order to analyze the system performances, both the power loss and annual energy capture/loss are of importance as the performance characteristic can be calculated from these indices. Although sound in theory, the practical implementation and realization of grid connected small wind turbine systems is a major technological challenge undertaken in this research. Moreover, the reliability is an imperative concern for most of the small wind turbine systems and is also an important part of the research. With the foregoing purpose in mind, the main objectives of this research are as follows:

- To identify the most preferable mainstream and an optimum surrogate system for a grid connected small wind turbine systems from the existing small wind energy sphere;
- To develop mathematical formulations and carry out numerical simulations in order to investigate the performance of the most preferable mainstream and the optimum surrogate system;
- To implement the systems and validate the performances established by the numerical simulation;
- To model the component level reliability of the optimum surrogate as well as the most preferable mainstream system in order to determine the most reliable system.

1.2 Motivations

The demand for cheap and environmentally friendly sources of energy has been increasing. An effective, low-cost and highly reliable mechanism for harnessing energy from the wind may revolutionize the scenario of rural power generation, especially in the developing world. A suitable topology for a small wind energy conversion system, although in progress, needs to be identified in the renewable energy family once its potential is established through research and development. Various existing topologies pertaining to small wind turbines have already indicated favorable outcomes for applications such as, home heating, battery charging and net metering. An in-depth analysis of the performance and reliability for grid connected residential application is considered necessary in the current state of the development of the SWT technology.

1.3 Thesis Layout

Starting with an introductory chapter, the layout of the thesis is organized as follows:

In chapter 2, an investigation of grid connected small wind turbine systems is presented in order to enhance the system level understanding. The investigation is expanded to include the power conditioning system followed by an overview of the reliability of the small wind energy conversion system. A comparison of the reliability for the various subsystems of a small wind energy conversion system is presented. Finally, it is decided to limit the scope of the rest of the research on the selected systems, i.e., grid connected Permanent Magnet Generator (PMG) and Wound Rotor Induction Generator (WRIG)-based systems, which are used for further investigation based on the research objective.

In chapter 3, a comprehensive literature review is presented on the PMG and WRIG-based systems. There is a summary of the market penetration, and a power loss

calculation of the power electronics of the systems is described. A survey of the wind turbine emulator is shown in order to differentiate this research from the previous attempts. The literature review is further extended to the reliability calculation of the power electronics and the scope for further development is identified. The need for the present work is described in the context of recent research in the area.

In chapter 4, a comparative study of PMG and WRIG-based systems for wind energy conversion system is presented. The study employs numerical simulation to investigate the power losses for both systems. The investigation is further enhanced by investigating the Annual Energy Capture (AEC), Annual Energy Loss (AEL) and efficiency for the wind speed information for eight different sites in Newfoundland and Labrador, Canada.

In chapter 5, the test bench development and associated results of the PMG and WRIG-based systems are presented. First, a furling control and associated dynamics based on Small Wind Turbine Emulator (SWTE) are developed. Afterwards, the grid connected PMG and WRIG-based systems are developed with the relevant power conditioning system as well as the Maximum Power Point Tracking (MPPT) control strategy. Power conditioning systems losses are determined and compared for both systems. Finally, AEC, AEL and efficiency of the systems are compared for the considered eight sites. The purpose of this chapter is primarily to validate the conclusion drawn during the theoretical investigation study presented in chapter 4.

In chapter 6, a reliability analysis and an identification of the least reliable component of the power conditioning system of PMG and WRIG-based grid connection arrangements are presented. Reliability of the systems is analyzed for a particular wind speed.

Moreover, the least reliable component within the power conditioning system is identified quantitatively.

In Chapter 7, a summary of the most important conclusions reached in the research and highlights of the contributions from the research, as well as suggestions for the direction, content and scope of future research are presented.

.

Chapter 2

Overview of Grid Connected Small Wind Energy Conversion System

The present commercial availability of small wind turbines incorporate a variety of innovative systems, with proven technology for both the generators and Power Conditioning Systems (PCS). The most frequently applied Small Wind Turbine (SWT) systems in industry are investigated in this research. The investigation is further extended to determine the failure modes of the wind turbine subsystems in order to identify the most common failure subsystems. The most preferable mainstream and an optimum surrogate system are identified and the characteristics, along with power conditioning system of each system are discussed in order to orient the research towards an optimum system for a small wind energy conversion system.

2.1 Overview of Grid Connected Small Wind Turbine Systems

The application grid connected of small wind turbines is a prominent research area in the

SWT industry. An extensive review is presented to investigate the most frequent generator system, control method, rated power, as well as the usual systems used by the manufacturers in their commercially available grid connected systems. The horizontal furling method is more common for mechanical power control [10 – 13]. Induction Generators (IGs) and Permanent Magnet Generators (PMGs) are used presently in most commercially available small wind turbines in the market for converting wind energy into energy. Furthermore, IGs and PMGs can be operated in grid connected mode using an inverter system, which is either manufactured specifically or commercially available [14]. The principal manufacturers of grid connected SWT, including the generator system and rated power are listed in Table 2.1. The table is based on information provided in web pages and owner manuals from the manufacturers.

The state-of-the-art for operating of SWTs in grid connected mode has changed over the years from being conventional-driven to being optimized-driven within the operating regime. In addition, the design of small wind turbines has progressed from fixed speed, flapping/passive pitching-controlled and drive trains with gearbox to variable speed, furling/soft stall-controlled with or without gearbox. The following discussion provides an overall outlook on the contemporary wind turbine systems, focusing on their general attributes over recent years.

The Wind Energy Conversion System (WECS) presented in Fig. 2.1a incorporates a Squirrel Cage Induction Generator (SCIG) and a soft starter for smooth grid connection. A large capacitor bank is required to cope with the reactive power demand by the generator from the grid. This configuration allows a small variation in rotor speed,

typically 1 to 3% and resembles a constant speed system. The system is also known as the "Danish System" in the market.

Table 2.1 Information regarding the grid connected SWT system

Manufacturer	Country	WT	Generator	Rated power (kW)
CleanField Energy	Canada	3.5 kW VAWT	PMG	3.5
WES Canada	Canada	WES TULIPO	AG	2.5
Wind Simplicity Inc.	Canada	Windancer	PMG	3
		Windancer	PMG	7
Aerojoule	Canada	AJT-15	IG	1.5
		AJT-30	IG	3
		AJT-45	IG	4.5
		AJT-100	IG	10
***Windmission**	Denmark	4 kW Windflower	PMG	4
Eoltec	France	Scirocco E5.6-6	PMG	6.6
Fortis	Netherland	Passaat	PMG	1.4
		Montana	PMG	5.8
		Alize	PMG	10
J.Bornay Aerogeneradores		Inclin 3000	PMG	3
		Inclin 6000	PMG	6
Proven Engineering Products Ltd (Proven Energy)	UK	WT2500	PMG	2.5
		WT6000	PMG	6
Southwest Windpower	USA	Whisper 200	PMG	1
		Whisper 500	PMG	3
		Skystream	PMG	1.8
Wind Turbine Industries Corporation	USA	Jacobs 10 kW	PMG	10
BERGEY	USA	BWC ExcelS	PMG	10
Abundant Renewable Energy	USA	ARE110	PMG	2.5
		ARE442	PMG	10
AVENTA AG	Switzerland	AV-7	PMG	6.5
Aircorn	Germany	Aircorn 10	PMG	10
Energotech SA	Greece	Butterfly 1K	PMG	1.5
		Butterfly 3K	PMG	3.5
		Butterfly 6K	PMG	7
Aerodyna and SMA	Germany	Aerosmart 5	AG	5

*Work in progress; PMG=Permanent Magnet Generator; AG=Asynchronous Generator;IG=Induction Generator

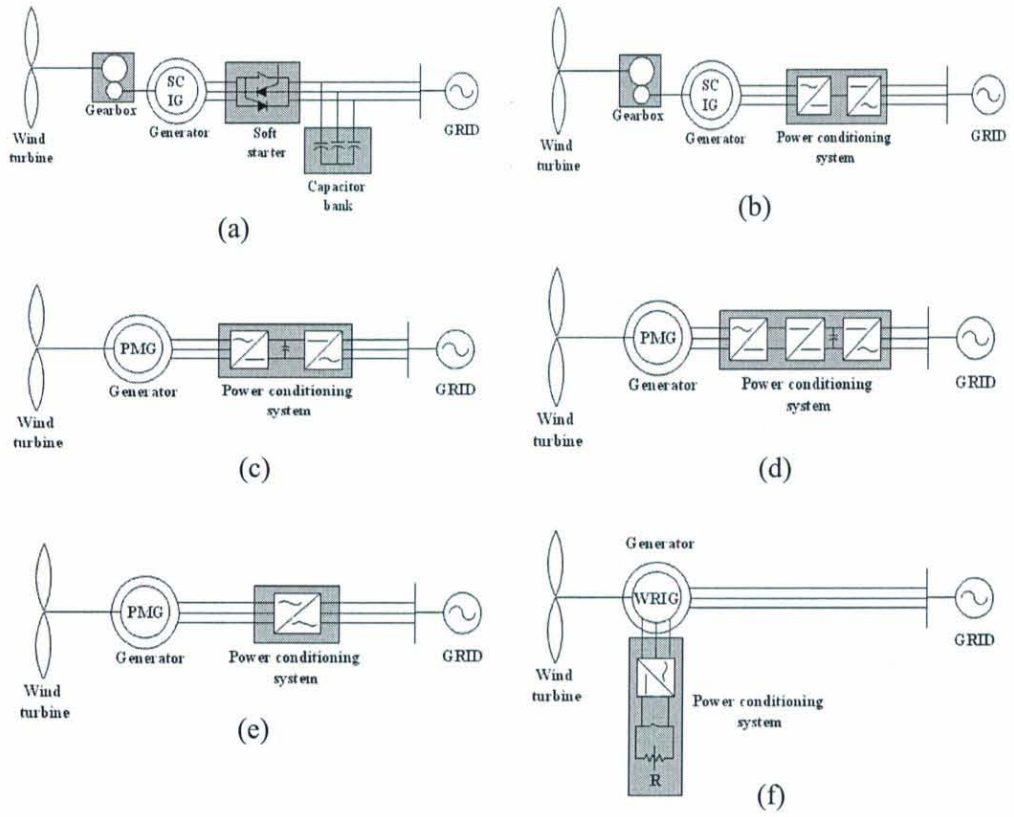

Fig. 2.1 Typical configurations of small wind turbine systems a) Type A, b) Type B, c) Type C1, d) Type C2, e) Type C3, f) Type D

The system shown in Fig. 2.1b changes the Danish system by inserting a converter/inverter to regulate the power between the grid and IG. Variable speed operation is achievable with a suitable control strategy. The power conditioning systems carry out the task of reactive power compensation as well as improvement in power quality. However, the variable voltage and frequency from the generator are adjusted by the converter/inverter system, requiring the power conditioning system to be dimensioned for the maximum power of the turbine and is therefore expensive. Higher power loss

compared to the Danish System in the power conditioning system is a major concern in this system.

Fig. 2.1c – e shows grid connected wind turbine systems that use permanent magnet generators. The machines generates electrical power at a frequency directly related to the shaft speed by some fixed ratio. The power conditioning system consists of a converter/inverter arrangement between the generator and grid to ensure smooth power transfer for variable speed operation. Permanent magnets may be used on the synchronous machine rotor to generate flux. This type of machine is referred to as a permanent magnet machine and is presently used by most of the manufacturers. Permanent magnets in the rotor overcome the barrier of field winding excitation that is required for synchronous generators. The problem for this system is the higher rating of the converter/inverter and consequently higher conversion power losses and system complexity, as well as system cost.

In the case of a SCIG, the rotor circuits are not accessible externally, and the induced current is a function of the slip and applied torque. However, in a Wound Rotor Induction Generator (WRIG), each of the three discrete rotor winding systems is electrically accessible via slip rings on the machine shaft. This access can provide a means for controlling the rotor currents, and therefore the electromagnetic torque production. The magnitude of the rotor current in such an arrangement is controllable over the operating speed range of the turbine by controlling the external resistor connected to the rotor circuit. This allows the control system to vary the slip-torque characteristic over a wide range of wind speed.

The power conditioning systems integrated at the stator side are associated with high current ratings and consequently an increase in cost. In such a scenario, a wound rotor induction generator with rotor resistance control can be a feasible surrogate system. In order to realize a better adoption during start-up, weak and high wind operating modes, the rotor resistance can be changed to compensate dynamically for the tower shadow effect on the power dissipation to the utility [15]. Moreover, the necessity of an inverter for grid connected operation can be eliminated since the power electronics circuitry in the rotor circuit is composed of a simple 3-phase bridge rectifier and a switch while the stator is directly connected to the grid. Flicker at the grid is minimized and electromagnetic compatibility can be attained using a small capacitor placed at the stator. It should be noted that the system also poses some restrictions such as higher power loss in the rotor circuit and constant maintenance of the slip rings. A basic schematic of the system is presented in Fig. 2.1f. Presently, the SWT industry does not use this system due to the fact that a gear box is necessary for the commercially available 4 pole wound rotor induction machines and hence is considered to be costly. However, the barrier posed by the gearbox can be overcome by designing an optimum machine with the number of poles as required for operation.

2.2 Overview of Failure Modes of Grid Connected Small Wind Turbine Systems

The uncertain nature of wind energy renders failure statistics and reliability analysis to be of great value before the installation of a wind turbine system. The need for long term field data is critical in evaluating the technical and economical performances. Long term failure and reliability data for wind turbine subsystems are readily available. This is

primarily due to the fact that a significant (and growing) number of wind turbines of various ages, types and locations are in existence across the world. This information represents a useful starting point for modeling the wind turbine systems subcomponents. It also allows optimization of the design features as well as the system. Most of the large commercial wind turbines have intense review of the reliability of the system components; however, small wind turbines lack this feature due to the additional cost involved. The following is a study performed from the published data to investigate the failure modes of various subsystems of the SWT systems. Small frequent failures have a minor impact on the availability of on-shore wind power generation. However, in grid connected off-shore wind turbines, these small failures can lead to high unavailability and high operational costs due to the difficult accessibility and expensive repair costs. As a whole, the least reliable components of a wind turbine system can be determined by investigating of the failure distribution of wind turbine systems. This also helps to improve the system level design for wind turbine systems.

Case study 1: [16]

The Scientific Monitoring and Evaluation Programme (WMEP) in Germany is one of the biggest funding programs involved with the development of SWT-based WECSs since 1989. SWT specific analysis and valuable information regarding the performance and reliability are published in their work. A recent publication deals with the failure rates of 235 SWTs for an observation over 10 years. The wind turbines have a rotor swept area of less than $200m^2$ and represent 16 different manufacturers. Moreover, investigating the SWTs is categorized into two groups: 205 SWTs that have a rotor diameter equal to or smaller than 7 m and 30 SWTs with rotor diameter greater than 7m. A total of 4200

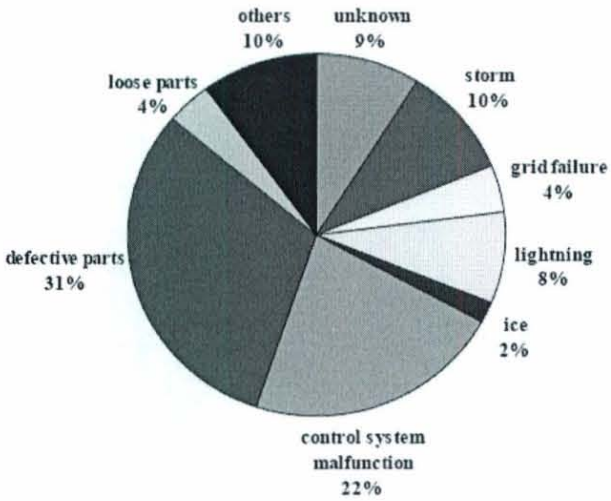

Fig. 2.2 Distribution of number of failures

reports have been selected by the authority from the local operator. These reports were analyzed and it was found that control system malfunctions account for 22% of the failures. Defective parts which include mechanical and electrical parts share 31% of the total failures. Fig 2.2 represents the frequency of failure of the SWTs subsystems investigated through the programme. Replacement and repair of components is usual for wind turbines and play a significant role as observed by the programme. Generally, an electrical control for a wind turbine includes an electronic control unit, relays, circuit breakers and others, while the electrical system incorporates the inverter, converter, fuses, switches, circuit breakers, cables and others. It has been found that the control unit and electrical system together with the sensors and generators account for 59% of the total repairs whereas the mechanical system, which includes drive train, yaw mechanism, hydraulic system, rotor blade, mechanical brake, rotor hub etc. and structures accounts for 41% of the total repair for the group of SWTs and has a diameter of less than 7 m. The pie chart is presented in Fig 2.3.

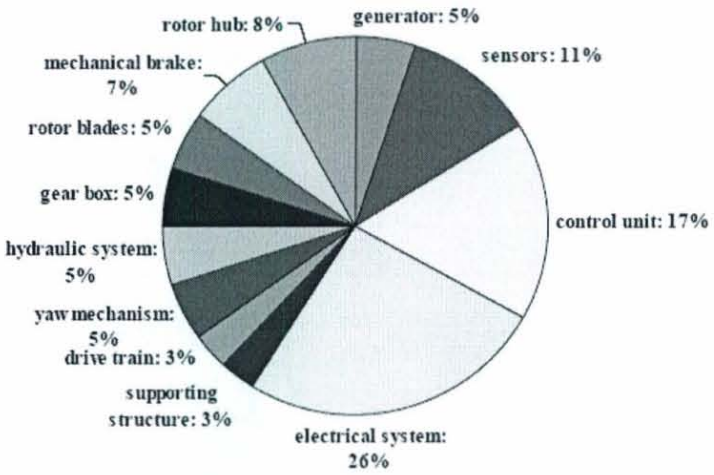

Fig.2.3 Share of repair measures on different sub systems for SWT

Case study 2: [17]

The task performed by Elsfork, Sweden is almost similar, i.e., publish reports on the performance of the turbines in Sweden. The statistical data from the wind power systems were collected by Vattenfall Power Consultant. Traditionally, the data are not automated, rather hand written reports were prepared by the individuals. The reports contain inform-

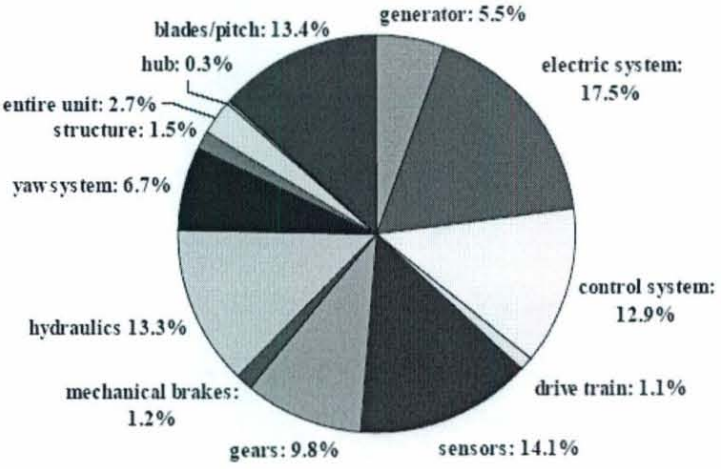

Fig. 2.4 Distribution of number of failures

-ation about the production and downtimes as well as failure statistics and reliability measures. A comprehensive study has been performed and presented in Fig 2.4 over the years 2000 to 2004. It follows a similar pattern, i.e., the failures involving the electric system, control systems, generators and sensors constitute 50% of the total failure.

Case study 3: [18]

The work performed in Germany investigated 3 turbines as follows: Enercon E66 rated 500 kW; Vestas V39 500 rated at 500 kW, and TW 600 rated at 600 kW. The data were

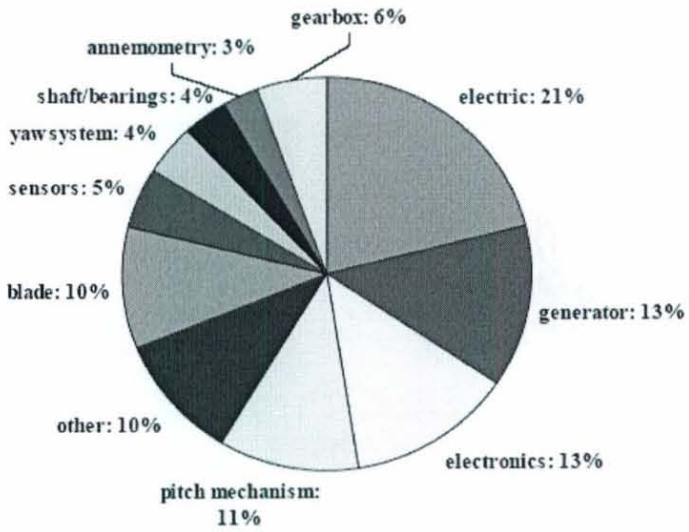

Fig. 2.5 Distribution of number of failures for Enercon E66

collected from Landwirtschaftskammer, Schleswing-Holstein, Germany (LWK). The results of the frequency of failure for Enercon E66 and Vestas V39 500 are presented in Fig 2.5 and 2.6 respectively. It should be noted that the rating is beyond the rating of small wind turbines. However, valuable information regarding the electrical system failures can be obtained. It is interesting to note that for all wind turbines the electric system failure accounts for at least 50% of all failures.

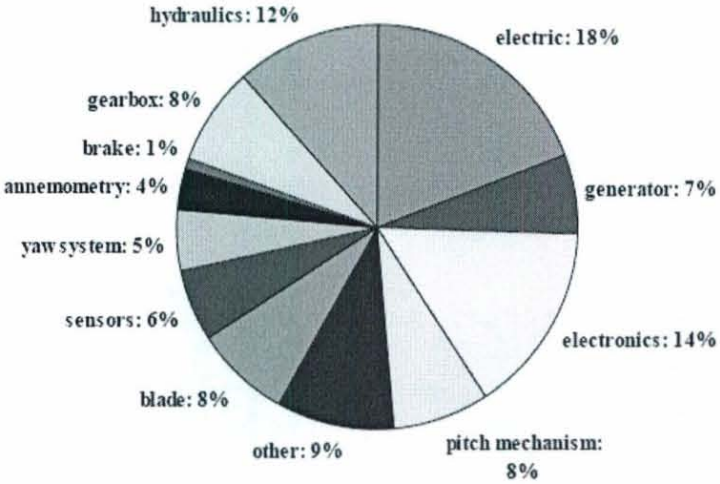

Fig. 2.6 Distribution of number of failures for Vestas V39 500

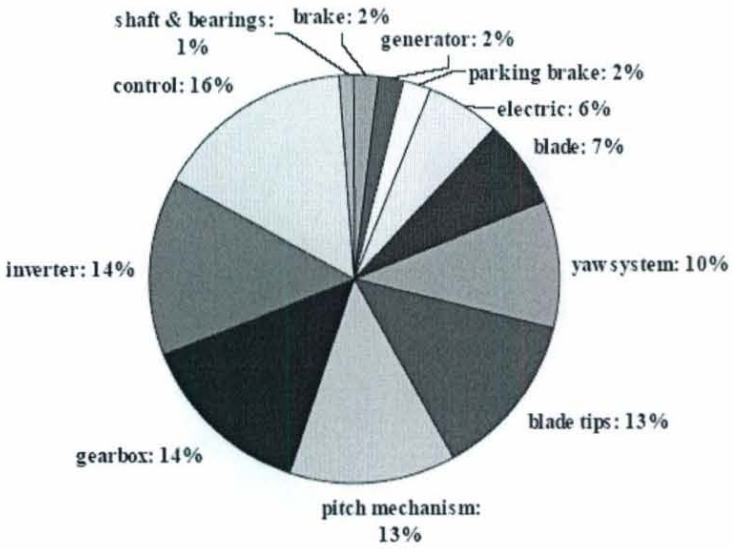

Fig. 2.7 Distribution of number of failures for large wind turbines

A significant difference is observed once the failure distribution of large wind turbines is carried out. Failure distribution and reliability of such large wind turbines was carried out in the DOWEC project at Netherland. The study also investigated the availability and maintainability of the wind turbine system. Part of the study focused on the opportunities

and drawbacks of different designs of extremely large wind turbines for large scale off-shore wind farms. The data presented in Fig 2.7 reflects the failure distribution of a large scale wind farm consisting of 100 units (5MW each) located in the North Sea. The interesting point revealed that for the large scale wind turbine, failure related with the electrical sub systems is minor. Most of the failures were due to the mechanical subsystems, which is entirely different than the SWT systems where the main causes of failure are due to the electrical sub systems [19].

The above discussion leads to a conclusion that the reliability of electrical related subsystems is a major concern for SWT systems as well as in the SWT industry and cannot be ignored. In order to have better penetration of the SWT in electrical power systems, high technical availability of the SWT is crucial to provide the needed security of supply. Research should be undertaken to improve the reliability of the electrical related subsystems due to the fact that the electrical related subsystems carry the major portion of the failure during operation. Attention should be given to a straightforward but reliable electrical design that ensures easy maintenance and repair as well as less complexity in the control architecture. However, in order to choose an optimum system, a valid motive should be established. As a result, this study undertakes a comprehensive performance and reliability analysis of the systems in order to find an optimum surrogate system as will be discussed in chapter 4, chapter 5 and chapter 6.

2.3 The Compared Systems

Today's SWT markets are primarily dominated by the PMG-based system that ensures a variable speed operation. Fig. 2.8 shows the schematic of the widely used system of a small grid connected PMG-based wind turbine system. The PMG is very interesting for

variable speed systems because it can be connected to a diode rectifier and, thereby, leads to a very efficient system. The power conditioning system has a diode rectifier, a dc-dc converter and an inverter. Usually the rectifier is chosen for its low price and low losses and the inverter because it produces high quality power to the grid. An alternative systems is the WRIG-based SWT system, shown in Fig. 2.9. The system is used in large wind turbines. In this arrangement the PCS consists of a 3-phase bridge rectifier, a switch and an external resistance. The high cost of the permanent magnet generator is offset by the reduced cost of the PCS, since only 20 – 30% of the rated power flows through the slip rings while most of the power flows to the grid from the stator. The resistance, R_e can be used as a heating element. The switch of the WRIG-based system allows the effective rotor circuit resistance to be varied hence ensuring variable speed operation.

The generic objective of power production by a wind turbine is to ensure variable speed operation in a wide wind speed range, maximize the energy yield, and improve the power quality. A subset of these goals is: to choose an optimum system; to improve the performances in terms of power production and efficiency; and to ensure high reliability in order to optimize the installation and maintenance costs. A popular belief is that the WRIG-based system is probably not useable because it suffers from high power loss in the rotor circuit, and only 0 – 10% speed variation is achievable, while a PMG-based system offers a speed variation of 0 – 100% and ensures high efficiency of the system. However, this research carries out an in-depth investigation and shows that the above mentioned belief is not correct. This is due to the fact that the optimum system should provide low cost of the energy, have lower failure rate and consequently increase the reliability as well as improve the serviceability and maintainability.

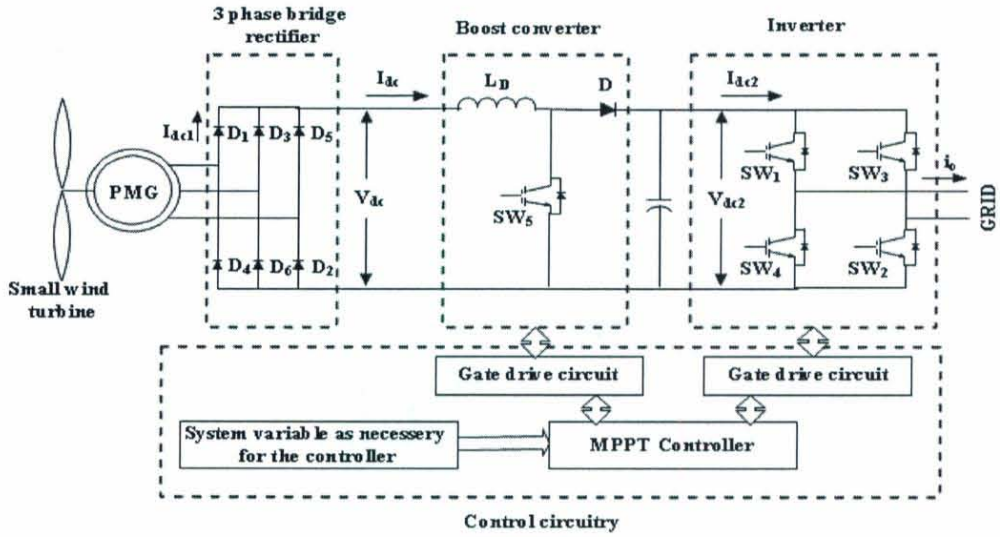

Fig. 2.8 A PMG-based small wind turbine system

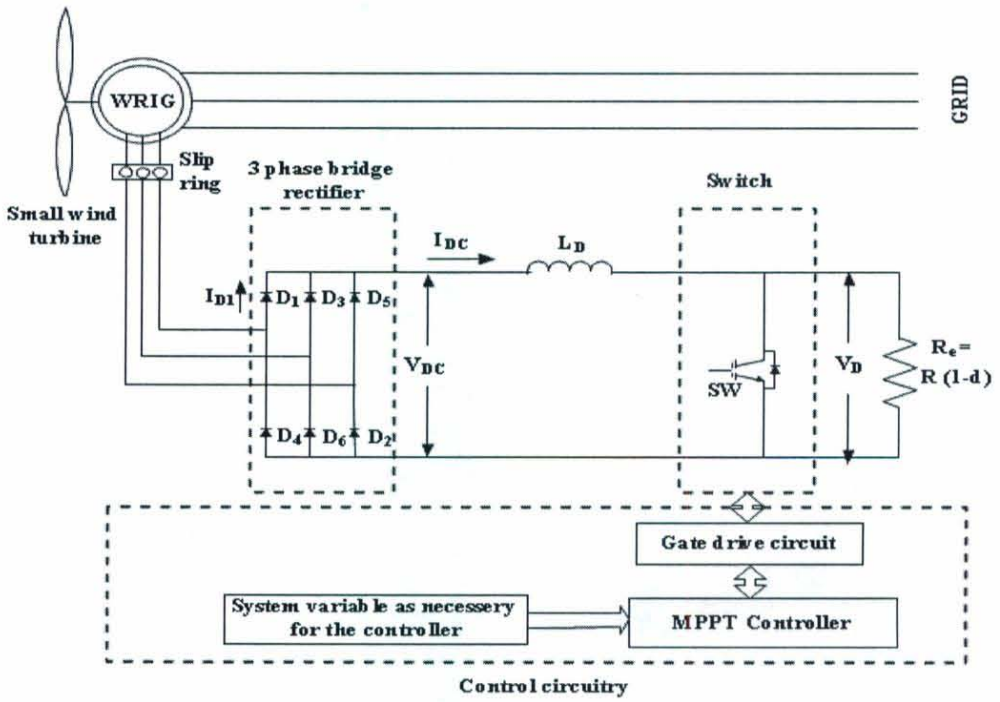

Fig. 2.9 A WRIG-based small wind turbine system

2.3.1 Overview of Power Conditioning Systems

In the early 80's, variable speed systems adopted rectifiers and converters made up of diodes or thyristors. Low frequency harmonics and low switching frequency resulted due to the line commutation of the switches [20]. With the advancement in technology, Insulated Gate Bipolar Transistor (IGBT) switches are very often used by the manufacturers which can operate at higher frequency and may have reduced switching losses. The rectifier system used at the generator terminal is usually of the uncontrollable type.

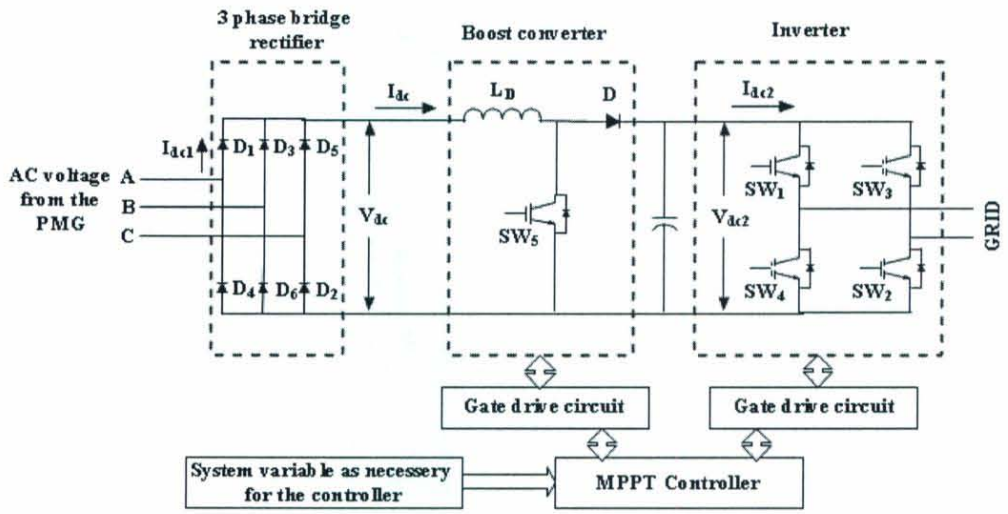

Fig. 2.10 Power conditioning system of a PMG-based system

A power conditioning system used for a PMG-based system is presented in Fig. 2.10. This technology employs a boost converter stage prior to the inverter. In general, the inverter used for grid connection requires a dc link voltage greater than the rectified line-to-line voltage. As a result, a boost in voltage level is required for the grid connection as the voltage level from the SWT system is low compared to the required dc link voltage.

This is achieved by using a boost converter. The dc link capacitor decouples the voltage source inverter and the boost converter and keeps the dc link voltage ripple to an acceptable level. The inverter can be programmed for maximum power extraction. It therefore yields a high reaction speed and in order to achieve an optimal system.

The use of a boost converter has the advantage of adapting the PMG voltage variation caused by the stochastic nature of wind and changing load. However, there are still a number of disadvantages:

- Traditionally, the conversion from dc to ac power is achieved using a conventional voltage source Pulse Width Modulation (PWM) inverter in a stand-alone load or grid connected system. Moreover, the stand-alone inverters need to ensure the voltage and frequency regulation as well as over-current protection and surge capabilities. The stand-alone inverter must be a self-commutated, voltage-controlled inverter, so that loads can be operated within their nominal voltage ratings. In terms of power quality, reliability and price, these stand-alone inverters are very competitive [21]. Almost no manufacturers use their own product in the case of the inverter. Most manufacturers typically use the modified version of inverters that are normally designed and optimized for Photovoltaic (PV) applications and change the control software if required. Moreover, the standards for small wind turbines are yet to be established and the technological development of SWT is not proceeding as fast as for the large Wind Turbine (WT). As far as the small wind turbines are concerned, most countries have their own recommendations about small wind turbines connected to the grid. This is understandable as the power quality aspects and standardization, as well as the

laws and regulations differ by country and governments set up their own rules to assure a good power quality. But, these actuations make it more difficult to introduce the SWT in countries, because the inverters have to pass all the tests in each country. Moreover, although most of the rules are more or less the same, they have to be approved and marked by some test centre approved or established to make this test in accordance with the rules of each country. In order to achieve these requirements a significant increase in cost of SWT could be observed and can be considered a major challenge for the penetration of small wind turbine in the market.

- The configuration consists of two stages, i.e., boost the voltage level (DC-DC boost converter) and grid connected (DC-AC inverter) which inevitably reduce the efficiency of the system.
- A complex control architecture is required, resulting in more components and hence reduced reliability. Due to the involvement of more components, an additional heat sink is required, consequently increasing the size and volume of the unit. Furthermore, more power electronics increase the cost of the system.

The boost converter based power conditioning system can be considered a better system compared to an AC-DC-AC link based power conditioning system. The low voltage produced by the wind turbine needs to adapt to the high main voltage level. A boost converter based power conditioning system increases the low voltage level to the main voltage level by using an IGBT. While in an inverter, two IGBTs or two diodes conduct at the same time for an AC-DC-AC link power

conditioning system and have to be sized for high current and voltage due to low voltage generation by the wind turbine.

- The inverters used in this system have low efficiency at low power levels. This is a very important point of consideration as most of the small wind turbines face low wind speed throughout a year and consequently operate at low power levels. The sharp drop of converter efficiency especially for a small wind turbine is not desirable but, it cannot be avoided [22].
- Most of the converters/inverters used for the grid connection use a PWM switching technique to optimize the performances. For instance, flexible control resulting in low switching losses may be used. The PWM modulation usually injects harmonics into the grid (and consequently, voltage drop or transient voltages) and is not advantageous in terms of power quality [22]. It should be mentioned that incorporating more converters in parallel can improve the power quality. However, this increases the cost of the total system and it is a severe problem for small wind turbines as they are very subject to installation and maintenance costs.

In contrast to the most common power conditioning systems for SWT systems presented above, the power conditioning circuitry for WRIG offers less complex architecture and components. The costs reduce dramatically due to the exclusion of the converter/inverter system. Furthermore, the power conditioning system consists of fewer components, and consequently provides lower control complexity. The stator of the machine is connected directly to the grid and the voltage induced in the rotor is rectified to DC by the diode

rectifier. An inductor is used to smooth the current in the rotor circuit. The current is then fed to an IGBT based shunt switch with an external resistance as presented in Fig. 2.11 and Fig. 2.12. The switch allows the effective rotor circuit resistance to be varied for the speed control of the machine. When the switch is on, $V_{DC} = 0$; the external resistance, R becomes short circuited. On the other hand, when the switch is off, $V_{DC} = V_D$; the resistance applied externally to the rotor is R. As shown in Fig 2.12, the effective external rotor resistance due to the PWM wave is

$$R_e = \frac{R.T_{OFF}}{T} = \frac{R(T - T_{ON})}{T} = R(1-d) \tag{2.1}$$

where, T is the total time period of the PWM wave,

d is the duty cycle of the switch and is equivalent to the total on-time over the entire period of the PWM wave.

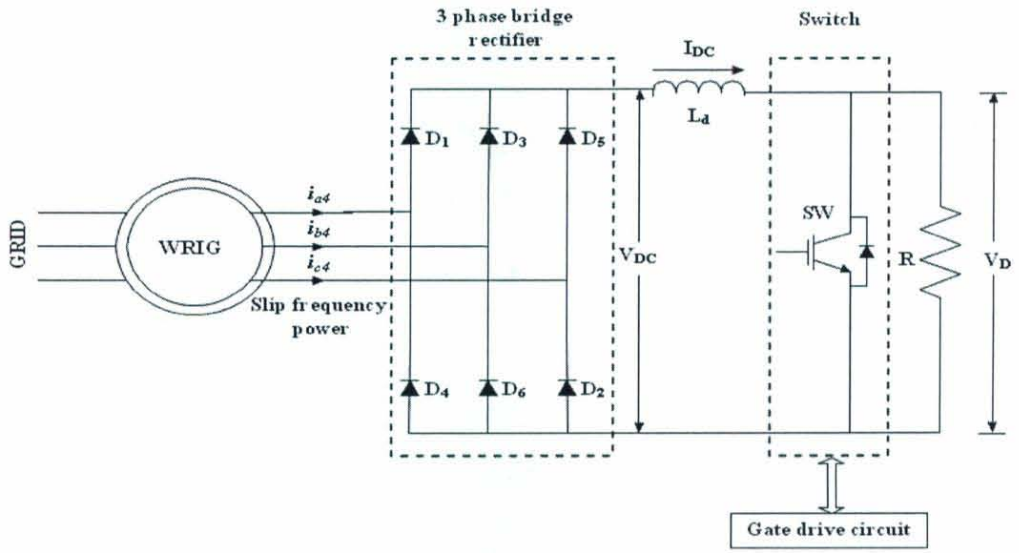

Fig. 2.11 Power conditioning system of a WRIG-based system

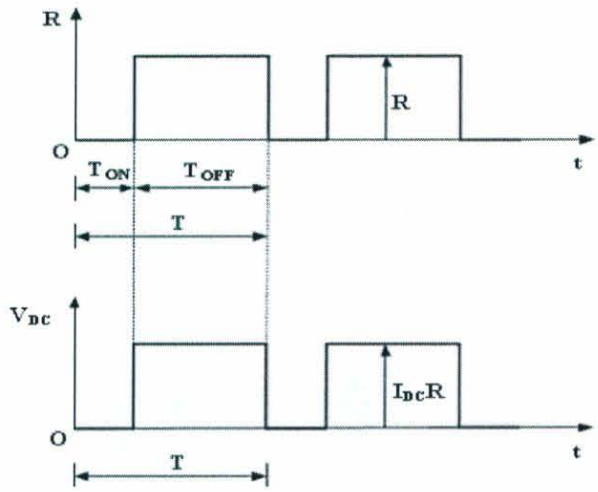

Fig. 2.12 Waveforms pertaining to Fig. 2.11

From (2.1) it is obvious that by changing the duty cycle of the switch, speed control of the machine can be achieved. The speed control of the wind turbine is thus attained using only a diode bridge rectifier and a controlled switch. The necessity of high rating of the components is lowered due to reduced slip power/voltage. Typically, the rectifiers and switch cope with 20% – 30% of the rated power. The reduced power rating of the components and driving circuitry leads to inexpensive components as compared to the most common configuration used for the SWT system. However, the main demerit of this method of control is that energy is dissipated in rotor circuit resistance, internal and external, and this energy is wasted in the form of heat. Bidirectional power flow is not possible with this system, while the PMG-based system exhibits the bidirectional power flow characteristic. A WRIG-based system also ensures a wide range of speed control of the wind turbine similar to a PMG-based system.

2.4 Summary

The discussion in this chapter raises several important issues that need to be examined. Synopses of the issues are presented below:

- Several systems exist in the market to connect a small wind turbine to the grid. The PMG-based system is favored while there is a lack of interest in the WRIG-based system. This lack of interest in the WRIG-based system is due to the popular belief that such a system waste higher power in the rotor circuit than the power loss in the power conditioning system of the PMG-based system.
- The reliability of the electrical subsystems is more important than the reliability of the mechanical subsystems for a small wind turbine system, while the opposite situation is observed for a large wind turbine system. The data collected from several wind turbine projects were used to validate this assumption;
- Quantitative evaluation of the performances of a PMG-based system and a WRIG-based system is required in light of the advantages and disadvantages described above.

Chapter 3

Literature Review

In the small wind energy domain, the existing knowledge of the system of a Permanent Magnet Generator (PMG)-based wind turbine system design and performance is quite rich. In sharp contrast, studies with emphasis on the system of Wound Rotor Induction Generator (WRIG)-based small wind turbine system are very few. The statement is factual when observing the market penetration between the systems for large wind turbines. Fig. 3.1a shows the market attention of the PMG and WRIG-based large wind turbines from the year 1995 to 2005. The diminishing nature of the WRIG-based system is observed whereas the PMG-based system maintains a steady market. The situation becomes more severe once the shares of cumulated installed power are considered over the years (Fig. 3.1b). The WRIG-based system has been decreasing over the years since 1997, while the PMG-based system maintained an increase from 1999 to 2002 in terms of

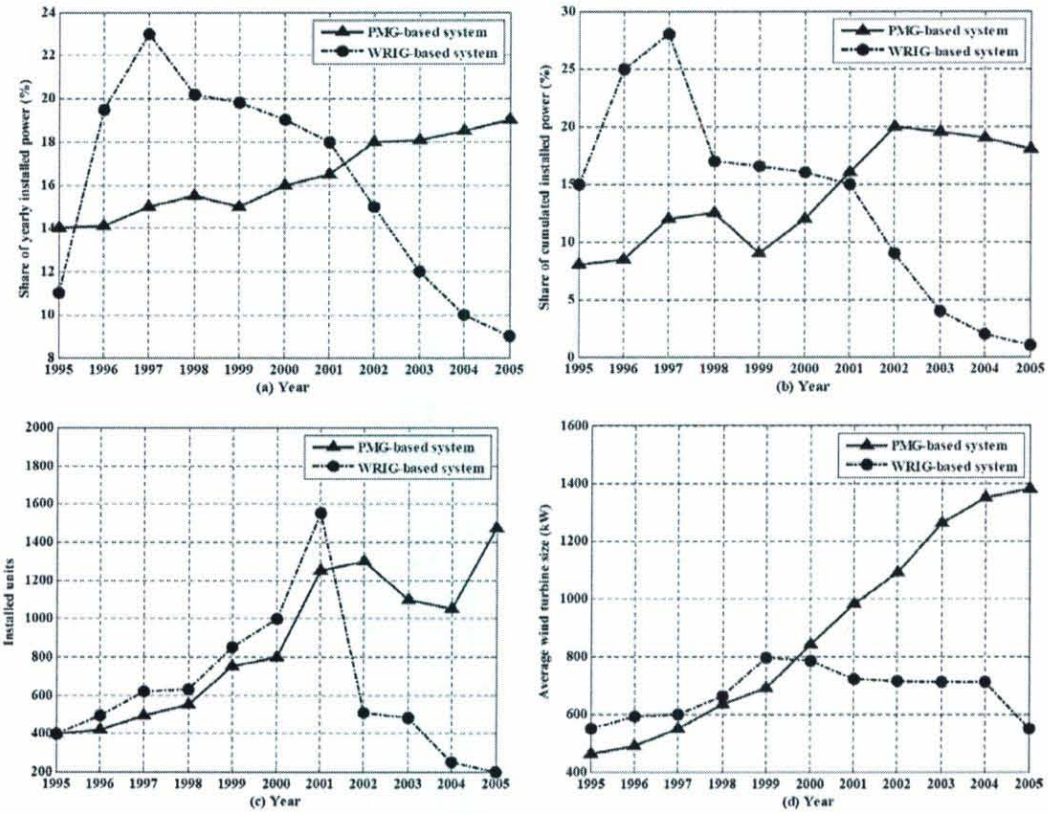

Fig. 3.1 Market penetration of the systems, a) Share of yearly installed power, b) Share of cumulated installed power, c) Installed units, d) Average wind turbine size

total installed wind power. It is observed from the number of installed units per year (Fig. 3.1c) that the WRIG-based system reached its peak in 2001, after which it decreased significantly [23]. In contrast to the WRIG-based system, the number of installed units for the PMG-based system increased slowly and is believed to be increasing after 2005. Finally, information on the installment of the commercial power of the wind turbine is significant in order to have an understanding for a preferred type of mainstream system. Fig. 3.1d presents the yearly average size of each wind turbine system over the years. It is

clearly visible that the WRIG-based system has almost always remained in the 600-800 kW power range, while the annual average size of the PMG-based system has increased almost linearly over the years. One of the main reasons for such a depressing picture of the WRIG-based system in contrast to the PMG-based system, is the ability of the PMG-based system to operate in a full variable speed operation with a more efficient manner. Variable speed operation is an attractive feature for wind turbines for a number of reasons, including reduced mechanical stress, increased energy capture and, not least, controllability, which is a primary concern for the grid connection of wind turbine systems [24, 25]. Recent advances in power electronics have been a leading cause in the dramatic advancement of the PMG-based system [26]. However, despite such rapid growth of the PMG-based system, it is difficult to predict the future for both systems. This is because ideas borrowed from other fields or other applications could have profound effects on future penetration. In this context, more investigation is essential on the PMG and WRIG-based systems not only on the basis of performance of power electronics of both systems but also with respect to the other aspects that significantly affect the global need of a wind energy conversion system. Indeed, performance evaluation of the individual systems is not unique; the author has, however, not found in the literature any evaluation of the comparison of performances of the PMG and WRIG-based system that could significantly dictate the future research to adapt an optimum system.

With the rapid improvement in the power electronics area, a lot of work has been done and is being done on the power conditioning system with a special focus on the electrical properties. However, with respect to the topic of this work, all those focusing entirely on

the power conditioning system improvement is not of big interest. Rather this research starts from a point that an optimized power conditioning system is integrated with the PMG and WRIG-based systems based on the market penetration of both systems. This assumption is required as general research approach on the wind energy conversion system emphasized on a specific system power conditioning system performance to a certain extent, while comparing a series of power conditioning system performance in the perspective of wind energy conversion system was left unanswered. This general approach could lead to a potential misjudgement on system performances as different results on the same question might arise. Moreover, without a test-bench validation, the final conclusion might fail to be consistent with the simulation results. On the strength of the discussion above, a comparison of the performances of the wind energy conversion systems is required, where the impacts of power conditioning system used by each system have to be included. This is of particular importance because the power conditioning system used by the PMG-based system is always considered as highly efficient as asserted by the manufacturers. However, manufacturers have a clear tendency to claim a higher performance of their power conditioning system for marketing purposes. Furthermore, factors, such as reliability, system complexity, control architecture also affect the performance of a PMG-based system. On the other hand, the power conditioning system for a WRIG-based system has long since improved from an external rotor resistance based system, Scherbius system to Kramer system. The power losses in the rotor circuit for the external rotor resistance control is one of the major disadvantages, while the use of other two power conditioning systems could reduce the power factor and complicate meeting the grid power constraints. Moreover, special attention should be

paid on the design of the mechanical system due to the fact that distorted rotor current produces low frequency torque pulsation [27, 28]. Although it is possible to integrate various power conditioning systems with the PMG and WRIG-based systems, the mainstream system is chosen in this research because of their vast existence in the market and the reliability concern as described in the previous chapter. An approach is undertaken by this research to clarify the performance of both systems in terms of power loss, Annual Energy Capture (AEC), Annual Energy Loss (AEL) and most importantly, in order to reach a global conclusion, analysis is extended on eight different regions of Newfoundland and Labrador, Canada and a performance characteristic, i.e., efficiency is compared. Finally, not only a high efficiency can help to penetrate a specific system but also the reliability of the system is essential. Therefore, a reliability comparison is also performed which will also support the use of a specific system.

The determination of power losses, which accordingly impact the efficiency of wind turbine systems have been studied by numerous literatures in the past [29–48]. There are principally three approaches for calculating the power losses in a Power Conditioning System (PCS), which are briefly discussed here. The first approach is the development of a non linear loss model of the PCS based on the on-state current of the semiconductor devices [29–32]. Because it is easy to relate the on-state current of the PCS and operating conditions of the wind turbine, this approach involves simple calculations and represents a good tool to distinguish between different PCSs. On the other hand, the non-linear loss model approach is unable to reflect the switching losses of the semiconductor devices, which could be a dominant factor during the high switching state. Indeed, switching losses have been considered [33–37], however excluding the dependency on the actual

commutation voltage or current or modulation index during conduction loss analysis could lead to ambiguous results.

The second approach is used to simulate the power electronic system with ideal switches and to obtain the current and voltage for these devices. The voltage and current waveforms, as well as the switch design, the conduction and switching losses for the semiconductor components can be determined using the information found either in data sheets for the components or in look-up tables based on experimental results. Theoretically, this approach offers the optimal solution as it considers both conduction and switching losses of the semiconductor devices. However, one of the main disadvantages is recognizable; the data provided by the manufacturers are ambiguous and calculation of the losses is time consuming due to the involvement of the experimental procedure [38–42].

The third approach makes use of physics-based simulation models and is suitable for designing new power electronic devices and converters. This approach requires implicit integration methods, leading to increased simulation times. It also requires detailed knowledge of the physical dimensions of the device [43, 44]. There have been numerous other efforts for calculating the power losses of PCSs used in wind turbine systems. Miaosen et al. [45] have presented the concept of switching device power loss of PCSs in used in wind turbine systems where the maximum device rating has been considered, however, this concept has not investigated the calculation of the switching losses. The switching losses have been considered in [46–48] using the same concept, i.e., maximum device rating, however, the calculation of conduction losses lacks the valid justification as the actual commutation voltage or current is neglected.

From the above discussion it is quite clear that previous researches prefer to work on the power conditioning system itself rather considering the influence of losses on the wind energy conversion system as one unit. However, very recently researchers started to have an interest on the comparison studies on the wind energy conversion system with a special focus on the power loss behavior. One of the attempts to calculate the power losses in the power conditioning systems of a wind turbine system can be found in the work reported by Grauers, et al. [49]. This attempt has investigated the power losses of the power conditioning system of an Induction Generator (IG), Synchronous Generator (SG) and PMG-based wind turbine systems are examined. In general, there is a need for a comprehensive mathematical analysis as well as analysis of the conduction and switching losses during the conduction and switching states of different switches. Recently, work reported by Akaira, et al. [50] emphasizes the efficiency calculation of an IG-based wind turbine and does not include the power conversion stage losses. Although losses in the power conditioning system are of great interest during calculation of the efficiency of a system, researchers more often assume a non-linear dependency of the losses on the rated power and speed, which is somewhat questionable [29]. A comparison study on converter systems used in WECSs has been performed by Orlando, et al. [51]. This study has proposed performance comparisons on the basis of control performances rather than the loss calculations. As a result, it is quite simple to conclude that the influence of power losses and comprehensive loss calculations for different components in wind energy conversion systems have not been fully investigated. Moreover, any evaluation of different PCS loss calculation methods for the PMG and WRIG-based systems and how they affect the efficiency is hard to find in the literature. A consequence for the efficiency

is an important issue since this parameter defines the revenue of a wind turbine project. Moreover, it is necessary to compare the effect of the low wind speed regime for the PMG and WRIG-based systems on the power losses, since high power extraction at low wind speed is a unique challenge for the small wind turbine industry [52–54]. As a result, considerable research is necessary to clarify the performances of the systems not only to the entire wind speed regime. This is examined with an emphasis on the low wind speed regime and is examined through this research work.

Afterwards the research focuses on the experimental justification of the influence of losses on the system performance. At first a Wind Turbine Emulator (WTE) is developed to simulate the wind turbine behavior in the laboratory environment. This is of particular importance as without the same wind turbine for both systems, the comparison result might be inconclusive. An emulator has been developed based on an induction motor (IM) which is rated at 125 HP [55]. The Wind Turbine (WT) model is incorporated in the Personal Computer (PC) using a static speed vs. power curve. At any given wind speed, the operating point of the wind turbine is determined by the intersection point of load and turbine characteristics. The feedback from the IM motor has been taken as torque and speed which determines the required torque for the wind turbine. The 3-phase Insulated Gate Bipolar Transistor (IGBT) converter is triggered on the base of the controlled stator current. Further research has been carried out [56, 57] based on the rating of a 10HP induction machine and using the same control strategy that has been described in the previous work [55]. A generalized approach has been developed by Nichita, et al. [58]. The proposed system has been implemented using a Direct Current (DC) motor and the emulator consists of a real time software emulator and an electromechanical tracking

system. By taking the reference from the wind turbine model the total structure can be implemented either in torque control or speed control mode which gives a lot of flexibility to the control. Research by Rabelo, et al. [59] emulates a wind turbine with a separately excited DC motor rated at 7.5 kW. In this work, the armature control method has been applied to control the DC motor and the wind turbine model is based on both the steady state and dynamic behavior. The steady state torque has been passed through a 3 mass model which represents the wind turbine, gear box and generator moments of inertia and the elastic shafts connecting them. For mechanical power control, a pitch angle control method has been incorporated with the wind turbine steady state model. The controller for the DC machine has been done with the frequency response method. The control has been performed using the armature voltage control method, i.e., by controlling the speed of the separately excited DC motor.

Research has been carried out by Manwell, et al. [60] on a wind/diesel system where the emulator is mainly based on the steady state characteristics. A 40 kW DC motor has been used to simulate the wind turbine behavior and the model of wind turbine based on the power coefficient vs. tip-speed ratio curve. The reference torque of the wind turbine is compared with the torque of the DC motor and based on this comparison, the controller determines the DC motor torque. Research by Pierik, et. al. [61] has considered the passive pitching mechanism to the wind turbine model and the rotor dynamics have been taken into account. A separately excited DC motor has been used to emulate the wind turbine and the motor is controlled using the armature current. A flywheel at the motor shaft represents the inertia of a wind turbine rotor. Aerodynamic torque of the wind turbine is calculated from the motor rotational speed and considered as the reference

torque of the wind turbine. Based on the difference between the reference torque and the torque produced by the motor, the DC motor armature current is controlled. A simple model of the wind turbine has been proposed by Barrero, et. al. [62]. To represent the torque dynamics; oscillatory, aerodynamic and dynamics components of the wind turbine torque are considered. The DC motor is controlled using the armature current.

Battaiotto, et. al. [63] has carried out a research work on the emulator by considering a separately excited DC motor. The control of the DC motor has been carried out through the armature current. To implement the control strategy, a dual Digital Signal Processor (DSP) board is used which increases the total cost of the emulator system. A brief review of research on the development of the emulator is given by A. D. Diop, et al. [64], which shows that the furling action is still not considered in the emulator raised area. From the previous investigations, it is viewed that although the static and dynamic aspects have been incorporated in the model in some way or other, a furling control and expected dynamics based emulator is rare to find in the literature. This conclusion is important because most of the small wind turbine uses a furling mechanism for aerodynamic power control [10–13]. Moreover, most of the studies on performance comparison of wind turbines are based on the simulation study and validation of the theoretical investigation is left for future work. There is thus a need to perform the complete test bench examination of the compared systems to support the theoretical investigation.

As shown in chapter 2, it is desirable to have a reliable power conditioning system for a wind energy conversion system. However, it is quite difficult to predict the reliability as the reliability analysis of a power conditioning system is greatly influenced by the operating conditions, i.e., covariates and therefore it is desirable to investigate the

magnitude of their effects on the system reliability. Reliability calculations consider the voltage or current as a covariate for an electromechanical system [65], while the reliability of power electronic components is strongly influenced by the component temperature and variations [66]. Knowledge of the reliability of power electronic components is a key concern when differentiating between systems. However, recent research intermittently endeavors to determine the reliability and advancement of the inverter rather than the PCS [66–68]. As far as the inverter is concerned which is an essential part for the power conditioning system of the PMG-based system, it is primarily designed for PV applications [21] Reliability of such grid connected inverters is ambiguous [21] and several key aspects to increase the reliability of such inverters have been identified by previous researchers [68–70]. The dominant factor that contributes low technical reliability is the heat generation caused by the power losses when the current flows through the semiconductor switches [66, 69, 71]. A reduction in heat generation can significantly increase the reliability. In addition, fans inside the inverter have a limited lifetime and deserve special attention [69]. Nevertheless, there are other aspects (e.g. humidity, modularity, and packaging) that also require special attention beyond the technical improvement and are not a part of this present study.

Most of the reliability calculations are based on the accessible data provided by the military handbook for reliability prediction of electronic equipment which is criticized for being obsolete and pessimistic [72, 73]. A comparative reliability analysis of different converter systems has been carried out based on the military handbook by Aten, et al [73]; however, the absence of environmental and current stress factors can pose grim constraints on the calculated reliability value. Rohouma, et al [74] provided a reliability

calculation for an entire PV unit which can be considered more useful, but the approach lacks valid justification as the data provided by the author is taken from the manufacturers' published data which is somewhat questionable. This is due to the fact that reliability calculations using purely statistical methods [75], manufacturers data [67, 74], or military handbook data [76] neglect the operating point of a component. Moreover, the total number of components could vary for two systems (which have the same objective) in order to meet a certain criterion of the overall system. Although higher components in the PCS will exhibit less reliability and vice versa, the effects of the covariates could be different and consequently could lead to a variation in the reliability [77]. Furthermore, a reliability evaluation for the PCS of a grid connected small wind turbine is essential in order to optimize the system performances as well as system cost [78]. Another important point to mention is that reliability analysis based on the covariate factor is strongly influenced by the standard reliability data book also. For example, it is shown in previous research that different values of covariate factor for a same covariate is possible by using a different reliability standard data book [79]. This variation in covariate factor also varies the reliability of an integrated system which is composed of numerous semiconductor devices. Moreover, it is well understood that an error in reliability prediction for a system could prove to be fatal for the high penetration of small wind power. On the strength of the above discussion, this research suggests performing a component level reliability calculation by considering temperature as a covariate as usually used in Highly Accelerated Lifetime Testing (HALT) procedure [69]. As a later part, this research prefers to calculate the Mean Time Between Failures (MTBF) of the

power conditioning system, which can be considered as the most widely informative parameter in reliability studies [72].

3.1 Summary

The literature review presented in this chapter raises several important research considerations that require further investigation. Synopses of the further research investigations are presented in the followings:

- A detail and comprehensive simulation for the power loss calculation of a grid connected PMG and WRIG-based small wind turbine system is essential. Moreover, an energy calculation is also essential to investigate the impact of efficiency of a PMG-based system over a WRIG-based system;
- Test bench verification should be carried out to ensure the simulation observations for a PMG and WRIG-based system. In order to achieve successful test bench verification, requirement of a small wind turbine emulator cannot be ignored. The furling as well as maximum power control should be incorporated with the emulator. A complete design of a grid connected PMG and WRIG-based system as well as the efficiency comparison should be carried out to identify an optimal system for high penetration of small wind power;
- A reliability calculation with the variation in temperature is required in order to eliminate the dependence on the manufacturers published data. The reliability calculation should be based on the component level in order to have an in-depth understanding of the reliability for a PMG and WRIG-based system.

Chapter 4

Performance Comparison

The aim of this chapter is to outline the approach for determining the power loss and the performance characteristic of a grid connected Permanent Magnet Generator (PMG) and Wound Rotor Induction Generator (WRIG)-based small wind turbine system. This is accomplished by establishing the procedure for obtaining the conduction and switching losses of the Power Conditioning System (PCS) used in a PMG-based system that is composed of a 3-phase bridge rectifier, a boost converter and an inverter. In a similar manner, formulation for the conduction and switching losses of a 3-phase bridge rectifier and switch, resistive loss of an external rotor resistance, and electrical and frictional losses of a slip ring for a WRIG-based system is developed. Afterwards, the wind turbine performance characteristic, i.e., efficiency is determined using the wind speed information for eight different regions of Newfoundland and Labrador, Canada. The

furling control method is assumed for aerodynamic power control for above rated wind speed. The analytical simulation procedure presented in the chapter assumes that the turbine maintains an optimum Tip-Speed-Ratio (TSR) below rated wind speed to ensure maximum power extraction. Some simplifications have been made when developing the analytical simulation program. The power losses in the control and drive circuitry are neglected since it will be about the same in both cases and a stiff grid is considered.

4.1 Operating Conditions of the System

The operating conditions for a PMG and a WRIG-based system must be known in order to investigate the power losses in the PCS. For a PMG-based system, the level of the Direct Current (DC) output voltage at the boost converter remains constant, while the output from the rectifier depends on the wind speed, the generator characteristics and the turbine control strategy. In this investigation it is assumed that the turbine is operated as a variable speed wind turbine. This implies that from low wind speeds to rated wind speeds, the wind turbine maintains a constant TSR to ensure maximum power production. The model of the wind turbine employed in the system includes the nonlinearities and dynamics of furling action of the considered wind turbine. The technical specification of the modelled wind turbine is presented in Appendix A. The wind turbine system considered is of the direct drive type, i.e., the gearbox is not considered in the model.

4.1.1 Wind Turbine Model

A wind turbine can be characterized by the non-dimensional curve of power coefficient, C_p as a function of TSR, λ, where, λ is given in terms of rotor speed, ω_s (rad/s), wind speed, w (m/s), and rotor radius, R_w (m) as

$$\lambda = \frac{R_w \omega_s}{w} \tag{4.1}$$

The relationship between C_p and λ can be approximated by a quartic equation. In this research, the curve is obtained from the literature [80]. A model for C_p as a function of λ is calculated and the curve generated by the approximate model and the actual data are presented in Fig. 4.1a. Statistical analysis shows that the R^2 value of the model is 99.8% and the p-value from the chi-square goodness-of-fit test is less than 0.0001, which shows that the predicted model for C_p with the fitted coefficients is acceptable. The resulting equation is found to be

$$C_p(\lambda) = 0.00044\lambda^4 - 0.012\lambda^3 + 0.097\lambda^2 - 0.2\lambda + 0.11 \tag{4.2}$$

The curve relating wind speed and furling angle is plotted using published data [81, 82]. An approximate model is used to determine the relation between wind speeds and furling angle. It is found that a fifth order model is sufficient to represent the relationship. The R^2 value and the p-value from the chi-square goodness-of-fit test of the expected model are found to be 98.19% and less than 0.0001 respectively, thus validating the modeling approach. The modeling equation for the wind turbine is determined as

$$\theta = 0.00019282w^5 - .011317w^4 + 0.21115w^3 - 1.179w^2 + 1.4072w + 3.1628 \tag{4.3}$$

where θ is the furling angle in degree and w is the wind speed in m/s. The actual data and approximated model curve are shown in Fig. 4.1b.

The furling action should be achieved within a reasonable time span and it is assumed that the furling action would take 10 seconds to attain the wind turbine rotor in its stable state after a change in wind speed. The second order dynamics, which can be expressed as $H(s)$ ensures a stable furling operation within 10 seconds after the change in wind

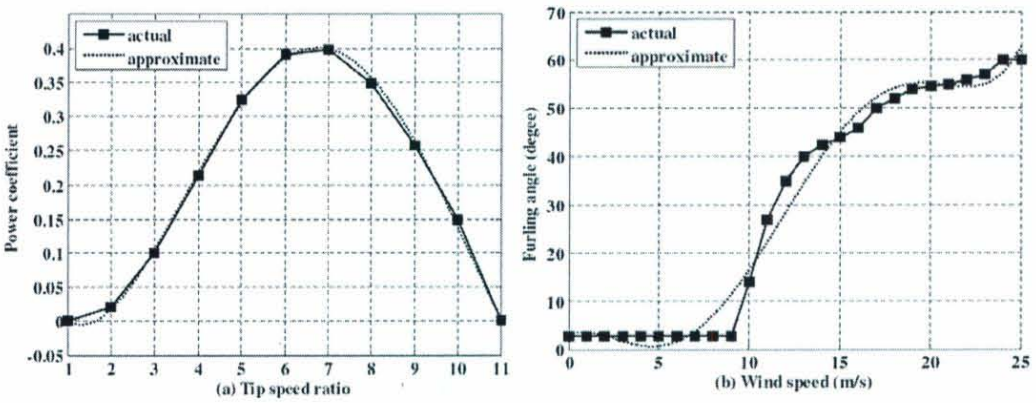

Fig. 4.1 a) Power coefficient as a function of TSR, b) Furling angle versus wind speed.

speed. The dynamics $H(s)$ is formulated as

$$H(s) = \frac{1}{1.3s^2 + .96s + 1} \tag{4.4}$$

The output power of the wind turbine can be expressed as

$$P_{aero} = 0.5\rho A C_p(\lambda) w^3 \tag{4.5}$$

where ρ is the air density (kg.m^{-3}) and A is the rotor rotational area, i.e., πR_w^2.

When the wind speed increases, small wind turbines yaw to an angle θ along its horizontal axis because of the furling action. The effective wind velocity at the rotor plane in that case will be $w\ cos\theta$ [83]. Incorporating the furling action, the theoretical power of the wind turbine can be written from (4.5) as

$$P_{aero} = 0.5\rho A C_p(\lambda)(w\cos\theta)^3 \tag{4.6}$$

Equation (4.6) represents the power for varying wind speed of the wind turbine rotor without accounting for maximum power production. Maintaining a constant optimum TSR can ensure the maximum power production. It should be noted that the value of the optimum TSR varies from one turbine to another. An optimum TSR of 7 is considered for

the small wind turbine and thus (4.6) is expressed in terms of the optimum power coefficient as

$$P_{max} = 0.5R_w AC_{p,OPT}(\lambda)(w\cos\theta)^3 \tag{4.7}$$

where $C_{p,OPT}(\lambda)$ is the optimum value of power co-efficient at the optimum TSR.

The theoretical maximum power of the wind turbine described in (4.7) serves as the dynamic power reference for both systems and presented in Fig. 4.2a. For the turbine under investigation, the cut-in wind speed, w_C is 2 m/s and the rated rotational speed is reached at a rated wind speed, w_R of 13 m/s, while the cut-out wind speed, w_F is 17 m/s.

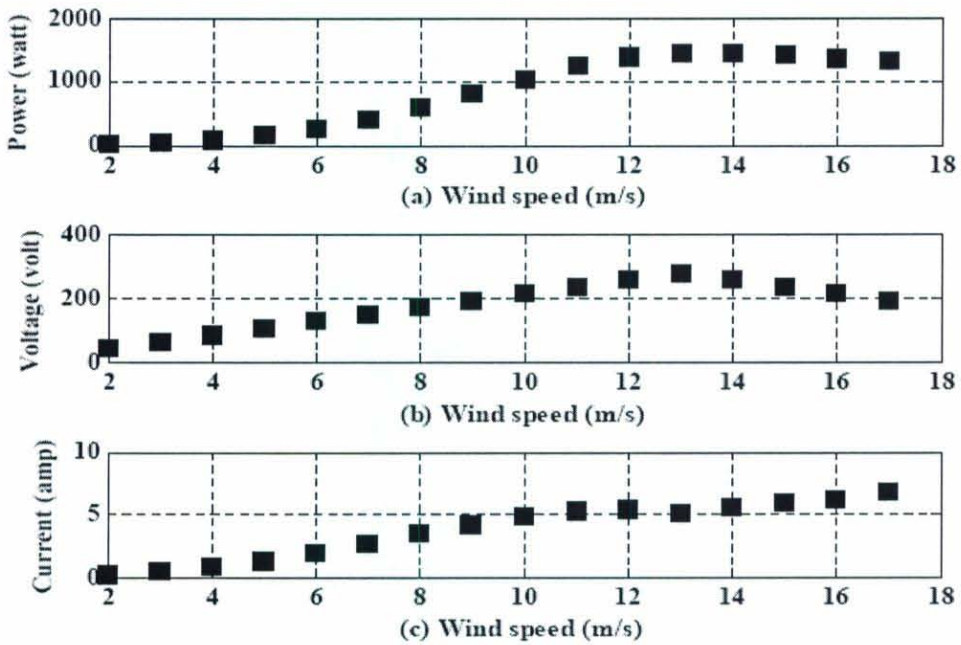

Fig. 4.2 Characteristics of the PMG-based system at the output of the rectifier a) Power, b) Voltage, c) Current

Since the PMG is connected to a diode rectifier, it is assumed that the output voltage of the rectifier is proportional to the rotational speed of the generator under unloded

condition. However, during the loaded condition the relation ship between PMG voltage and RPM remains more or less linear unless the voltage reaches to a saturation level. In this research, the variation of wind speed causes the PMG not to go enough to it's saturation level and assumed that it operates in the liner region. The voltage is assumed to be 40V at 2m/s wind speed and 280V at 13m/s wind speed as shown in Fig. 4.2b. The corresponding current curve at the rectifier output is shown in Fig. 4.2c. The drop in turbine speed and output voltage above 13m/s wind speed is due to the automatic furling of the wind turbine. The cubic nature of the effective wind velocity in (4.5) reaches maximum at 13 m/s and leading to a reduced output power.

4.2 Power Loss Calculation

In this section, the origins of the losses in the different components of the power conditioning system are explained. Here "components" refers to either a 3-phase bridge rectifier, or a boost converter or an inverter for the PMG-based system, and to either a 3-phase bridge rectifier, or a switch and an external resistance for the WRIG-based system. The losses for the power conditioning system are strongly dependent on the voltage and current waveforms of each semiconductor device. The analytical derivation of voltage and current equations of the individual semiconductor components is used to determine the losses [84, 85]. The following section describes the approach used to calculate the losses of the PCS for the PMG and WRIG-based system as presented in Chapter 2, section 2.3, Fig. 2.8 and Fig. 2.9 respectively.

4.2.1 Loss Calculation in a PMG-based System

In this section, the focus is on the loss calculation of the PMG-based system that varies with the wind speed. The losses for the power conditioning system are strongly

dependent on the voltage and current waveforms. Simplified analytical derivation of voltage and current equations associated with the individual semiconductor components are derived to determine the losses. The loss calculation presented in this investigation focuses on the loss originating during the conduction and switching states of the semiconductors.

4.2.1.1 Loss Calculation of the 3-phase Bridge Rectifier

For the 3-phase diode bridge rectifier, the losses are calculated for a single diode from the known voltage and current equations. It is assumed that the current and voltage in the 3-phase diode bridge rectifier are equally distributed in the diodes. Knowing the voltage and current for one diode, the losses can be obtained for all the diodes in the bridge rectifier. The losses are then added for all the diodes giving the losses for the bridge. The circuit diagram of the 3 phase bridge rectifier used during this calculation along with the commutation voltages and currents in shown is Fig. 4.3, which represents the part of the entire power conditioning system of the PMG-based system used in this research (Fig. 2.8).

The conduction losses of a diode can be calculated using the on-state characteristics for the diode. The electrical characteristic of a diode or IGBT, which is a function of device current, can be approximated as a linear function [86]

$$V_{for} = V_{thr} + r_{on} I_{on} \tag{4.8}$$

where V_{for} is the forward voltage drop of the diode or IGBT, V_{thr} represents the threshold voltage of the diode or IGBT, r_{on} and I_{on} are the on-state resistance and current respectively for the diode or IGBT. The electrical characteristic for a diode, V_f of the 3-phase bridge rectifier can be written as

$$V_f = V_{f0} + r_d I_{dc1} \tag{4.9}$$

where V_{f0} and r_d constitute the diode threshold voltage and resistance respectively.

The current at the output of the three phase rectifier is I_{dc} and the conduction current of the diode of the 3-phase bridge rectifier is represented as [87]:

$$I_{dc1} = \frac{1}{3} I_{dc} \tag{4.10}$$

The conduction losses, $P_{cd1,d}{}^{DB}$ for the diode can be expressed as

$$P_{cd1,d}{}^{DB} = V_f I_{dc1} \tag{4.11}$$

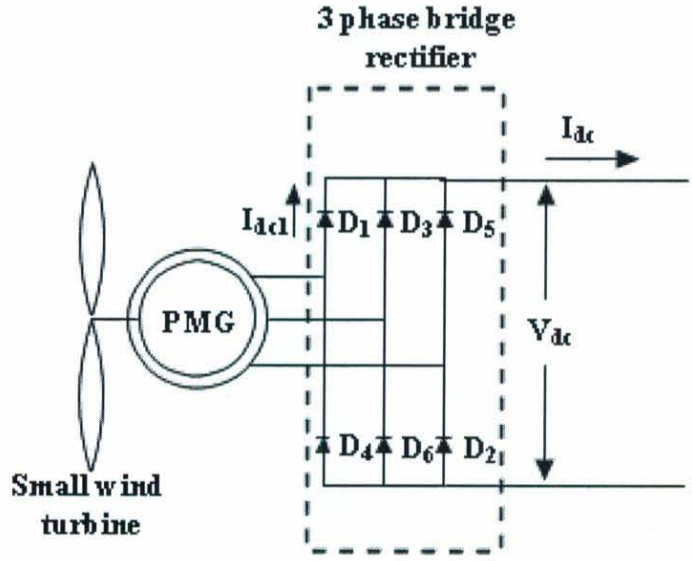

Fig. 4.3 3-phase diode bridge rectifier for a PMG-based system

The major switching losses of a pn-diode are primarily due to the turn-off losses since the turn-on losses are negligible in comparison with the turn-off ones [88]. The energy dissipation at turn-off is dependent on the charge stored in the depletion region and not lost due to internal recombination [89, 90]. During the reverse recovery, the current flows

in the reverse direction while the diode remains forward biased, and this results in a high instantaneous power loss in the diode. Under the assumption of a linear loss model for the diodes, the switching loss in each diode is given by [91].

$$P_{sw1,d}{}^{DB} = f_{WT} E_{SR} \cdot \frac{V_{dc}}{V_{ref,d}} \cdot \frac{I_{dc}}{I_{ref,d}} \tag{4.12}$$

where f_{WT} is the frequency of rotation of the wind turbine, E_{SR} signifies the rated switching loss energy given for the reference commutation voltage and current $V_{ref,d}$ and $I_{ref,d}$, while V_{dc} and I_{dc} indicate the actual commutation voltage and current respectively. The total losses of the 3-phase diode bridge rectifier, $P_{t,d}{}^{DB}$ for all 6 diodes is given by

$$P_{t,d}{}^{DB} = 6P_{cd1,d}{}^{DB} + 6P_{sw1,d}{}^{DB} = P_{cdt,d}{}^{DB} + P_{swt,DB}{}^{DB} \tag{4.13}$$

4.2.1.2 Loss Calculation of the Boost Converter

The conduction and switching loss of the Boost Converter (BC) is calculated by assuming an ideal inductor (L_D) at the boost converter input. For a boost configuration, the IGBT is turned on for the duration δ, while the diode (D) conducts for the duration $(1-\delta)$. The circuit diagram of the boost converter used during this calculation along with the commutation voltages and currents in shown in Fig. 4.4, which represents the part of the entire power conditioning system of the PMG-based system used in this research (Fig. 2.8). The on-state or commutation current of the IGBT is the input current I_{dc}, while the inverter input current I_{dc2} is given by

$$I_{dc2} = I_{dc}(1-\delta) \tag{4.14}$$

The forward voltage drop of the diode of the BC corresponding to the on-state current can be expressed as

$$V_{f1} = V_{f0} + r_d I_{dc} \tag{4.15}$$

In the similar way as for the diode, the linear electrical characteristic for an IGBT can be expressed as a function of the on-state current as

$$V_{ce} = V_{ce0} + r_{ce} I_{dc} \tag{4.16}$$

The value of the threshold voltage, V_{ce0} as well as the on-state resistance, r_{ce} can be found in the data sheet provided by the manufacturer for any specific IGBT.

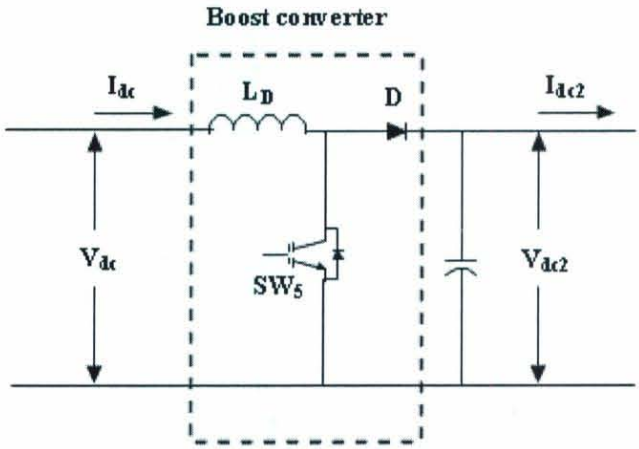

Fig. 4.4 Boost converter for a PMG-based system

The conduction loss for the diode and IGBT can be obtained by multiplying their on-state voltage and current with the respective duty cycle and is given by

$$P_{cd,d}{}^{BC} = I_{dc}\left(V_{f0} + r_d I_{dc}\right).(1-\delta) \tag{4.17}$$

$$P_{cd,IGBT}{}^{BC} = I_{dc}\left(V_{ce0} + r_{ce} I_{dc}\right).\delta \tag{4.18}$$

The actual commutation voltage and current for the boost converter are the DC link voltage, V_{dc2} and input current to the converter, I_{dc1} while, the reference commutation voltage and current for the diode and IGBT is $V_{ref,d}$, $I_{ref,d}$ and $V_{ref,IGBT}$, $I_{ref,IGBT}$ respectively.

E_{ON} and E_{OFF} signify the turn-on and turn-off energies of the IGBT as can be found in the datasheet. The switching loss for a specific switching frequency, f_{SW} of the diode and IGBT in the BC are given by

$$P_{sw,d}{}^{BC} = f_{sw} E_{SR} \cdot \frac{V_{dc2}}{V_{ref,d}} \cdot \frac{I_{dc}}{I_{ref,d}} \tag{4.19}$$

$$P_{sw,IGBT}{}^{BC} = f_{sw} \left(E_{ON} + E_{OFF}\right) \cdot \frac{V_{dc2}}{V_{ref,IGBT}} \cdot \frac{I_{dc}}{I_{ref,IGBT}} \tag{4.20}$$

The sum of (4.17) to (4.20) gives the losses of the BC as

$$P_{t,(d+IGBT)}{}^{BC} = \left(P_{cd,d}{}^{BC} + P_{sw,d}{}^{BC}\right) + \left(P_{cd,IGBT}{}^{BC} + P_{sw,IGBT}{}^{BC}\right) \tag{4.21}$$

4.2.1.3 Loss Calculation of the Inverter

Most of the small wind turbine systems integrate a single phase inverter for commercial as well as residential application. With the exclusion of the snubber circuit, the single ph-

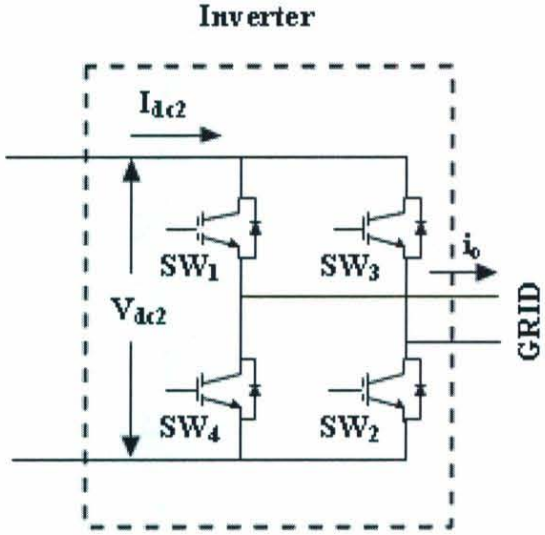

Fig. 4.5 Inverter for a PMG-based system

-ase inverter consists of 4 switches and 4 anti-parallel diodes as presented in Fig. 4.5. It should be noted that when the inverter is operated in the linear region (i.e., not including

the over modulation region), the switching losses have no dependency on the modulation index and power factor. However, the modulation index greatly dominates the conduction losses in contrast to the switching losses of the inverter. In addition, the method of modulation has also a great significance on the conduction losses. Several analyses for calculation of the conduction losses depending on the modulation function have been presented [92, 93, 94]. The modulating function for the inverter considered in this research is pure sinusoidal and can be described by

$$F(\alpha+\varphi)=\sin(\alpha+\varphi) \tag{4.22}$$

where α is the current angle and φ is the angle between current and voltage.

The conduction losses of a diode and IGBT for the inverter can be expressed respectively as [84]

$$P_{cd1,d}{}^{INV}=\left(\frac{1}{8}-\frac{M}{3\pi}\cos\varphi\right)r_d I_{om}{}^2+\left(\frac{1}{2\pi}-\frac{M}{8}\cos\varphi\right)V_{f0}I_{om} \tag{4.23}$$

$$P_{cd1,IGBT}{}^{INV}=\left(\frac{1}{8}+\frac{M}{3\pi}\cos\varphi\right)r_{ce}I_{om}{}^2+\left(\frac{1}{2\pi}+\frac{M}{8}\cos\varphi\right)V_{ce0}I_{om} \tag{4.24}$$

where M the modulation index $(0\le M\le 1)$ and I_{om} is the maximum amplitude of the output current of the inverter.

An approximated, closed solution for the IGBT switching losses at a phase leg output current i_o is given by [85]

$$P_{sw1,IGBT}{}^{INV}=\frac{1}{\pi}f_{sw}\left[E_{ON}+E_{OFF}\right]\frac{V_{dc2}}{V_{ref,IGBT}}\frac{I_{om}}{I_{ref,IGBT}} \tag{4.25}$$

Similarly, with the assumption that on-state losses of the diode are negligible, the diode switching loss of the inverter can be found as [95]

$$P_{sw1,d}^{INV} = \frac{1}{\pi} f_{sw} E_{SR} \frac{V_{dc2}}{V_{ref,d}} \frac{I_{om}}{I_{ref,d}} \tag{4.26}$$

The loss of a single phase inverter is obtained as the sum of (4.23) to (4.26) and expressed by (4.27), while the total loss for the PCS of the PMG-based system is expressed by (4.28).

$$P_{t,(d+IGBT)}^{INV} = P_{cd,d}^{INV} + P_{cd,IGBT}^{INV} + P_{sw,d}^{INV} + P_{sw,IGBT}^{INV} \tag{4.27}$$

where $P_{cd,d}^{INV} = 4P_{cd1,d}^{INV}$ and $P_{cd,IGBT}^{INV} = 4P_{cd1,IGBT}^{INV}$ and

$P_{sw,d}^{INV} = 4P_{sw1,IGBT}^{INV}$ and $P_{sw,IGBT}^{INV} = 4P_{sw1,IGBT}^{INV}$

$$P_t^{PMG} = P_{t,d}^{DB} + P_{t,(d+IGBT)}^{BC} + P_{t,(d+IGBT)}^{INV} \tag{4.28}$$

4.2.2 Loss Calculation in a WRIG-based System

In a WRIG, a variable resistance in the rotor circuit effectively controls the rotor current as well as the speed of the wind turbine as has been discussed in Chapter 2. The actual circuit of a 3-phase WRIG in conjunction with the diode rectifier and switch is shown in Fig. 4.6. If the rotor leakage reactance are neglected compared to inductor L_D, the equivalent circuit of Fig. 4.7 is obtained. In the figure, r_1 and x_1 are the stator resistance and reactance respectively; r_2 and x_2 are the rotor leakage resistance and reactance respectively; I_1, I_2 is the stator and rotor current; R_e, R and d represent the effective rotor resistance, actual rotor resistance and duty cycle respectively. The stator voltage V_1, referred to the rotor circuit, results in a slip frequency voltage, sE_2 given as

$$\left(s.V_1.N_2\right)/N_1 = s.a.V_1 = sE_2 \tag{4.29}$$

where s is the slip, N_1 and N_2 are the number of turns of the stator and rotor windings respectively and a represents the turn ratio of rotor to stator turn.

The output voltage of the rectifier can be expressed as [96]

$$V_{DC} = \left(3\sqrt{6}s.a.V_2\right)/\pi \tag{4.30}$$

The voltage V_2 can be expressed as

$$V_2 = \left(s.a.V_1 - I_2 r_2\right) \tag{4.31}$$

The total slip power is given by

$$P_{t,slip} = sP_s \tag{4.32}$$

where P_s is the power delivered by the stator of the generator and represents the maximum power, P_{max} of the wind turbine.

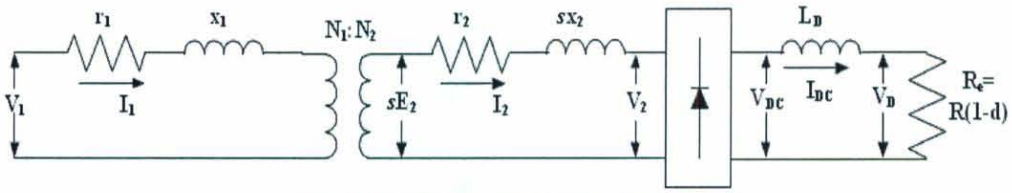

Fig. 4.6 Equivalent circuit of a WRIG

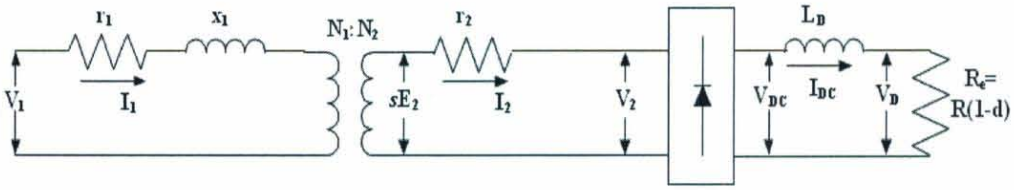

Fig. 4.7 Approximate equivalent circuit of a WRIG

The losses in the external rotor resistance and switch are given by

$$P_{l,ex}{}^{R} = V_{DC} I_{DC} \tag{4.33}$$

where V_{DC} and I_{DC} are the rectified output voltage and current at the rotor respectively.

The sum of the losses in the rotor resistance, rectifier, external rotor resistance and switch is equal to the slip power entering the rotor. Equating the losses to the slip power and assuming that $r_{d1} << R$, results in

$$I_{DC} = \frac{sP_S - 3I_2^2 r_2}{\left[2V_f + \frac{6f_{WT}E_{SR}V_{DC}}{V_{ref1}I_{ref1}} + V_{DC}\right]} \tag{4.34}$$

The total of the losses of the 3-phase diode bridge rectifier for the WRIG-based system is the sum of conduction and switching losses and is given by

$$P_{l,rec}{}^{DB} = P_{cd2,d}{}^{DB} + P_{sw2,d}{}^{DB} = 2V_f I_{DC} + \frac{6f_{WT}E_{SR}V_{DC}I_{DC}}{V_{ref1}I_{ref1}} \tag{4.35}$$

The construction of the rotor in case of a phase wound rotor induction generator has a 3-phase double layer distributed winding made up of coils, similar to that of an alternator. Typically, the rotor winding is star connected and is wound to the number of stator poles. The terminals are brought out and connected to three slip rings mounted on the rotor shaft with the brushes resting on the slip rings. The brushes are externally connected to the rotor resistances to modify the torque - speed torque characteristics. A schematic of the WRIG including slip ring is presented in Fig. 4.8.

The losses in the slip ring consist of electrical and friction losses. The electrical losses are the sum of the resistive losses in the brushes and slip ring and the losses from the contact voltage drop between the slip ring and the brush. The friction losses are dependent on various factors, such as the area of the brush, number of brushes, friction coefficient, spring force and the speed of the slip ring. In addition, the electrical and friction losses are also dependent on the brush material. The electrical and friction losses due to the

rotation of the rotor are given by (4.36) and (4.37) respectively, while the total loss of the slip ring is expressed by (4.38)[97]:

$$P_{l,elec}^{SR} = K_{\omega}\omega \tag{4.36}$$

$$P_{l,fric}^{SR} = K_{\delta}\omega \tag{4.37}$$

$$P_{l,sring}^{SR} = P_{l,elec}^{SR} + P_{l,fric}^{SR} \tag{4.38}$$

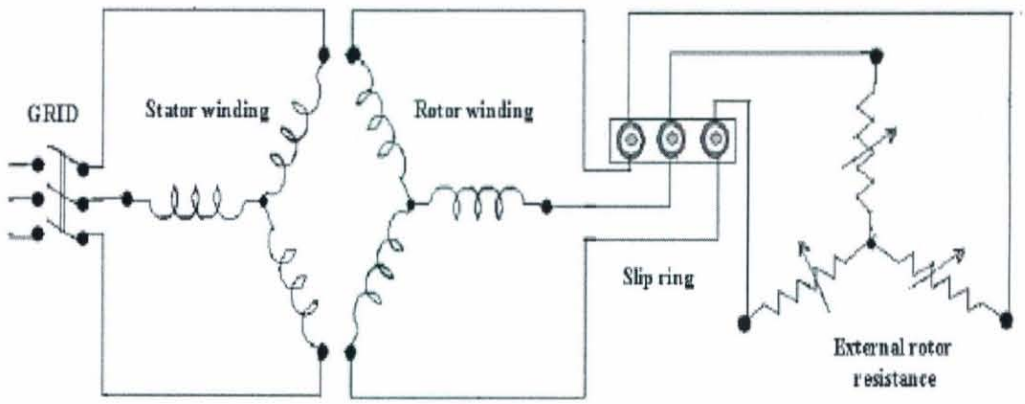

Fig. 4.8 A schematic of the WRIG including slip ring

where K_{ω} and K_{δ} are constants that depend on the contact voltage drop and friction coefficient respectively. Thus the total losses of the WRIG can be expressed as

$$P_t^{WRIG} = P_{l,rec}^{DB} + P_{l,ex}^{R} + P_{l,sring}^{SR} \tag{4.39}$$

4.3 Performance Characteristic Calculation of the Systems

After the simulation of maximum power and power losses for each wind speed has been explained, the next step is to calculate the performance characteristic namely, efficiency. The efficiency is of importance because in order to deploy any wind energy conversion system. It is necessary to recognize the characteristic for best fit in terms of installment

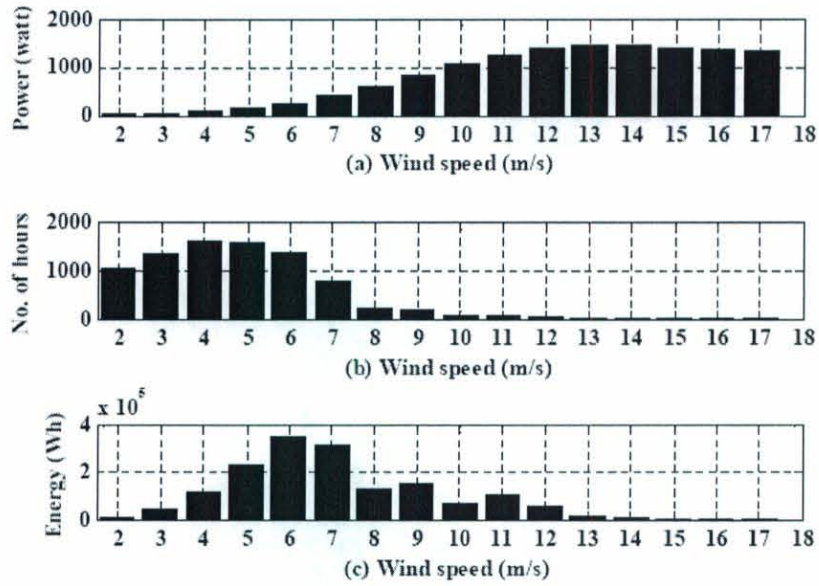

Fig. 4.9 Calculation of the annual energy capture a) Maximum Power, b) Wind speed distribution, c) Energy Capture (Example, PMG or WRIG-based system, St. John's)

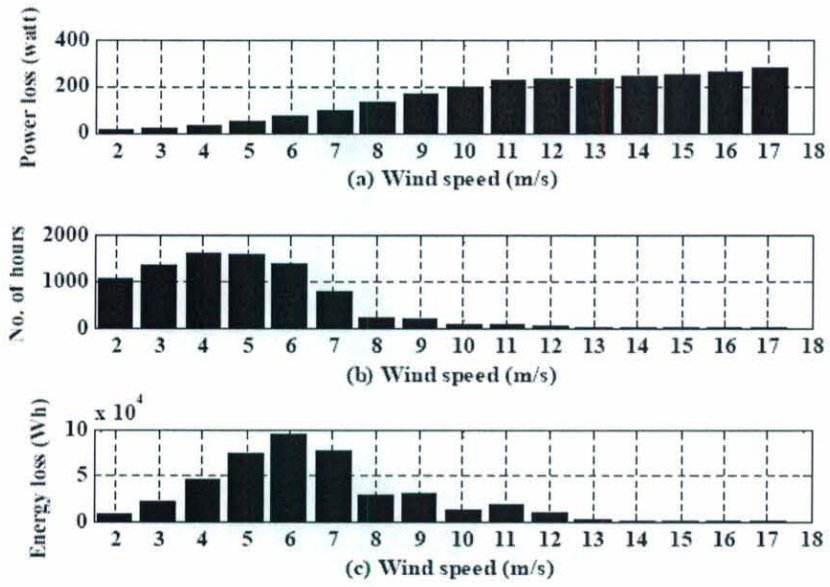

Fig. 4.10 Calculation of the annual energy capture a) Maximum power loss, b) Wind speed distribution, c) Energy loss (Example, PMG-based system, St. John's)

cost, economies of various sizes and brands of wind turbines as well as power conditioning systems. The problem becomes more difficult when the wind energy conversion system is small as high cost/kWh of a system could lead a potential discouragement on deploying a particular system. Indeed, efficiency is not the only factor that should be considered but it affects the feasibility of the installment of a wind energy conversion system. Nevertheless, efficiency has a great dominant effect for penetration of a specific system. In view of this, a procedure to calculate the efficiency of the systems is required and performed as described below:

After all the simulation was done for the systems, the output power and power losses are known for discrete wind speeds. This relation generates the power curve and power loss curve and is plotted in the Fig. 4.9a and Fig. 4.10a respectively.

In order to calculate the Annual Energy Capture (AEC) and Annual Energy Loss (AEL) from the power and power loss curves, the relation between the wind speed over a time interval of one year during which this wind speed occurs is needed. There are two approaches to reproduce this characteristic. Firstly, employ an ideal distribution, which approximates the real wind distribution for a region in a year, and secondly, use yearly real wind information for a region in consideration. This research considered the second approach as the efficiency for any wind energy conversion systems can be calculated more precisely than the first approach, which employs an ideal wind speed distribution. In the second approach, as soon as the real wind information is available, considering a bin of 1m/s, the time in one year interval during which the wind speed lies within the wind speed band is then found (Fig. 4.9b and Fig. 4.10b). Once the wind speed distribution and thus the power curve (power loss curve) is plotted for discrete wind

speed, the energy capture (energy loss) by a particular wind speed is known by a multiplication of the wind speed distribution (No. of hours in a year) curve and power curve (power loss curve) on a bin by bin basis as presented by Fig. 4.9c (Fig. 4.10c) and can be expressed as

$$E_{g,i}(w_i) = P_{g,i}(w_i) f_{dis}(w_i) \tag{4.40}$$

where $E_{g,i}(w_i)$ is the energy capture for a wind speed of i m/s, $P_{g,i}(w_i)$ is the maximum power for a wind speed of i m/s, $f_{dis}(w_i)$ is the number of hours for the wind speed of i m/s, and i signifies any wind speed between cut-in to cut-out.

The energy loss for the wind speed of i m/s, $E_{l,i}(w_i)$ can be found by replacing $P_{g,i}(w_i)$ of (4.40) with $P_{t,i}^{PMG}$ and $P_{t,i}^{WRIG}$ using (4.28) and (4.39) for the PMG and WRIG-based system respectively.

Finally, the annual energy capture and annual energy loss in the one year time interval found by summing up all the bars in the lower diagram in Fig. 4.9 and Fig. 4.10 respectively, which can be expressed mathematically by (4.41) and (4.42) respectively.

$$E_g = \sum_{i=cut-in}^{cut-out} E_{g,i}(w_i) \tag{4.41}$$

$$E_l = \sum_{i=cut-in}^{cut-out} E_{l,i}(w_i) \tag{4.42}$$

The efficiency of the systems is then calculated as,

$$\eta = \frac{E_g - E_l}{E_g} \times 100\% \tag{4.43}$$

It can be seen that the efficiency of the wind energy conversion system is greatly dominated by the wind speed distribution. As stated earlier, efficiency is a dictating factor for potential investors and is meaningful for evaluating turbine performance.

4.4 Simulation Results

The analytical expressions described in the preceding sections were numerically simulated to determine the total power losses of the power conditioning systems for the PMG and WRIG-based systems under varying wind speed condition. The rated power for the wind turbine is assumed to be 1.5 kW with a rated wind speed of 13 m/s. A wind speed variation of 2 m/s to 17 m/s was considered, which represents the cut-in and cut-out wind speed respectively. Furthermore, in order to differentiate between the low and high wind speed regime, a wind speed up to 8 m/s is considered as a band between the low and high wind regime. It should be noted that a wind speed above 8 m/s can be considered as a high wind situation as found by the previous research [49, 50]. The way the results are plotted is as follows: Firstly, the simulation results are presented for both systems then the performances characteristic is presented. Afterwards the performance characteristic is compared based on the wind speed distribution for eight different sites of Newfoundland and Labrador, Canada.

4.4.1 Power Loss in the Systems

The grid connected PMG and WRIG-based small wind turbine system numerical simulation results found from the power loss calculations are presented in this section. For the numerical simulation the data sheet on the EUPEC IGBT-module of FP15R12W1T4_B3 was selected as the source for the necessary data for the PMG and WRIG-based system and the parameter values are provided in the Appendix B [98]. Each

leg of the module consists of two IGBTs connected in series and an inverse diode beside each IGBT. During calculation of the losses, it is assumed that the heat sink is adequate to maintain the semiconductors at proper working temperature. Power wasted in the power supplies of the inverter and boost converter control circuits is also ignored as it could vary between 10W to 15W, however, due to the inclusion of less control circuitry with the WRIG-based system, as a rule of thumb, control circuitry losses will be less in the WRIG-based system than the PMG-based system.

4.4.1.1 Power Loss of the PMG-based System

In order to investigate the worst-case scenario of the power loss in this numerical simulation study, the modulation index is assumed to be unity and the load current is assumed to be in phase with the output voltage. The inverter switching frequency is considered as 20 kHz. It is also assumed that the inverter operates in the linear modulation region.

The conduction and switching losses in the 3-phase diode bridge rectifier of the PMG-based system are presented in Fig. 4.11a followed by the losses in the IGBT and diode of the boost converter in Fig. 4.11b as a function of wind speed. Fig. 4.11c shows the conduction and switching losses of the IGBT and anti parallel diodes of the inverter for a similar wind variation. The total losses in the power conditioning system in the PMG-based system are presented in Fig. 4.11d from cut-in to cut-out wind speed variation. It is understood that as soon as the wind speed starts to increase, the operating state of the PCS starts to shift from low to high voltage and current level and increase the power losses of each component. The results of the conduction and switching losses for the PMG-based system show that the power loss is higher for a wind speed of 12m/s than for

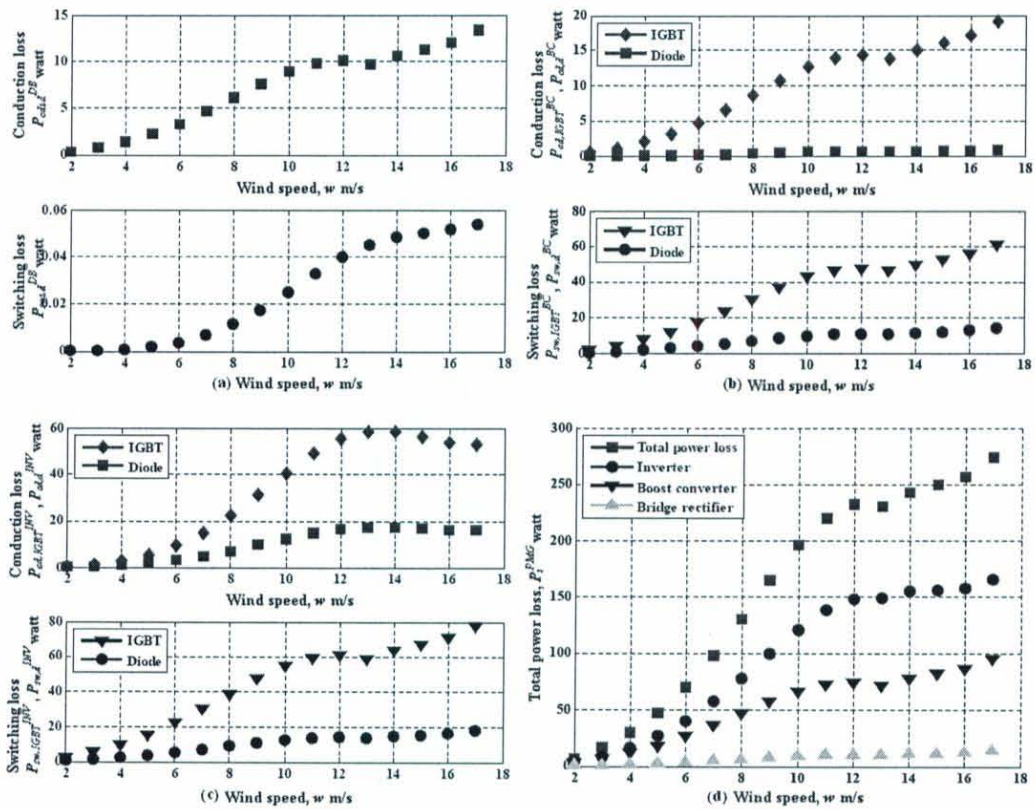

Fig. 4.11 Variation of the power losses for the PMG-based system a) Conduction and switching losses for the rectifier, b) Conduction and switching losses for the IGBT and diode of the Boost Converter, c) Conduction and switching losses for the IGBT and diode of the inverter, d) Total power losses of the PCS

the rated wind speed of 13 m/s and is due to the furling action. The furling angle varies abruptly as wind speed increases from 9 m/s to 13 m/s with a negligible change close to the maximum speed. Meanwhile, the voltage remains linear from cut in to rated and from rated to cut-out wind speed. As a result, the captured aerodynamic power as well as the current is asymmetrical on either side of the rated wind speed.

The individual efficiency of the components as well as the efficiency of the PCS is presented in Fig. 4.12a. It is evident that the inverter efficiency has the lowest value due

to the high losses, while the rectifier has the highest efficiency and the efficiency of the boost converter is in between the inverter and rectifier. The PCS efficiency is also plotted and as expected, efficiency is lower than any other components of the PCS and significantly drops at light load condition. It is observable that inclusion of more power electronic stages into the PCS will lower the efficiency of a wind energy conversion

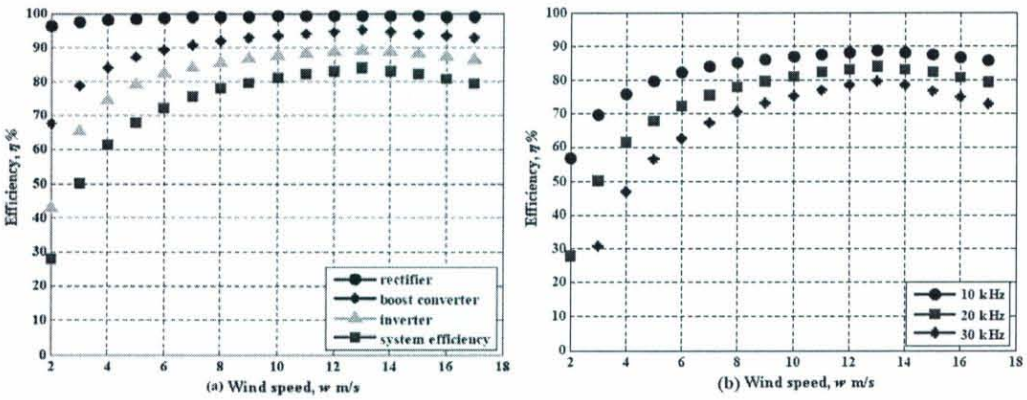

Fig. 4.12 a) Variation of efficiency for the PMG-based system a) Rectifier, Boost Converter, Inverter and the PCS b) Total PCS with the change in switching frequency

system and consequently will decrease the efficiency as well as increase the cost of a system. However, the efficiency can be increased by decreasing the switching frequency of the PCS and can be observed in Fig. 4.12b, which represents the variation of efficiency with switching frequency. Though, it should be considered that for a low switching frequency, the ripple in the current is substantial, and there could be a considerable difference in turn-on and turn-off losses. On the other hand, the switching losses usually dominate the converter losses at high frequency. Therefore, a tradeoff should be made between the switching frequency and desired performance of the system. It is clearly seen from the figure that at a lower switching frequency of 10 kHz, the efficiency of the PCS

remains more than 87%, while 30 kHz provides an efficiency of the PCS of less than 80%. The efficiency of the PCS is about 84% at a switching frequency of 20 kHz, which is a typical switching frequency value of such PCS operation. Moreover, 84%@20kHz is not an under ambitious value as several other PCS also exhibit almost the same value [45, 99-103]. It should be noted that usually the manufacturers assert the efficiency is more than 90% for most of the PCS. As an example, the manufacturer of the GridTek Inverter asserts an efficiency of 92% in the specification sheet [103], while the actual efficiency was found by the National Renewable Energy Laboratory (NREL) laboratory to be 87% or lower [99, 100]. This discrepancy occurs because manufacturers usually do not disclose the operating condition during testing as well as the way the testing is performed. As a consequence, the expected behavior does not coincide with the actual behavior of a system. Such inconsistency may increase the large penetration of a particular system which might not have occurred if the actual behavior is noticed initially.

4.4.1.2 Power Loss of the WRIG-based System

The WRIG-based system was subjected to the same conditions as the PMG-based system. The switching frequency of the switch is considered as 20 kHz. It is worthwhile to mention that the change of wind speed will change the slip of the WRIG-based system and calculation should be proceeding based on the respective slip values. Higher values of slip result in high power losses and vice versa, while a low variation of slip resembles almost constant speed system. The conduction and switching losses for varying wind speed of the 3-phase bridge rectifier in the rotor circuit of WRIG are presented in Fig. 4.13a. A WRIG-based system suffers from the dilemma of power loss in the external rotor resistance. The power loss for the external rotor resistance and switch is presented

in Fig. 4.13b for a variation in the wind speed. The electrical, frictional and total losses of a slip ring results are presented with the variation of wind speed in Fig. 4.13c. The electrical and frictional loss in a slip ring is strongly dependent on the speed of rotation of the WRIG. The variation in total power losses in the PCS for the WRIG-based system is presented in Fig. 4.13d. The decrease in power loss after 13m/s is because of the lower

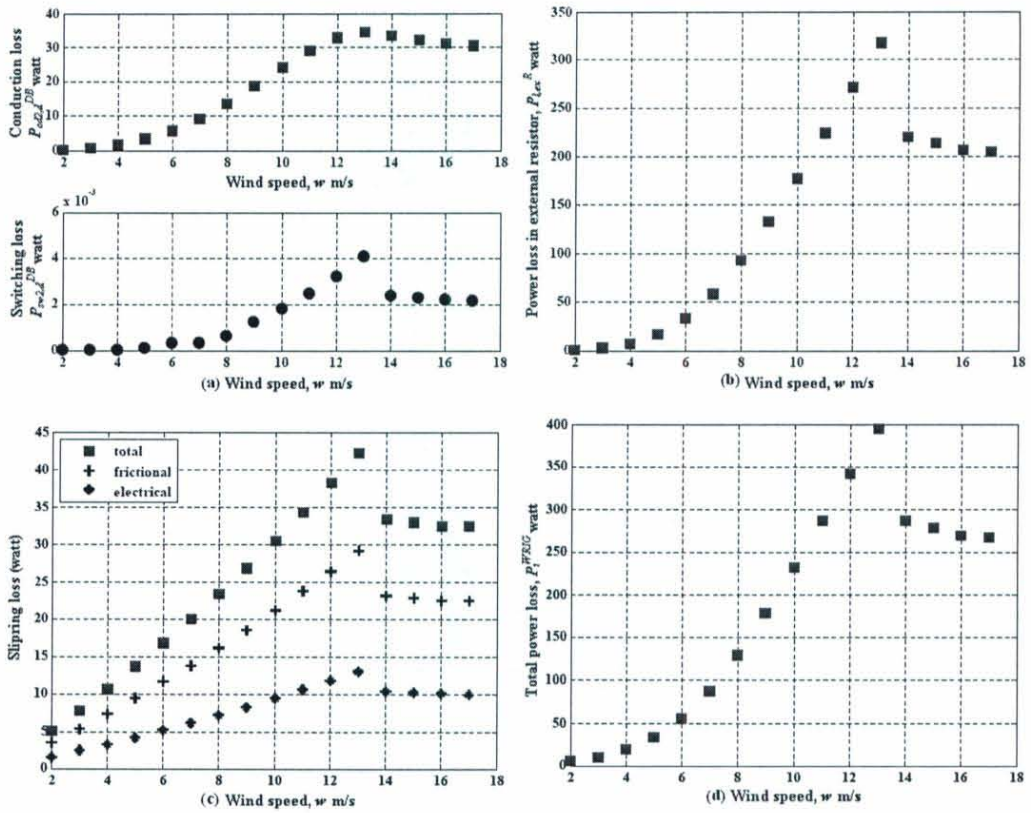

Fig. 4.13 Variation of the power losses for the WRIG-based system a) Conduction and switching losses for the rectifier, b) External rotor resistance losses, c) Electrical, frictional and total losses of the slip ring, d) Total power losses of the PCS

tip-speed-ratio of the wind turbine at higher wind speed region. It is well understood that typically a small wind turbine system operates at low wind speeds most of the time during a year [53-55]. Thus in order to achieve economic feasibility, it is extremely

important to investigate the influence of losses at low wind speed regime. Generally rated power of a wind turbine system is considered before deployment of a wind energy conversion system even though mostly the wind turbine operates at a fraction of the rated power. As a result, low power losses at low wind speed regime are an important aspect from a system for high penetration of wind power to the community. However, interesting enough, from the simulation results of total losses for both system, losses at low wind speed regime is higher for the PMG-based system than the WRIG-based system. Moreover, it is proved from the previous simulation results that the efficiency of the power conditioning system for the PMG-based system falls off rapidly at low wind speed regime. This behavior can significantly increase the power loss of the PMG-based system and consequently, lower the performance of the system. In contrast to the PMG-based system, the WRIG-based system could provide less power loss at low wind speed situation and thus, could increase the efficiency of the system. As a whole, the WRIG-based system appears to be a better option than the PMG-based system in terms of power losses and circuit complexity in the low wind regime.

4.4.2 Performance Characteristic of the Systems

Efficiency is an important criterion for any wind energy conversion system and one of the major concerns of this research. In this section the efficiency of the grid connected PMG and WRIG-based small wind turbine systems are compared. This is achieved for eight regions, i.e., Battle Harbour (BH), Cartwright (CW), Little Bay Island (LB), Mary's Harbour (MH), Nain (NA), Ramea (RA), St. Brendan's (SB) and St. John's (SJ) of Newfoundland and Labrador, Canada. The hourly average wind information of the regions is presented in Fig. 4.14 and Fig. 4.15. The power curve and power loss curve

from cut-in to cut-out wind speed is found from the aforementioned section. Once these curves and wind distribution are known, the energy capture and energy loss for both systems can be calculated as described in section 4.3. The results of the calculation are presented by Fig. 4.16 to Fig. 4.17. It is clearly visible that for all the regions energy loss remains higher for the PMG-based system especially at the low wind regime. Although

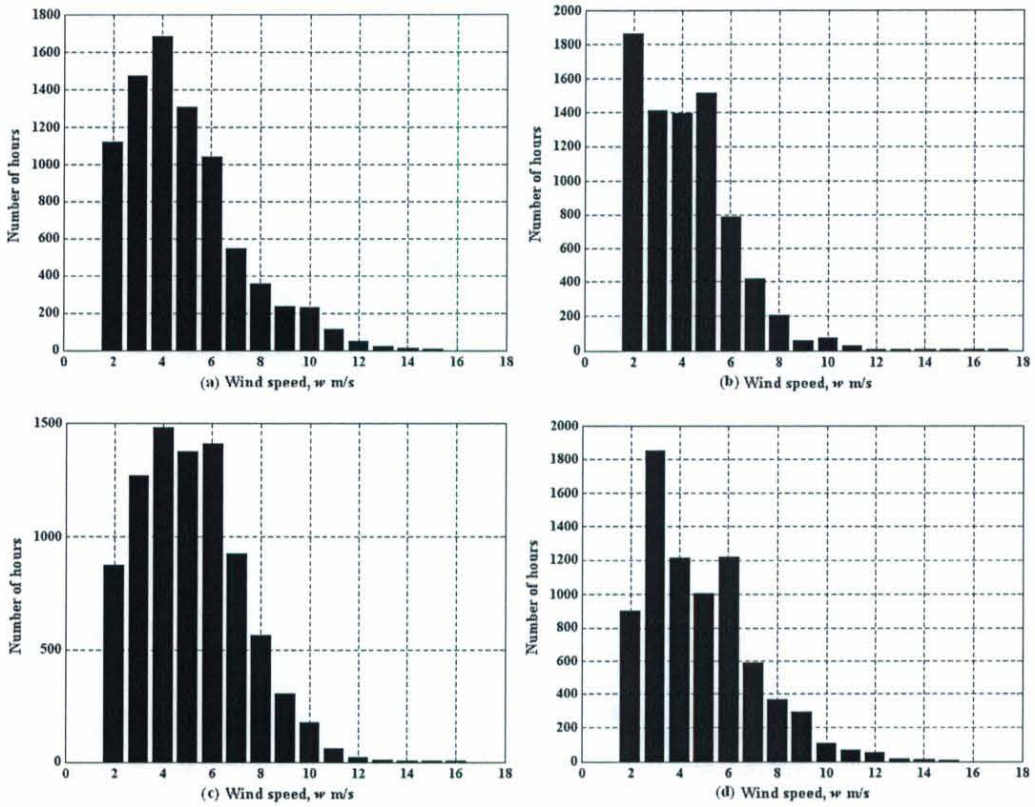

Fig. 4.14 Wind speed distribution for a) Battle Harbour (BH), b) Cartwright (CW), c) Little Bay Island (LB), d) Mary's Harbour (MH)

due to the increase of slip at high wind speed, higher losses observed at high wind speed for the WRIG-based system, which consequently increases the energy loss of the system.

due to the increase of slip at high wind speed, higher losses observed at high wind speed However, the high energy loss at high wind speed will not decrease the performance of the WRIG-based system because of the high frequency of occurrence of the low wind speed will produce high losses and consequently, total losses will be more in the PMG-based system compared to the WRIG-based system. Finally, the annual energy capture is calculated for the considered regions and is presented in Fig. 4.18a, while the annual

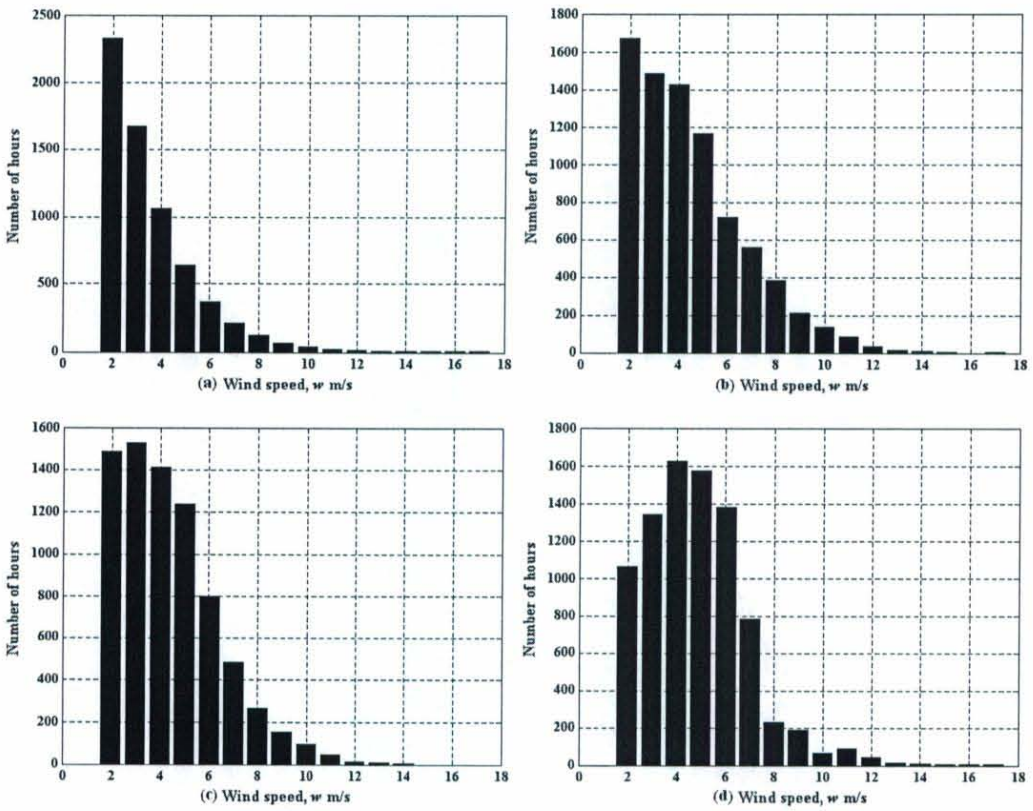

Fig. 4.15 Wind speed distribution for a) Nain (NA), b) Ramea (RA), c) St. Brendan's (SB), d) St. John's (SJ)

energy loss for the respective regions of both systems is presented in Fig. 4.18b. The annual energy loss figure clearly demonstrates that high losses at high wind speed for the WRIG-based system is not a significant disadvantage of the system. The corresponding efficiency based on the annual energy capture and annual energy loss for each region is presented in Fig. 4.19 for both systems. The comparison shows that the WRIG-based system is more efficient than the PMG-based system with an increase in efficiency of about 2%. Even though the absolute difference is not a significant amount, the relative consequences are much more important. A short example will make this clear: If one has

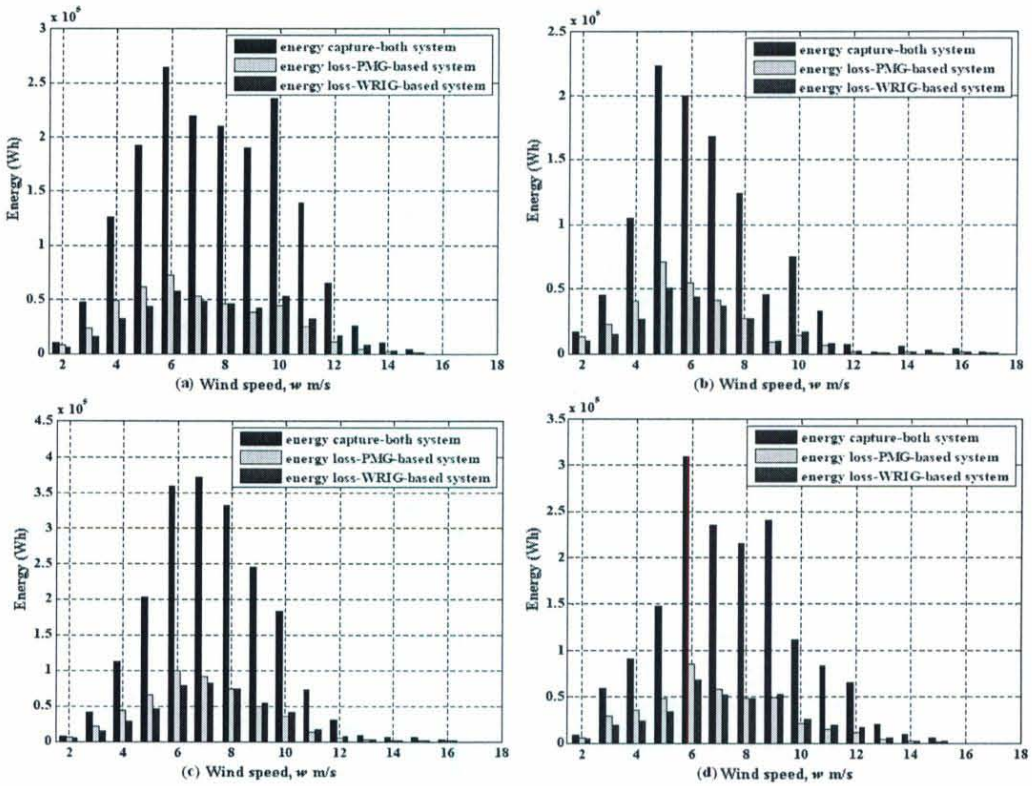

Fig. 4.16 Energy capture and energy loss from cut-in to cut-out wind speed for a) Battle Harbour (BH), b) Cartwright, c) Little Bay Island (LB), d) Mary's Harbour (MH)

the choice between a wind energy conversion system "X" and another wind energy conversion system "Y" which is 2% more efficient (or, which is the same but less complex in maintaining and complexity) than "X", then wind energy conversion system "Y" will be more preferable at a particular region than "X". Otherwise "X" will be preferable. In view of this, even if the WRIG-based system is not that much more efficient than the PMG-based system, it would be an optimum preference when anyone has a choice between the PMG and WRIG-based system. Moreover, the PCS of the WRIG-based system composed of fewer components than the PMG-based system. This is certainly advantageous as less complexity in PCS architecture of the WRIG-based system

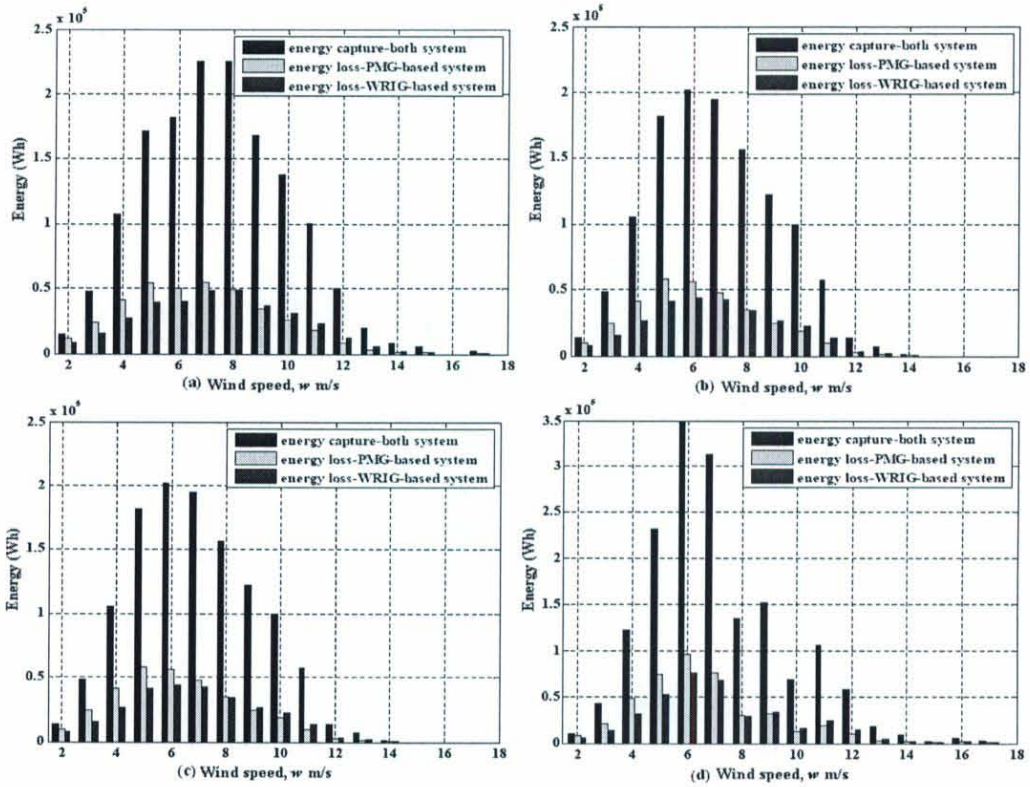

Fig. 4.17 Energy capture and energy loss from cut-in to cut-out wind speed for a) Nain (NA), b) Ramea (RA), c) St. Brendan's (SB), d) St. John's (SJ)

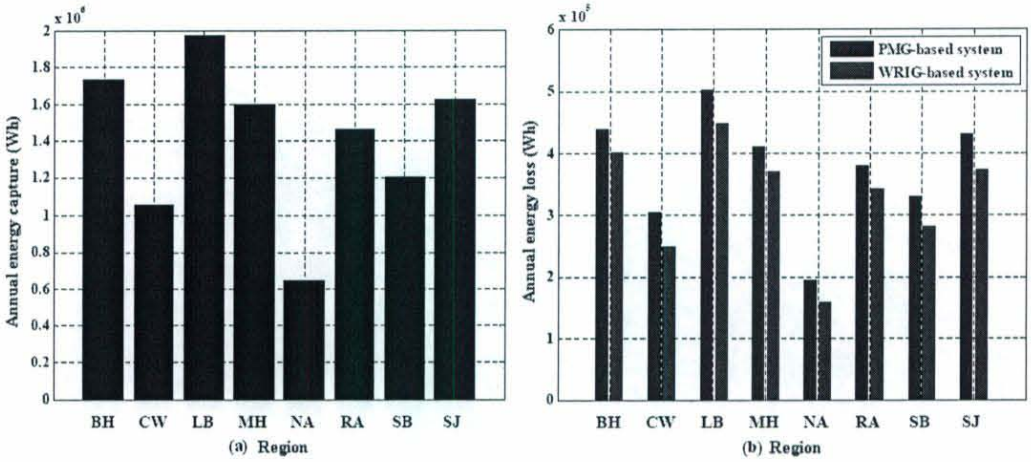

Fig. 4.18 a) Annual energy capture for the systems, b) Annual energy loss for the systems

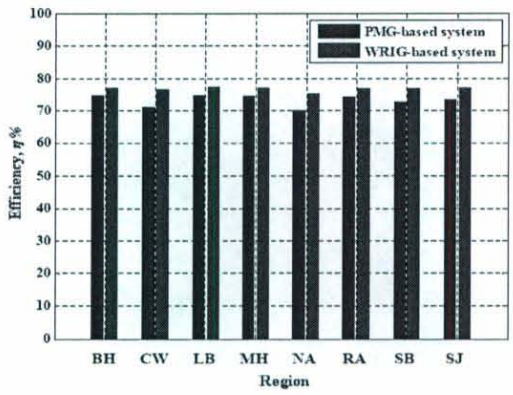

Fig. 4.19 Variation of efficiency of the systems

is possible than the PMG-based system. So it can be concluded that focus should be paid on the low wind speed situation for a small wind energy conversion system and in such situation, a higher efficiency is possible to achieve from a WRIG-based system than a PMG-based system. As a whole, a WRIG-based system appears to be a better option than a PMG-based system in terms of power losses, annual energy loss and efficiency.

4.5 Summary

This chapter provides details of loss calculation and system analysis. The proposed analysis in this chapter reveals several important observations which make a significant contribution to the field of wind energy. Synopses of the observations are presented below:

- The requirement for high efficiency at low wind speed is a unique challenge to the small wind power industry and off-the-shelf converters are unable to satisfy the requirement. The proposed analysis therefore suggests from the point of view of efficiency that a PMG-based system is not the best system for small grid connected installations;
- Detailed analysis reveals that the power losses of a WRIG-based system for low wind speed are lower than that for a PMG-based system;
- The annual energy loss is lower, while the efficiency is higher for a WRIG-based system than a PMG-based system. Therefore, a WRIG-based system is the preferred option for small grid connected wind installations.

Chapter 5

Testing the Grid Connected Small Wind Turbine Systems

In chapter 2, the Power Conditioning Systems (PCS) were studied and in chapter 4, the power losses, Annual Energy Capture (AEC), Annual Energy Loss (AEL), and finally efficiency were calculated for the application in grid connected small wind turbine systems. It was found that the Wound Rotor Induction Generator (WRIG)-based system is a more appropriate choice than the Permanent Magnet Generator (PMG)-based system for a small grid connected application due to lower power losses and lower AEL, which subsequently result in higher efficiency. In order to verify the conclusions from the numerical simulations of the power losses, AEC, AEL and efficiency, experimental test benches of the systems using a Wind Turbine Emulator (WTE) were constructed and detailed tests were carried out over a period of almost a year. Details of the design and test results are provided in this chapter.

First, since the systems are based on the same wind turbine, a WTE is developed in the laboratory. Then the development of the systems with required PCS is described along with their control strategy. Afterwards, a procedure to calculate the power loss is described. Finally, the experimental results and relevant findings are presented and discussed.

5.1 Description of the Test Bench

The majority of the comparison analysis results presented in the literature are obtained by theoretical investigations that were carried out by means of numerical simulation. It is well understood that simulation provides preliminary analysis and prediction of any

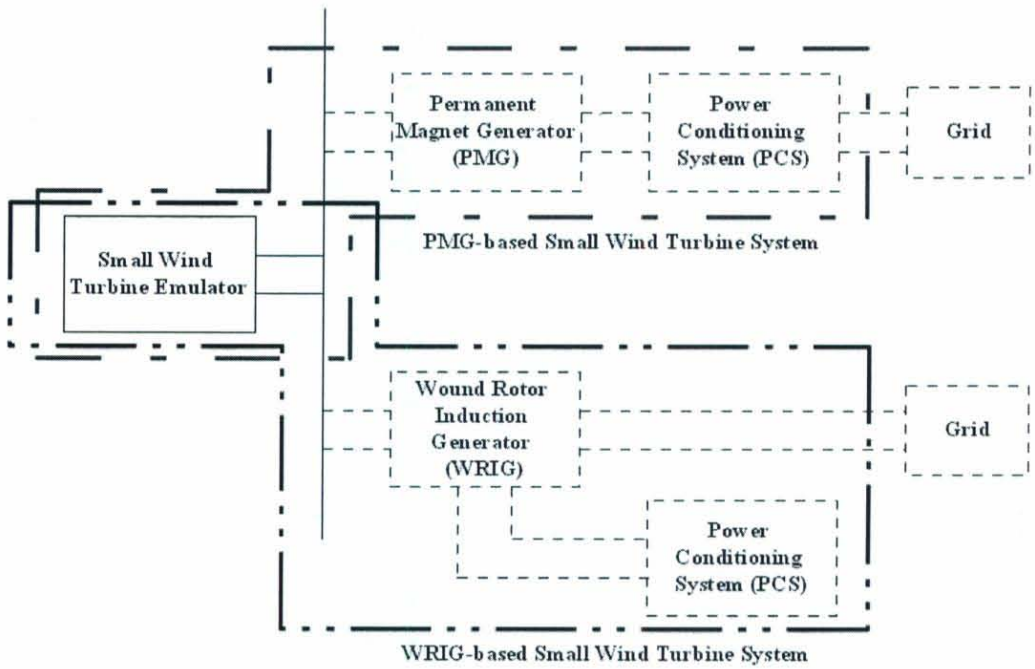

Fig. 5.1 Basic structure of the PMG and WRIG-based system test bench

system performance. However, in order to validate the results found by the simulation, laboratory experimentation is essential. In this study an attempt has been made to verify the simulation results by developing test benches for the systems as opposed to full-scale tests, which are usually not possible in an academic laboratory environment. The overall arrangements of the test bench are shown in Fig. 5.1 and each main component is described in the following subsections.

5.1.1 Small Wind Turbine Emulator

In chapter 4 the modeling of a wind turbine, which is used to compare the performances of grid connected PMG and WRIG-based systems through numerical simulation is presented. In order to ensure fair comparison, the same wind turbine is used in both systems. In view of this, a small laboratory WTE is developed to emulate the behavior of a wind turbine. The furling control and resulting dynamics are implemented within the emulator to control the aerodynamic power as well as to avoid the over speed situation. The following sections describe the essential implementation issues of the WTE in detail.

5.1.1.1 Basic Structure

A WTE is fundamentally a representation of the operation of a practical wind turbine in a laboratory environment. The general structure of a WTE consists of a Personnel Computer (PC) where the model and characteristics of the wind turbine are programmed either in high or low level language, a motor to represent the wind turbine rotor, feedback circuit from the motor, and power electronics equipment to control the motor. The feedback signal is normally acquired by a PC through an Analogue to Digital (A/D) converter and the signal for driving the power electronics equipment emerges from the

PC through a Digital to Analogue (D/A) converter. The representation of the wind turbine rotor could be achieved using an Alternating Current (AC)/Direct Current (DC) motor [50 - 59]. Researchers more often prefer an AC motor mainly due to the benefit of low cost and maintenance in contrast to a DC motor. Furthermore, a DC motor is bulky and costly. In general, the primary disadvantages of an AC motor are that the speed control of an AC motor requires expensive power electronic equipment and the control is more complex than a DC motor. Also, it should be noted that an AC motor is not suitable to operate below 1/3 of its rated speed, i.e., it will not properly reflect the actual turbine characteristic below 1/3 of its rated speed. On the other hand, the speed or torque control of a DC motor is less complex. A DC motor operates more accurately at low speeds.

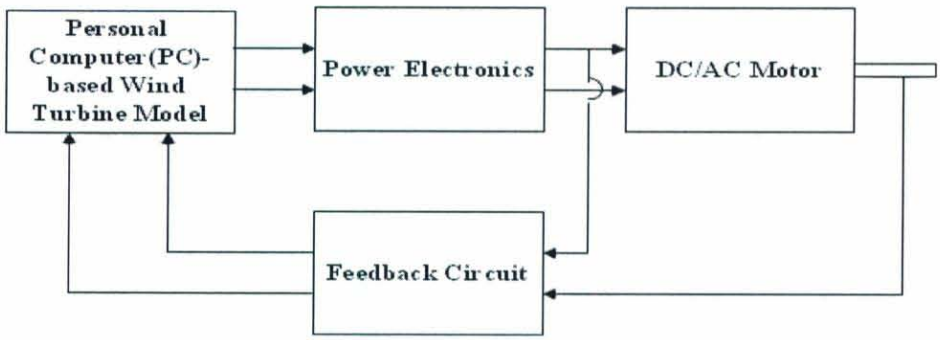

Fig. 5.2 Typical structure of a wind turbine emulator

Finally, in a DC motor, the torque and speed can be adjusted by controlling the armature current and voltage respectively. The cost of the controlling equipment of a DC motor is lower than the cost of an AC motor. Due to the above discussed reasons, this research used a separately excited DC motor to represent the characteristics of the wind turbine rotor. The structure of a typical emulator system is shown in Fig. 5.2.

5.1.1.2 The Developed Emulator

In order to enhance the research and development of wind turbines, it is necessary to better understand the steady state and dynamic behavior of wind turbines. Typically, a wind turbine is a highly nonlinear system and to represent a realistic wind turbine several dynamics should be included in the model. In this research, a furled wind turbine emulator is developed and certain criteria are imposed for an acceptable performance.

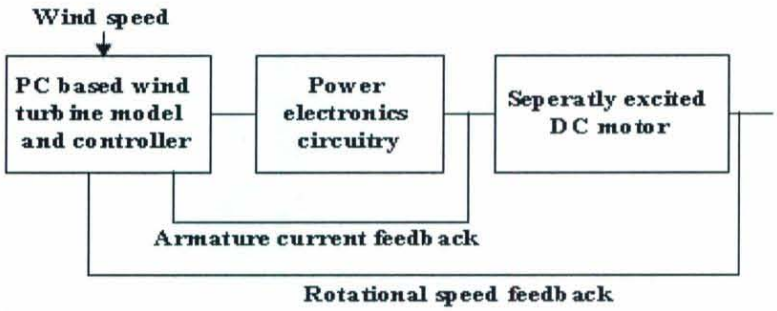

Fig. 5.3 Basic structure of the developed wind turbine emulator

The acceptable performance of the emulator is evaluated based on two criteria: firstly, representation of the furling control and resulting dynamics; secondly, tracking the theoretical optimum shaft speed of the wind turbine rotor by the DC motor. In view of these, furling action and resulting dynamics are incorporated in the emulator with the use of a PC based wind turbine model. In order to follow the optimum shaft speed of the wind turbine rotor, the reference shaft speed is determined from the motor shaft torque (determined from the DC motor armature current) and compared with the actual shaft speed. The difference of these two speeds introduces an error, which is decreased as quickly as possible through a specially designed controller. In this way, the emulator would reproduce different optimum shaft speeds for different wind speeds situation.

Indeed, the precision of the representation depends on the performance of the tracking controller and the precision of the armature current (torque) and speed sensor circuits. The basic structure of the small WTE developed in this research is presented in Fig. 5.3.

5.1.1.3 DC Motor Initial Armature Current Limitation

It is well known that if the dynamics of the motor are slow, an initial high armature current could develop and may damage the motor [104]. The impact of this problem increases when the motor is subjected to uncertain changes. The DC motor of the emulator serves as the wind turbine rotor, that my experience sudden changes in speed. These sudden changes in speed are to emulate the wind gusts. Such variation in DC motor speed demand a limitation of the initial armature current while implementing the emulator. There are several methods to limit the initial current in the motor armature. Current limiting is achieved by limiting the reference of a cascaded current regulating system [105, 106], or it can be achieved by a parallel interventionist system [105, 107]. However, the drawback of the first method is a complex controller. The problem raised by the interventionist system is that, to perform the current limit effectively, the first over shoot of the current should be allowed [106, 107]. Also complex analogue circuitry could be a potential issue to implement such methods in terms of cost and available laboratory facility. A straightforward solution to the problem of limiting the armature current can be achieved by limiting could be to limit the current within the digital controller algorithm which will effectively eliminate complex electronics circuitry. Several research papers discuss how to limit the initial current to a motor by the digital algorithm [105, 106, 108]. Minkova, et. al. [108] proposed a simple adaptive speed control technique to limit the armature current. An approach which applies a slightly smaller amplitude voltage to the

motor in the next sampling instant if the armature current at any instant is too large could limit the armature current. It is also noticed that using such control technique could significantly limit the initial current. In this research, an initial current limiting controller is implemented inside the emulator controller algorithm. The initial current limiting controller works as follows:

The motor armature voltage is dictated by the controller output. A gradual increase in voltage, which is dependent on the controlled voltage, is determined at the output of the controller. At any particular instant *t*, the difference in voltage between the instant *t* and *(t-1)* is calculated for both the controlled and linear voltage. The smaller difference in voltage is applied to the motor armature. Initially the controller will be producing a large variation in the output until it settles to a constant controlled value. Therefore, the difference between the instant *t* and *(t-1)* of the controlled voltage will be higher and the linear voltage will slowly speed up the motor, thus limiting the armature current.

5.1.1.4 Reference Rotor Shaft Speed

The wind turbine model used in this research is implemented in QBASIC 4.5 and the modeling equations are described in Section 4.1.1 in Chapter 4. From (4.7), the optimum shaft speed of the wind turbine can be written as

$$\omega_{m\_ref} = \frac{0.5\rho AC_{p,OPT}(\lambda)(w\cos\theta)^3}{T_w} \tag{5.1}$$

The relationships between the power coefficient and tip-speed ratio and between the wind speed and furling angle are given in (4.2) and (4.3) respectively.

5.1.1.5 Furling Dynamics Discretization

The second order furling dynamics is represented by (4.4). A zero order hold method for 0.1 second sampling time is used to convert the continuous dynamics of the furling action to its discrete equivalent $\left(H(z)\right)$ given by (5.2), which is derived from (4.4) and then converted to a difference equation form.

$$H(z)=\frac{0.003751z+0.00366}{z^2-1.921z+0.9288} \tag{5.2}$$

5.1.1.6 Controller

A simple controller used most of the time is a Proportional Integral (PI)/Proportional Integral Derivative (PID) controller, as it is easy to implement and requires less computing power. In the time domain, the PID controller equation can be written as [104]

$$u(t)=K_p e(t)+\frac{K_p}{T_i}\int_0^t e(t)dt+K_p T_d\frac{de(t)}{dt}+u_0 \tag{5.3}$$

where $u(t)$ is the output of the PID controller at any instant t.

K_p is the proportional gain of the PID controller.

T_i is the integral time of the controller.

T_d is the derivative time of the controller.

$e(t)$ is the error between reference and actual control variable.

In order to implement the controller in a PC, an approximation of the continuous function of (5.3) is required. Approximations of the integral and derivate terms of (5.3) can be written as

$$\frac{de(t)}{dt} \approx \frac{e(t)-e(t-1)}{T_s} \text{ and } \int_0^t e(t)dt \approx T_s \sum_o^t e(t) \tag{5.4}$$

where T_s is the sampling time.

$e(t-1)$ is the previous state error.

From the above approximations, the discrete equivalent of the continuous PID controller algorithm can be written as

$$u(t) = K_p e(t) + \frac{K_p T_s}{T_i} \sum_0^t e(t) + \frac{K_p T_d \{e(t)-e(t-1)\}}{T_s} + u_0 \tag{5.5}$$

where u_o is the base level of the control signal.

Equation (5.5) is called the positional PID controller algorithm and it can be easily implemented using a PC. One of the major drawbacks of the positional algorithm is that the value of u_o is stiff to determine and requires extensive trial and error. By shifting one sampling interval of the PID controller equation (5.5), it can be written as

$$u(t-1) = K_p e(t-1) + \frac{K_p T_s}{T_i} \sum_0^{t-1} e(t-1) + \frac{K_p T_d \{e(t-1)-e(t-2)\}}{T_s} + u_0 \tag{5.6}$$

Subtracting (5.5) from (5.6) gives

$$u(t) = u(t-1) + K_p [e(t)-e(t-1)] + \frac{K_p T_s}{T_i} e(t) + \frac{K_p T_d}{T_s} [e(t)-2e(t-1)+e(t-2)] \tag{5.7}$$

Equation (5.7) describes the velocity PID controller equation. There are several advantages of the velocity PID algorithm over the positional PID algorithm such as:

- The summations of errors are not explicitly calculated so there is an anti reset wind up accumulated with this controller algorithm.

- A base value is not required for velocity PID controller algorithm, i.e., it depends on the previous state value and no prior assumption is necessary.

Due to the above reasons, the velocity PID controller algorithm was used to track the theoretical rotational speed of the wind turbine rotor by the DC motor. As there are three types of controllers which can be implemented, the obvious question that could arise is

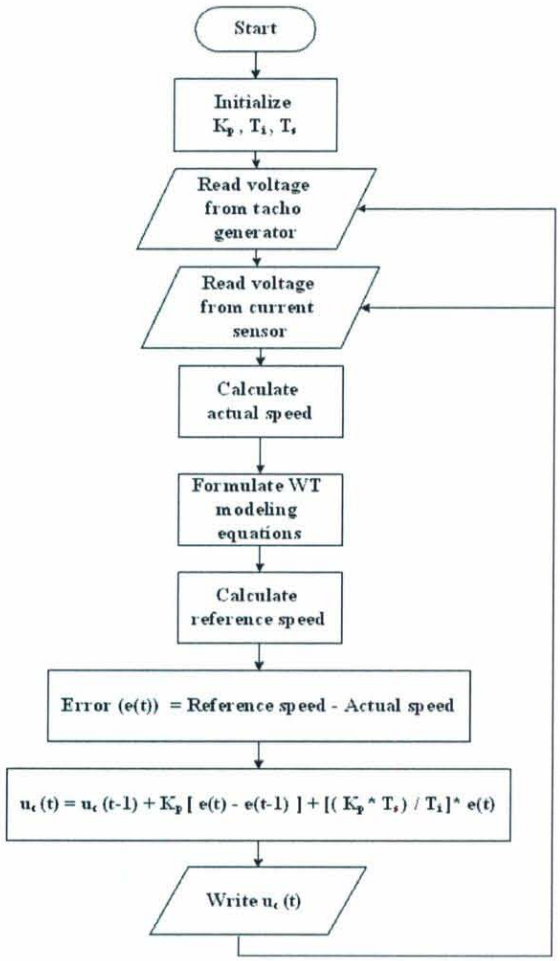

Fig. 5.4 Controller flow diagram for the wind turbine emulator

which controller would be the most suitable to implement. A Proportional (P) only controller is the easiest to tune, however, zero steady state error with only proportional control is not possible. On the other hand a PID controller is the most complicated to tune and the derivative term might be affected by noise. To avoid these complexities, a PI controller was used as it has the ability to make the steady state error zero and is also less complex to tune. Although, it should be noted that a trade off is required before implementing a PI/PID controller based on the consideration of time span, accuracy and tuning issues. Due to the use of a PI controller, the derivative term will become zero, and (5.7) will be reduced to

$$u(t) = u(t-1) + K_p * \left[e(t) - e(t-1) \right] + \frac{K_p * T_s}{T_i} e(t) \tag{5.8}$$

A flow chart for the controller algorithm is given in Fig. 5.4.

5.1.1.7 System Integration

The emulator developed in this research consists of a 3HP separately-excited DC motor. The parameters of the motor are given in Appendix C. This motor serves as the wind

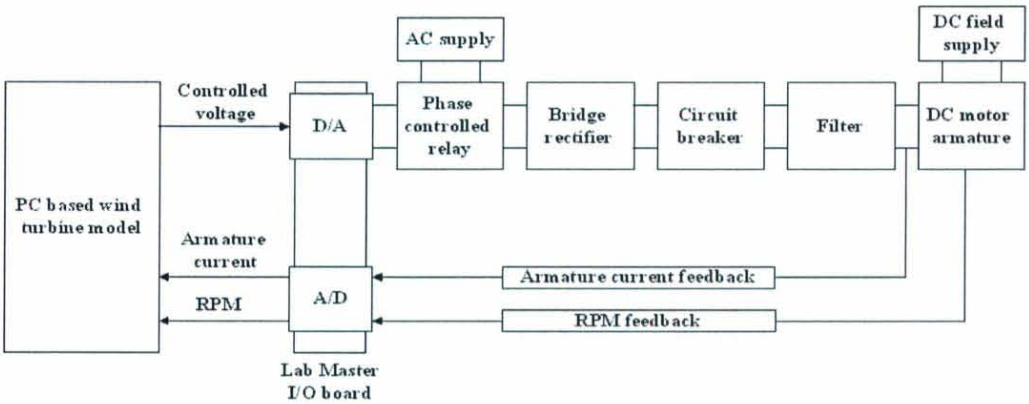

Fig. 5.5 Schematic of the wind turbine emulator test bench

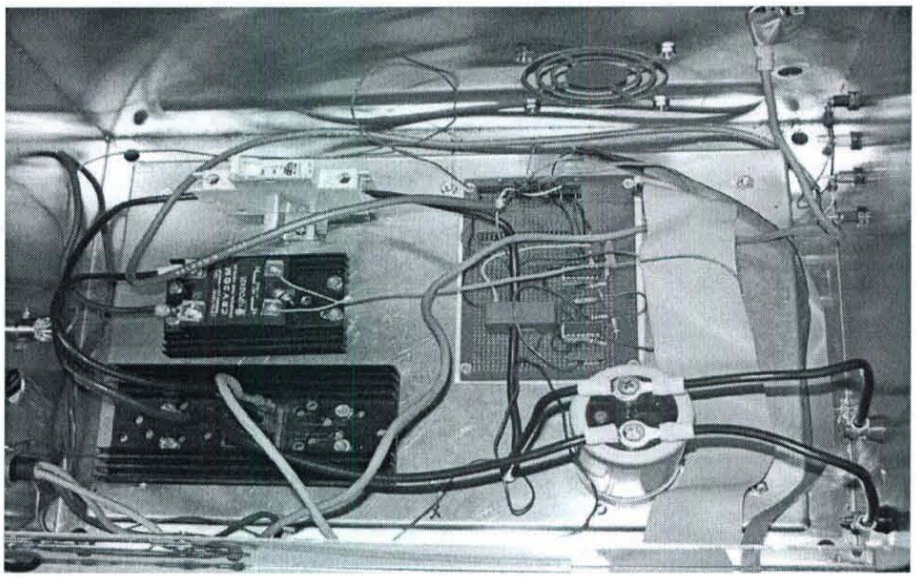

Fig. 5.6 Photograph of the emulator power electronics

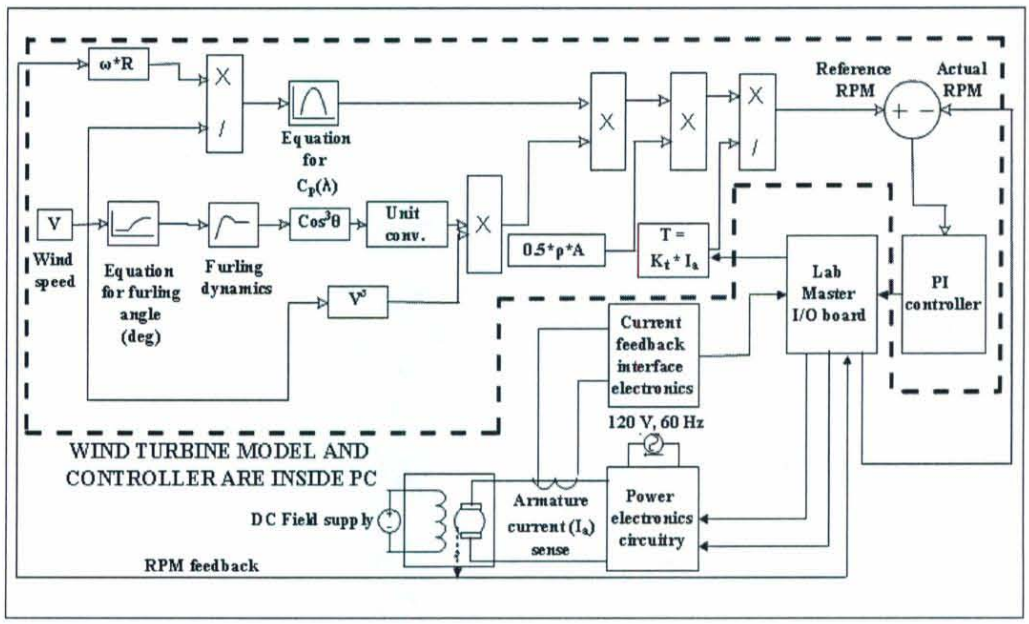

Fig. 5.7 Wind turbine emulator with controller and peripheral

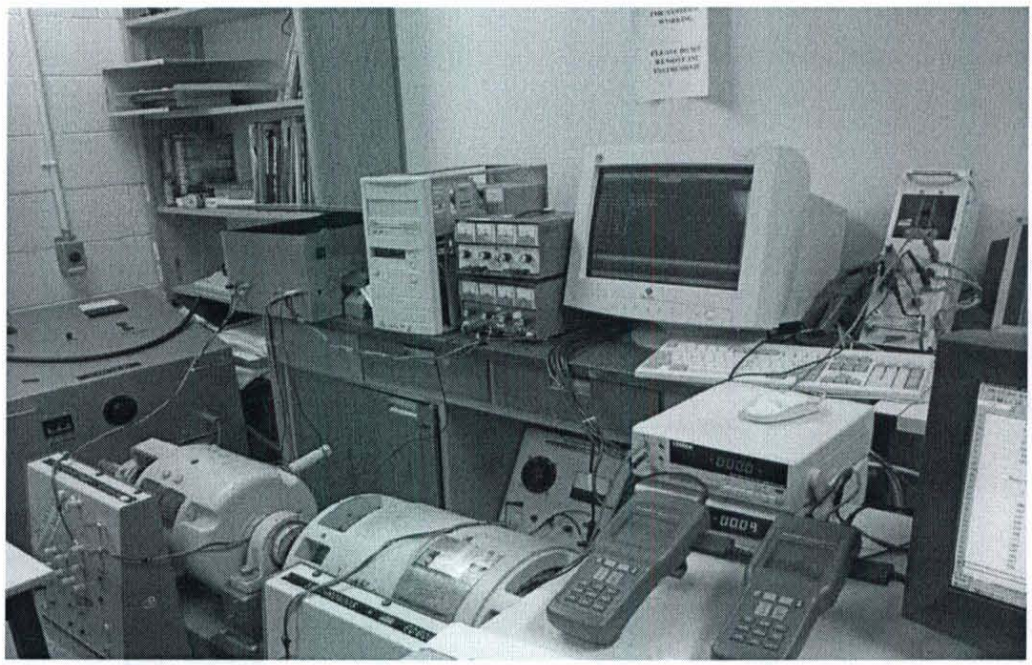

Fig. 5.8 Photograph of the wind turbine emulator test bench

turbine rotor, which literally drives a PMG or WRIG in order to emulate a PMG and WRIG-based system. The PC-based controller produces the required control voltage which passes through the D/A converter to trigger the phase controlled relay. A simple amplifier and a filter circuit are used in conjunction with the current sensor. Saturation of the armature current is eliminated by adjusting the gain of the amplifier stage. The output of the phase controlled relay is rectified and then filtered using a capacitor to remove the noise from the rectified voltage. During the tuning of the parameters it was necessary to use a circuit breaker in the armature side of the system. Fig. 5.5 and Fig. 5.6 show the schematic of the emulator and photograph of the power electronics of the emulator respectively. The complete emulator with the controller and peripheral and photograph of

the test bench are depicted in Fig. 5.7 and Fig. 5.8 respectively. More details of the emulator may be found in [109].

5.1.2 Grid Connected PMG-based Small Wind Turbine System

The grid connected PMG-based system is developed by using available laboratory facility as well as commercially available components. The following sections describe the development procedure in detail.

5.1.2.1 Basic Structure

The grid connected PMG-based small wind turbine system is composed of the wind turbine emulator (described in Section 5.1.1), a PMG, a 3-phase bridge rectifier, a Boost Converter (BC) and an inverter. The changes in wind speed result in changes to the shaft speed of the emulator, and hence the speed of the PMG. The shaft of the emulator is coupled to the PMG through flexible coupling. Thus the PMG output has the

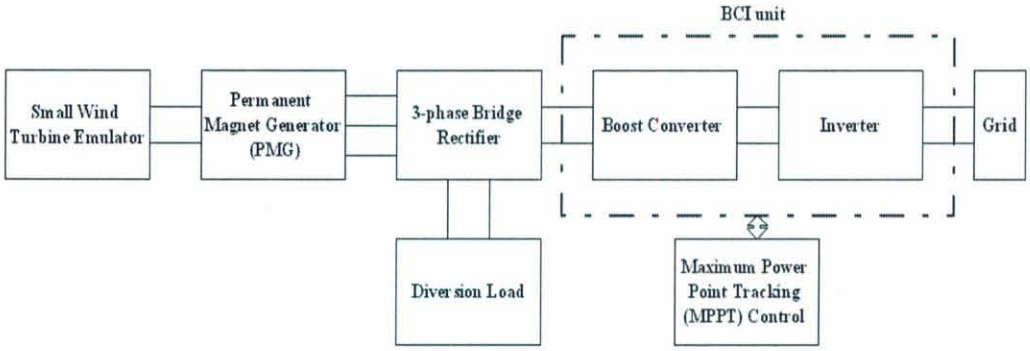

Fig. 5.9 Basic structure of the PMG-based system test bench

characteristic of variable voltage, current and frequency. The output of the PMG is fed to a 3-phase bridge rectifier. A diversion load (dump load) is connected to the output of the rectifier in order to ensure safe operation of the system in case of very high wind speed.

The output DC voltage of the rectifier is fed to BC, which acts as a mid stage between the rectifier and grid inverter. The regulated DC output voltage is fed to the inverter, which supply to the grid at a predetermined nominal voltage and frequency. The BC and inverter modules are considered as a single unit in this thesis (BCI), since both of these components are supplied by the manufacturer as a single unit. The BCI unit is programmed with the wind turbine model specific power curve. The model specific power curve is used for the Maximum Power Point Tracking (MPPT) control to extract the maximum amount of power from the emulator at a specific shaft speed. A block diagram structure of the PMG-based system is presented in Fig. 5.9.

5.1.2.2 Control strategy

The basic idea behind this control strategy is to ensure optimum tip-speed-ratio at all wind speeds. In order to achieve this objective, the following approach is employed:

The emulator optimum speed, ω for a specific wind speed, w is controlled by the emulator controller and the corresponding rectified DC voltage, V_{dc} is determined. As a result, a table with one input as the emulator shaft speed and one output as the rectified DC voltage is recorded. In addition, a table of shaft speed versus maximum power, P is known in advance from the modeling equations of the emulator. Thus at a given wind speed, a lookup table, containing rectified DC voltage versus maximum power characteristic, is programmed into the BCI unit using a serial interface. The BCI unit uses the lookup table to create a curve by interpolating between points as needed and ensures the variable speed operation. The control strategy described above is presented in Fig. 5.10.

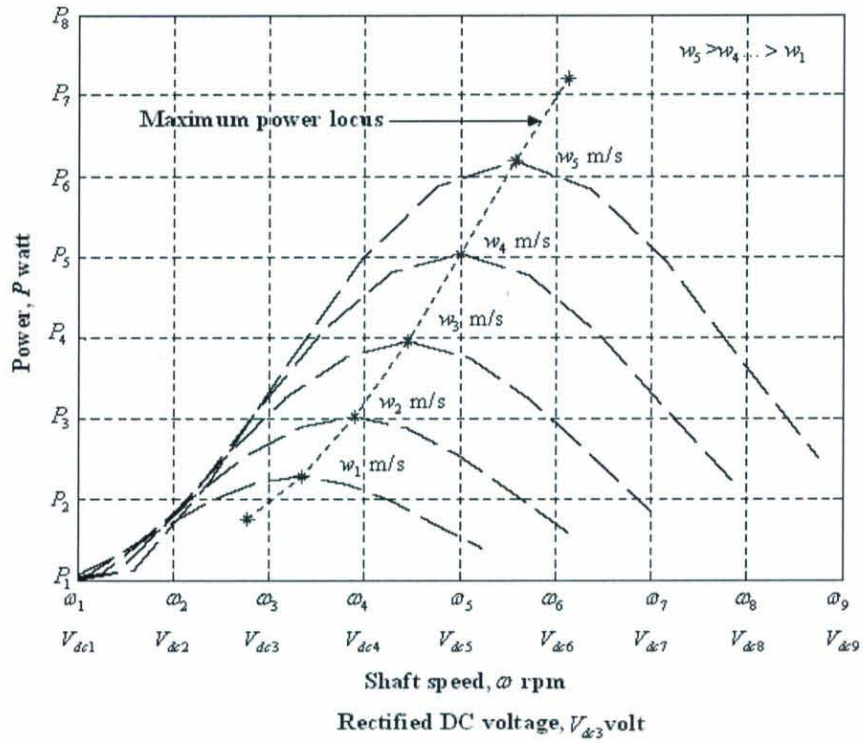

Fig. 5.10 Control strategy for the PMG-based system

5.1.2.3 System Integration

The DC motor based wind turbine emulator was coupled to a 1.6kW permanent magnet machine, which has a rated terminal line to neutral voltage of 120 volts. Appendix D provides the nameplate information for the PMG. A circuit breaker was connected in between the 3-phase bridge rectifier and the output of the PMG. A diversion load resistor was connected to the output of the rectifier in order to limit the rectifier output voltage during gusts and very high wind speed conditions. When the rectifier output voltage exceeds $530 V_{dc}$, the diversion load is switched on and remains on until the rectifier output voltage decreases to approximately $430 V_{dc}$. The output of the rectifier was connected to

an ammeter and voltmeter and afterwards a circuit breaker. The output from the circuit breaker was connected to the input of the BCI unit. The BCI unit is equipped with several protective devices to protect the BCI unit from Anti-Islanding and Ground Fault. Furthermore, the BCI unit is equipped with additional protections to guarantee safe operation under all circumstances. The protections include a continuous monitoring of the grid voltage to ensure the frequency and voltage values are within the proper operational limits. The BCI unit is installed using watertight wiring methods, which required the use of watertight components and locknuts with the applicable wiring method. On the bottom of the unit there are four 29mm diameter holes (Trade size 3/4") covered with cap Elektrozubehör, type H 400 P (model designation K 426 21 P) or equivalent to UL listed

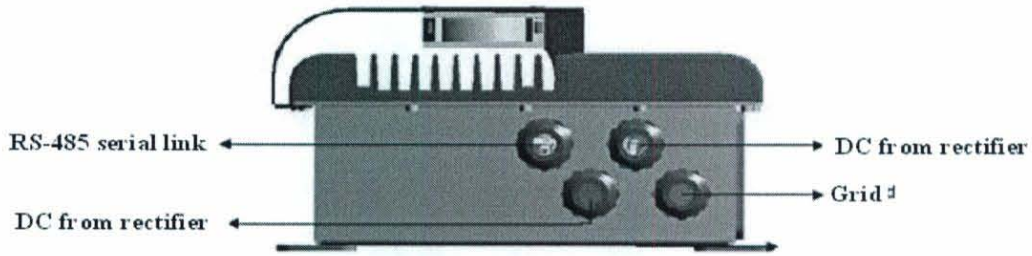

Fig. 5.11 Hole assignment of the BCI unit

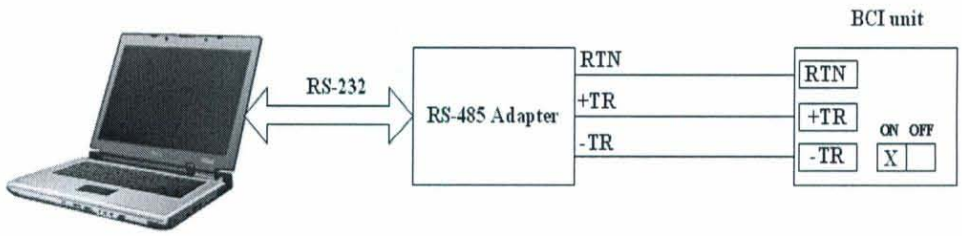

Fig. 5.12 Communication between the BCI unit and PC

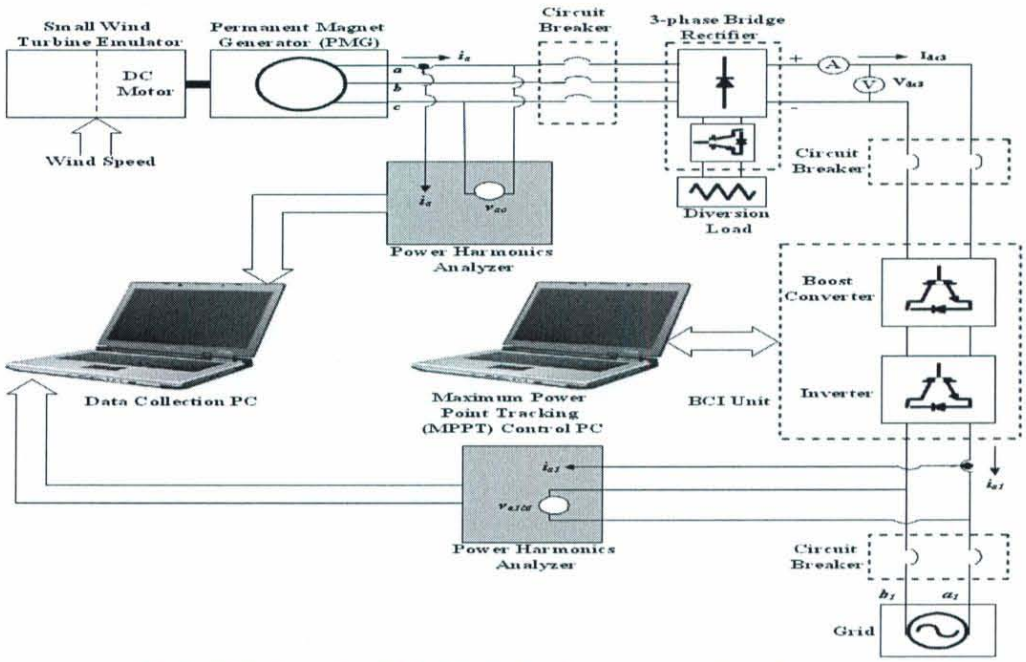

Fig. 5.13 Schematic of the PMG-based system test bench

Fig. 5.14 Photograph of the PMG-based system test bench

watertight cap. Un-used holes were left sealed by the caps. Fig. 5.11 shows an example of hole assignment of the BCI unit. To program the BCI for the MPPT control, a communication with the external PC was required. The BCI has a RS-485 link to communicate with the PC. The RS-485 link uses two wires for signals plus a third wire for signal ground, which is different from the equipment grounding of the BCI unit. The wires are run in a watertight conduit through the bottom of the BCI unit.

Despite the RS-485 link, an adapter was used to convert the communication from RS-485 to RS-232 in order to optimize the operation. A diagram of the communication between the PC and BCI unit is shown in Fig. 5.12. The lookup table for the MPPT control is sent through the serial interface whether the BCI unit is online or offline. The BCI unit can also provide the necessary real time values and can be stored in the PC. The single phase output of the BCI unit was connected to a circuit breaker and finally to the grid. Two Fluke power harmonics analyzers are used to acquire the time sampled voltage and current from the output of the PMG and from the input of the grid. The power harmonics analyzers are connected to another PC through serial port to store the instantaneous voltage and current values to a file for further calculation. A detail schematic is presented in Fig. 5.13 and a photograph of the test bench is given in Fig. 5.14. Appendix F provides the list of the components used to integrate the system.

5.1.3 Grid Connected WRIG-based Small Wind Turbine System

The grid connected WRIG-based system is developed by using the available laboratory facility as well as the commercially available components. The following sections describe the development of the system in detail.

5.1.3.1 Basic Structure

The grid connected WRIG-based system is composed of a wind turbine emulator, a WRIG, a 3-phase bridge rectifier, and a variable resistance. The shaft of the WRIG is coupled to the shaft of the emulator through flexible coupling. The stator of the WRIG is directly connected to the grid, while the rotor is connected to a 3-phase bridge rectifier and a variable external resistance. The variation of shaft speed of the emulator due to

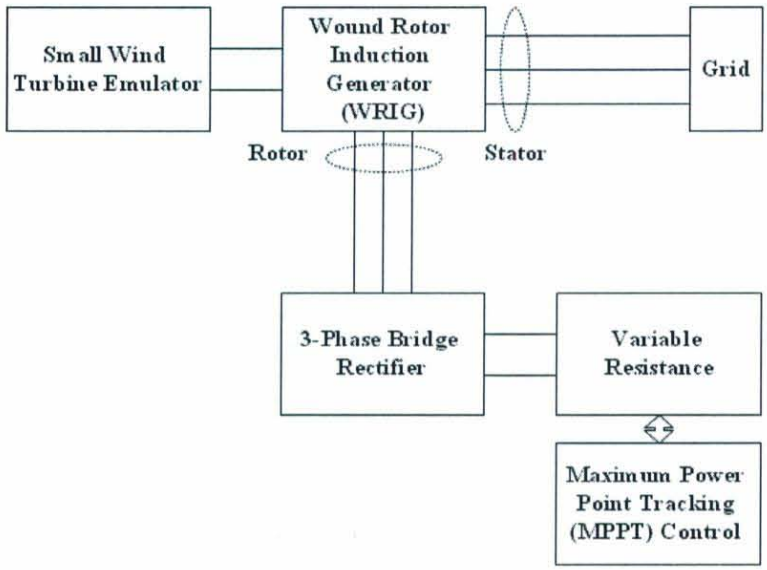

Fig. 5.15 Basic structure of the WRIG-based system test bench

changes in wind speed, changes the speed of the WRIG and subsequently injects power to the grid. The model specific wind turbine power curve used for the WRIG-based system is identical to the PMG-based system. The power curve is used to provide MPPT control to extract maximum power from the wind turbine. A block diagram of the structure of the system is presented in Fig 5.15.

5.1.3.2 Control strategy

An optimum tip-speed-ratio control method is adapted with the WRIG-based system to optimize the power production. This requires a continuous change of the power speed characteristics of the system. The convenient parameter that can be used to modify the torque-speed characteristics of the WRIG is the external rotor resistance. The change of rotor resistance can be realized by changing the duty cycle, d of a switch connected in parallel with the external rotor resistance. At a fixed value of the external resistance, the

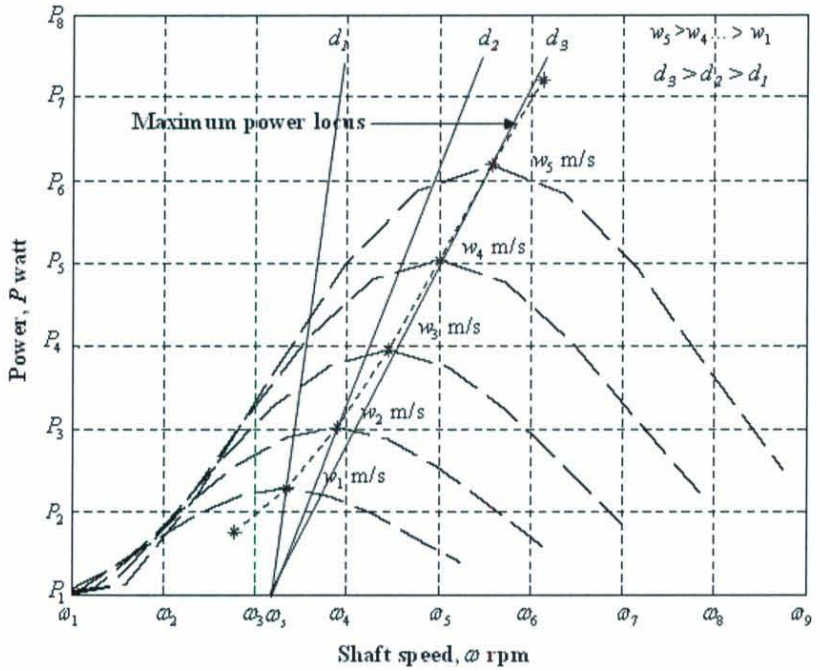

Fig. 5.16 Control strategy for the WRIG-based system

emulator can operate at a maximum power, P at one wind speed, w and shaft speed, ω only, as can be seen from Fig. 5.16. For the system to operate at maximum power at all wind speeds, the rotor resistance is continuously changed, so that under varying wind

speed conditions, the system always follows the maximum power locus. In this manner, maximum power is extracted from the system through the WRIG stator.

5.1.3.3 System Integration

The emulator used with the PMG-based system was coupled to a 1.8kW WRIG, which has a rated terminal line to neutral voltage of 120 volts. Appendix E provides the nameplate information for the generator. A circuit breaker was connected in between the stator of the generator and grid. The three phase output from the rotor of the generator was connected to a 3-phase bridge rectifier. The output of the rectifier was connected to an ammeter and voltmeter, and afterwards to an external variable resistance. The variable resistance is varied to ensure maximum power flow to the grid at the optimum shaft speed for a specific wind speed. Two Fluke power harmonics analyzers are used to acquire the time sampled voltage and current values from the stator and rotor output of the WRIG. A current probe is used to acquire the current values, while a voltmeter is used for voltage from the output of the rectifier. The power harmonics analyzer is connected to another PC using serial port to store the instantaneous voltage and current values. A detail diagram and a photograph of the test bench are given in Fig. 5.17 and Fig. 5.18 respectively. Appendix F provides the list of the components used to integrate the system

5.2 Power Loss Determination

The test benches for the grid connected systems comprised several laboratory and commercial components. Some of the commercial components (for example, the BCI unit) are entirely sealed by the manufacturer. As a consequence, the switching and conduction loss for the individual switches in the BCI unit could not be reproduced.

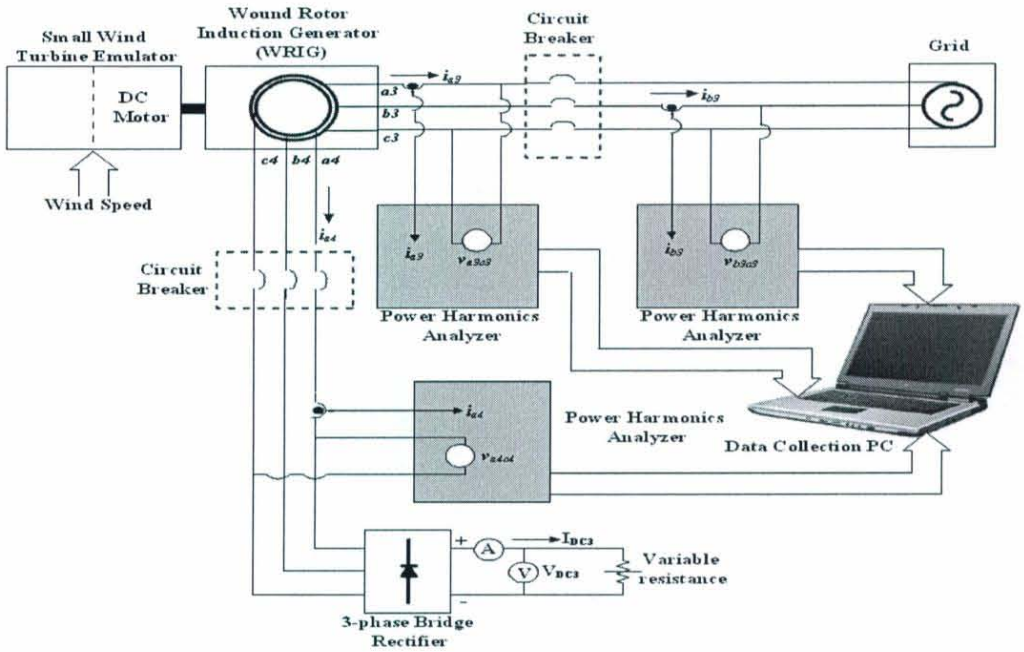

Fig. 5.17 Schematic diagram of the WRIG-based system test bench

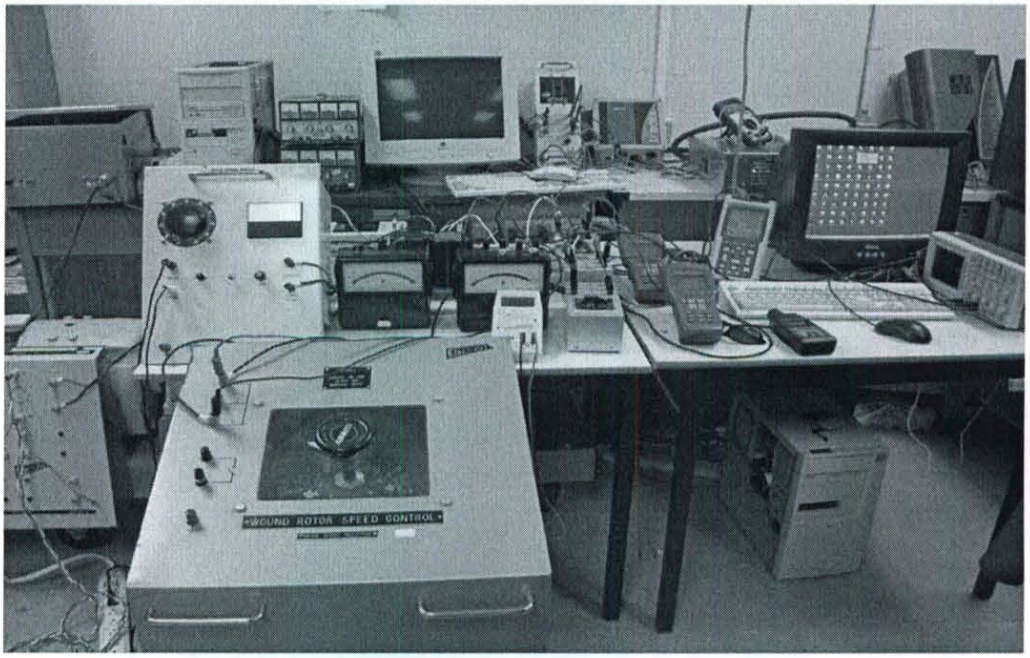

Fig. 5.18 Photograph of the WRIG-based system test bench

Considering rather the conduction and switching power loss for the individual switches, the total power loss of each block is calculated. Here a "block" refers to the 3-phase bridge rectifier and BCI unit for the PMG-based system and 3-phase bridge rectifier and external rotor resistance for the WRIG-based system. The following section describes the procedure used to determine the losses for each block.

5.2.1 Loss Determination of the PMG-based System

The PMG used in this research has a star connected stator with balanced and identical three phases denoted as a, b, c, while the neutral is absent. The Root Mean Square (RMS) value of the PMG output voltage and current for phase a, b and c is $V_a, I_a; V_b, I_b$; and V_c, I_c respectively. The instantaneous power at time t, $P(t)$, is expressed as

$$P(t) = v_a i_a + v_b i_b + v_c i_c \tag{5.9}$$

where v_a, v_b and v_c are the instantaneous values of PMG output voltages for phase a, b and c respectively

i_a, i_b and i_c are the instantaneous values of PMG output currents for phase a, b and c respectively

The characteristic of a balanced 3-phase generator is that at any instant the summation of all instantaneous currents is zero and can be written as

$$i_a + i_b + i_c = 0 \tag{5.10}$$

Substituting the value of i_c in (5.9), the power is expressed as

$$P(t) = (v_a - v_c) i_a + (v_b - v_c) i_b \tag{5.11}$$

As the generator phases are 'balanced', both terms in (5.11) are equal, hence

$$P(t) = 2(v_a - v_c)i_a = 2(v_b - v_c)i_b \tag{5.12}$$

Averaging over one period T of (5.12) will give the average power. So the output power of the PMG, which consequently acts as the input AC power to the 3-phase bridge rectifier, $P_{out,gen}{}^{PMG}$ is expressed as

$$P_{out,gen}{}^{PMG} = \frac{1}{T}\int_{cycle} P(t)dt = \frac{1}{T}\int_{cycle} 2(v_a - v_c)i_a dt \tag{5.13}$$

An approximation uses a digital oscilloscope to obtain instantaneous values of $V_{ac} = v_a - v_c$ and $I_a = i_a$. If there are n samples in one period then by definition of the integral, (5.14) becomes the power generated by the PMG.

$$P_{out,gen}{}^{PMG} \cong \frac{1}{n}\sum_n 2V_{ac}I_a \tag{5.14}$$

The output DC power from the 3-phase bridge rectifier can be expressed as

$$P_{out,rec}{}^{PMG} = V_{dc3}I_{dc3} \tag{5.15}$$

Subtracting (5.15) from (5.14), the rectifier power loss is found as

$$P_{t,rec}{}^{PMG} = P_{out,gen}{}^{PMG} - P_{out,rec}{}^{PMG} \tag{5.16}$$

The PMG-based small wind turbine system has a single phase output with phases $a1, b1$ and a neutral (ground). As a consequence, a similar kind of formulation expressed by (5.9) to (5.15) is derived to compute the power flowing into the grid, $P_{out\_exp,grid}{}^{PMG}$, and can be written as

$$P_{out\_exp,grid}{}^{PMG} \cong \frac{1}{n}\sum_n V_{a1b1}I_{a1} \tag{5.17}$$

Equation (5.17) expresses the power flowing into the grid by the actual voltage and current; however, the BCI unit itself is able to calculate the power flowing into the grid

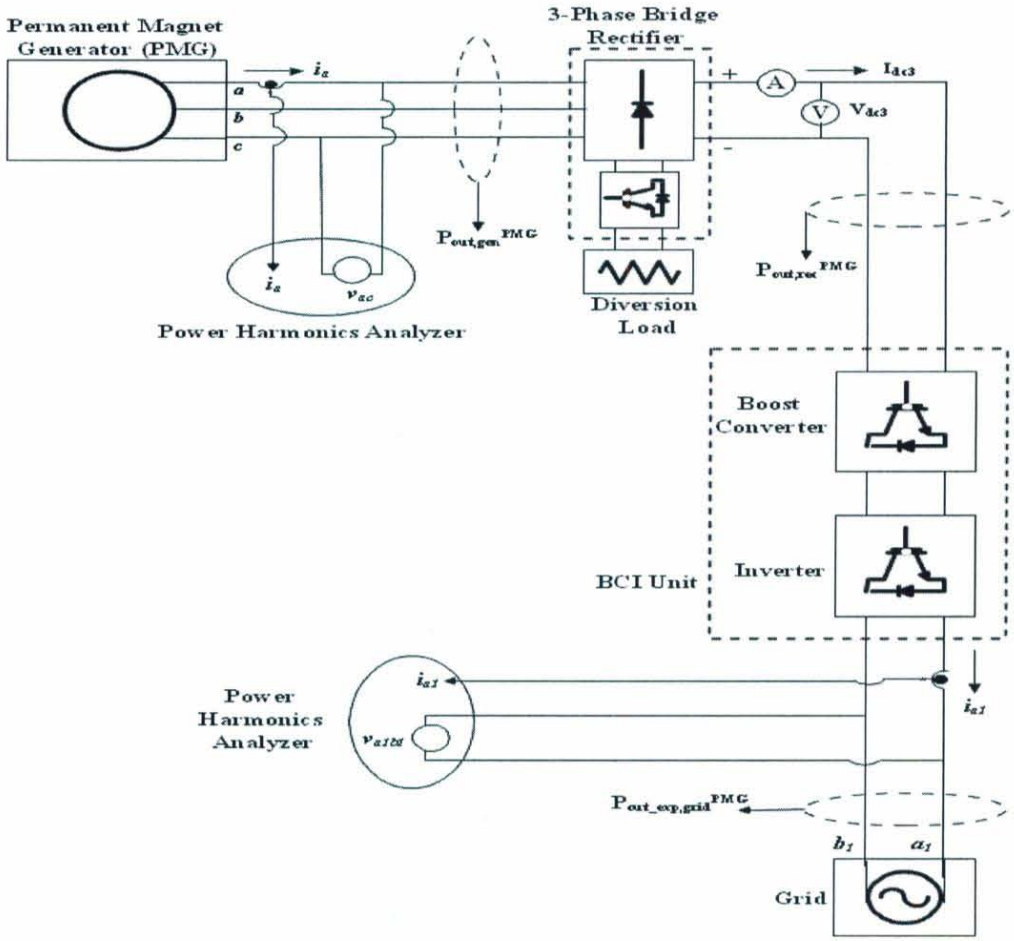

Fig. 5.19 Power loss calculation diagram for the PMG-based system

by its own data acquisition system and denoted in this research as commercial or expected value. The commercial power production values from the BCI unit is also stored in the PC and denoted by $P_{out\_com,grid}^{PMG}$. These commercial power output values are recorded in

order to observe the commercial power loss values. This is of particular importance because the expected and experimental outcomes from a system will be clearly identified and any misconception about a system performance will certainly be evaluated.

The BCI unit loss is computed by subtracting (5.16) from (5.17) and is given by (5.18), which represents the experimental power loss of the BCI unit. In contrast to the experimental power loss, subtracting the commercial output power from the BCI unit will provide the commercial power loss of the BCI unit as expressed in (5.19).

$$P_{t\_exp,BCI\_unit}^{PMG} = P_{out\_exp,grid}^{PMG} - P_{out,rec}^{PMG} \tag{5.18}$$

$$P_{t\_com,BCI\_unit}^{PMG} = P_{out\_com,grid}^{PMG} - P_{out,rec}^{PMG} \tag{5.19}$$

The experimental and commercial total power losses for the PMG-based system can be expressed by (5.20) and (5.21) respectively, and a complete schematic diagram is given in Fig. 5.19.

$$P_{t\_exp}^{PMG} = P_{t,rec}^{PMG} + P_{t\_exp,BCI\_unit}^{PMG} \tag{5.20}$$

$$P_{t\_com}^{PMG} = P_{t,rec}^{PMG} + P_{t\_com,BCI\_unit}^{PMG} \tag{5.21}$$

The efficiency of the individual component is calculated as follows: Equation (5.22) expresses the rectifier efficiency, while (5.23) and (5.24) represent the respective experimental and commercial efficiency of the BCI unit. The composite experimental and commercial efficiency of the PCS is also calculated and expressed by (5.25) and (5.26) respectively.

$$\eta_{rec} = \frac{P_{out,rec}^{PMG}}{P_{out,gen}^{PMG}} \tag{5.22}$$

$$\eta_{exp,inv\_unit} = \frac{P_{out\_exp,grid}^{PMG}}{P_{out,rec}^{PMG}} \tag{5.23}$$

$$\eta_{com,inv\_unit} = \frac{P_{out\_com,grid}^{PMG}}{P_{out,rec}^{PMG}} \tag{5.24}$$

$$\eta_{exp,composite} = \eta_{rec} \times \eta_{exp,BCI\_unit} \tag{5.25}$$

$$\eta_{com,composite} = \eta_{rec} \times \eta_{com,BCI\_unit} \tag{5.26}$$

5.2.2 Loss Determination of the WRIG-based System

The three phases, $a3$, $b3$ and $c3$ of the stator of the wound rotor induction generator is directly connected to the grid for the grid connected WRIG-based system. Two power harmonics analyzers are used to determine the total real power and the connection diagram is presented in Fig. 5.20. A similar formulation expressed by (5.9) to (5.15) is derived to compute the power flowing into the grid and can be written as

$$P_{out\_ac,grid}^{WRIG} \cong \frac{1}{n}\sum_{n} V_{a3c3} I_{a3} \tag{5.27}$$

$$P_{out\_bc,grid}^{WRIG} \cong \frac{1}{n}\sum_{n} V_{b3c3} I_{b3} \tag{5.28}$$

where V_{a3c3} and V_{b3c3} are the line-to-line voltages of the stator, and I_{a3} and I_{b3} are the line currents of the stator.

The total real average power flowing into the grid is given by

$$P_{out\_exp,grid}^{WRIG} = P_{out\_ac,grid}^{WRIG} + P_{out\_bc,grid}^{WRIG} \tag{5.29}$$

The rotor of the generator is star connected and balanced. As a result, a similar attempt described by (5.9) to (5.15) is used to determine the power losses in the rotor and results in:

$$P_{t,rotor}^{WRIG} \cong \frac{1}{n}\sum_{n} 2V_{a4c4}I_{a4} \tag{5.30}$$

where V_{a4c4} is the line-to-line voltage of the rotor, and I_{a4} is the line current of the rotor.

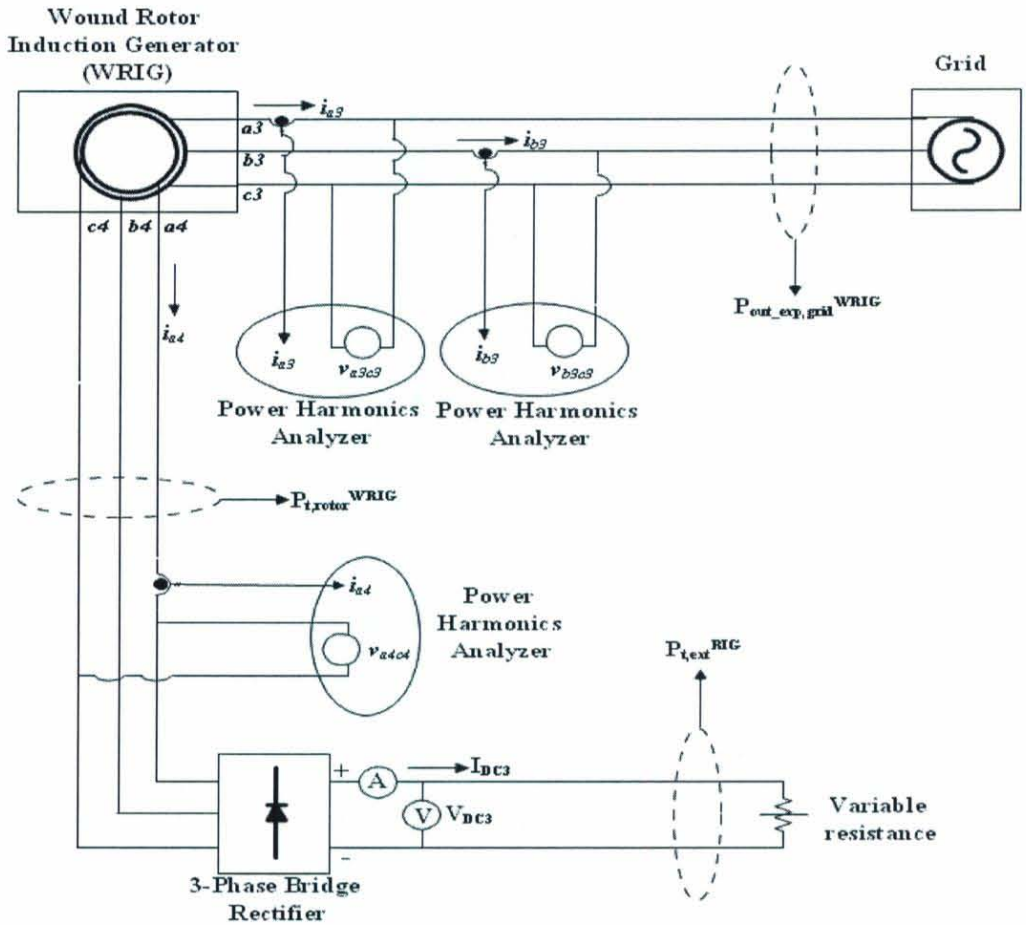

Fig. 5.20 Power loss calculation diagram for the WRIG-based system

The output power of the 3-phase bridge rectifier is eventually the external rotor resistance loss and can be expressed as

$$P_{t,ext}^{WRIG} = V_{DC3} I_{DC3} \tag{5.31}$$

Subtracting (5.31) from (5.30), the rectifier power loss is found as

$$P_{t,rec}^{WRIG} = P_{out\_exp,grid}^{WRIG} - P_{t,ext}^{WRIG} \tag{5.32}$$

The electrical and frictional losses in the slip rings are determined based on the slip of the generator and expressed by (5.33) and (5.34) respectively, while the total slip-ring loss is expressed by (5.35). The sum of (5.30) and (5.35) reflects the total power loss of the WRIG-based system and is represented by (5.36).

$$P_{elec\_slipring}^{WRIG} = K_{\omega}\omega \tag{5.33}$$

$$P_{fric\_slipring}^{WRIG} = K_{\delta}\omega \tag{5.34}$$

$$P_{t,slipring}^{WRIG} = P_{elec\_slipring}^{WRIG} + P_{fric\_slipring}^{WRIG} \tag{5.35}$$

$$P_{t,exp}^{WRIG} = P_{t,rec}^{WRIG} + P_{t,ext}^{WRIG} + P_{t,slipring}^{WRIG} \tag{5.36}$$

5.3 Test Results

The grid connected small wind turbine systems described in this chapter were implemented and tested in the laboratory environment. It should be mentioned that the operating range of the systems was greatly dominated by the available laboratory facility as well as safety regulations in the laboratory environment. Based on these, a specific wind speed range was selected and corresponding results are presented. First, the emulator test results are presented and afterwards, the power losses for both systems are described based on the computation procedure described in Section 5.2. Finally, AEC,

AEL and efficiency are compared based on the wind speed distributions for eight different sites in Newfoundland and Labrador as employed in Chapter 4. In order to reduce the volume of results that can be presented for the 8 different sites and 8 different wind speeds for each system, representative results for each system are presented in the thesis.

5.3.1 Small Wind Turbine Emulator

The wind turbine emulator developed in the laboratory environment has been subjected to a changing wind speed w. This changing wind speed is prepared as pseudorandom wind speed profile (Fig.5.21a); the input to the emulator as a series of steps, equi-duration. Although real wind does not occur with such abrupt slopes, a series of equi-duration steps is a standard testing signal, which permits a clear interpretation of the system behavior. The wind speed was limited to values between 6 m/s and 13 m/s. As discussed in Section 5.1.1.3, limitation of the armature current is of importance in order to protect the motor armature and this was taken into consideration during the development of the wind turbine emulator using an initial current limiting controller. The performance of the controller with current limitation of 4 amperes is illustrated in Fig. 5.21b from the initial start-up of the emulator. The variation in armature current characteristic corresponding to the change in wind speed is recorded and averaged to generate a uniform distribution over the entire wind speed range. It can be seen that the proposed controller limits the amplitude of the armature current of the DC motor below 4 amperes. System stabilization is also achieved, as after some initial transient, the armature current settled to a new value and remained more or less constant. Furthermore, with the increase in wind speed, the

motor started to draw more current from the main, while no unwanted overshoot of the current was observed. The experimental results proved that the current limitation functioned well. The controller performed well, independent of the speed and of the motor dynamics.

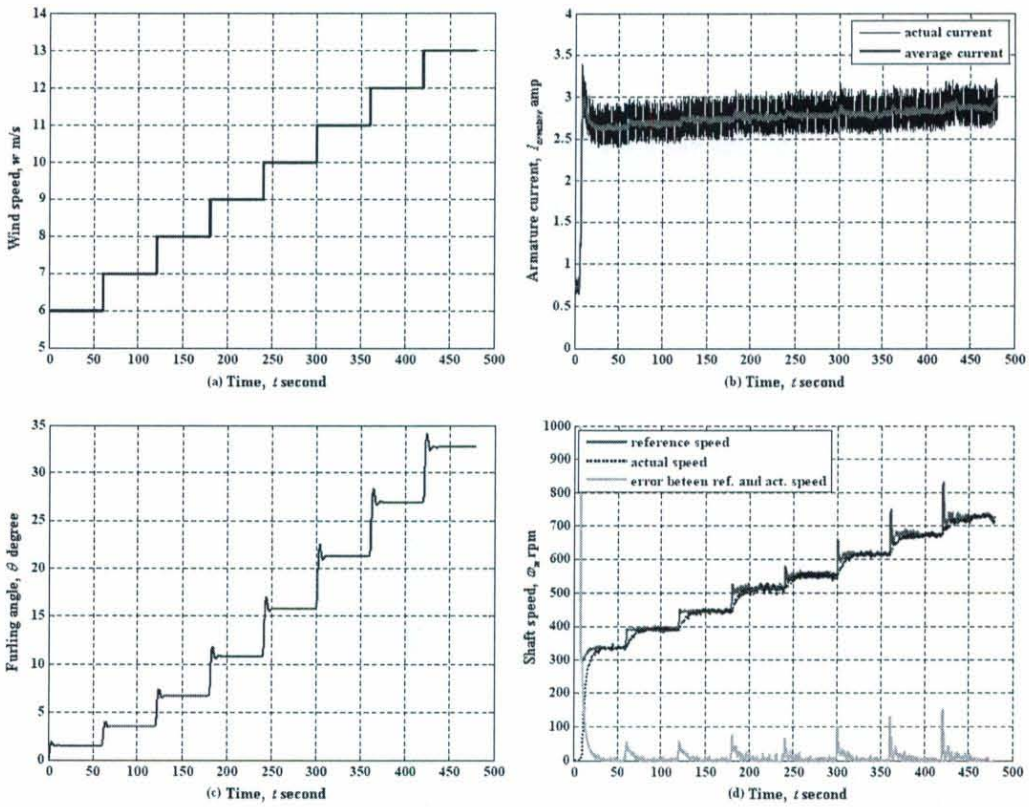

Fig. 5.21 Variation of the emulator characteristics, a) Wind speed, b) DC motor armature current, c) Furling angle and expected dynamics, d) Shaft speed

The response of the furling angle, θ and expected dynamics are shown in Fig. 5.21c. During the wind speed increase, within 10 seconds, the rotor reached a stable state at a furling angle corresponding to the value obtained in (4.4) in Chapter 4. This settling time

is required in order to avoid any excessive overloading of the mechanical part of the wind turbine.

In the emulator controller, the theoretical or reference rotor shaft speed was compared with the actual speed measured from the shaft of the DC motor in order to find the speed error. The controller forced the actual speed of the emulator to trace the reference rotor speed. The reference speed, actual speed and error between them in rpm of the emulator are shown in Fig. 5.21d. The upper trace shows that after some transients, the speed of DC motor always followed the reference speed of the controller. Therefore, the error was always minimized at steady state. It can be observed that the transition time takes less than 12 seconds at the startup of emulator before the algorithm reaches its steady states. As discussed in Section 5.1.1.2, an acceptable performance of the emulator is determined by two criteria namely, achieving the furling control and expected dynamics; and tracking the theoretical speed of the rotor by the DC motor. Both criteria were achieved as demonstrated by the experimental results described above.

5.3.2 Power Loss in the Systems

The grid connected PMG and WRIG-based small wind turbine system experimental power loss results are presented in this section. The emulator was coupled to the PMG and WRIG and the required power conditioning system was implemented as described in Section 5.1.2. The MPPT control was implemented through an external PC for the PMG-based system, while the external rotor resistance was varied for the WRIG-based system. The instantaneous values for the voltage and current were recorded through a power harmonics analyzer, which was connected to an external PC using serial interface. The

gear ratio for the PMG-based system was 2.2 and the emulator was operated at the corresponding optimum speed for each wind speed. Both of the systems were subjected to the same wind speed input as used for the emulator and the corresponding voltage and current values were used for computation of the power losses for each component as described in Section 5.2. The system was allowed to rotate at different speeds with the varying wind speeds in order to ensure the maximum power transfer to the grid. It should be mentioned that the experimental voltage and current used for computation of the power losses are presented only for a wind speed of 6 m/s.

5.3.2.1 Power Loss of the PMG-based System

Fig. 5.22a shows instantaneous line-to-line output voltage, v_{ac} of the PMG, while Fig. 5.22b depicts line current, i_a input to the rectifier when the PMG is operating at 25 Hz, i.e., 749 rpm. It is observed that the generated voltage waveform is non-sinusoidal in nature, with saturated maximum and minimum values. This is mainly due to the mechanical arrangement of the generator, i.e., number of poles and the diameter of the generator. There is not enough width for the magnets to cover 3 coils at same time for the sinusoidal waveform to form properly due to the fast rotation of the stator magnet transversing across the stator winding, resulting in saturation of the maximum values. Furthermore, in order to quantify the distortion of the voltage and current, the harmonic content and Total Harmonic Distortion (THD) of the generated PMG voltage and current were obtained. The results are summarized in Fig. 5.23a and Fig. 5.23b. The fundamental components were omitted in these figures, in order to highlight the harmonic content. From the figures it is observed that 5^{th}, 7^{th}, 11^{th}, 13^{th}, 17^{th} and 19^{th} harmonics are

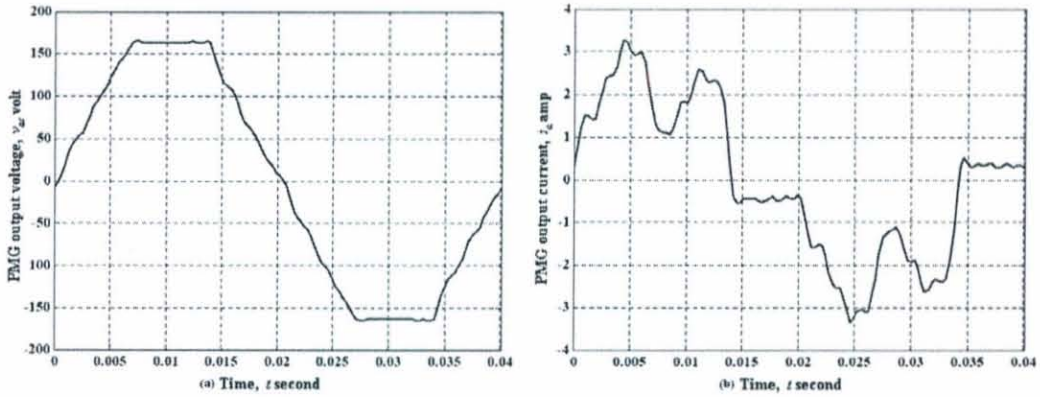

Fig. 5.22 Instantaneous value of the PMG output a) Line-to-line voltage v_{ac}, b) Line current i_a

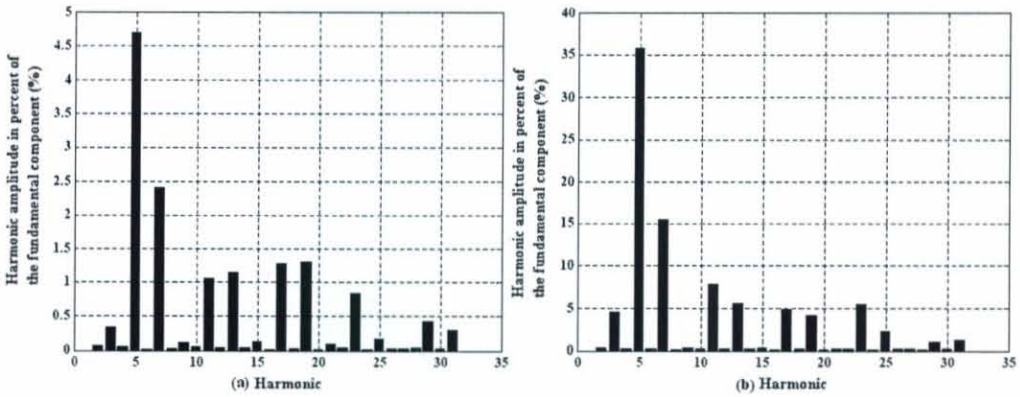

Fig. 5.23 Harmonic content of the PMG output a) Voltage, b) Current

significant for the voltage, while the 5th, 7th, 11th, 13th, 17th, 19th and 23rd harmonics are significant for the current. The total harmonic distortion (THD) was determined to be 5.89% and 41.4% for the voltage and current respectively, which is quite high. The presence of the high and low-order harmonics in the voltage and current is obviously not undesirable. High-order harmonics can interfere with sensitive electronics and communication systems, while low-order harmonics can cause over heating of the generator and conductors which is not undesirable for a small wind turbine system. In

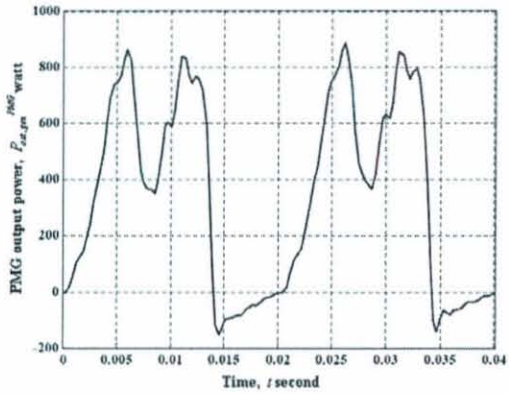

Fig. 5.24 Instantaneous power of the PMG output

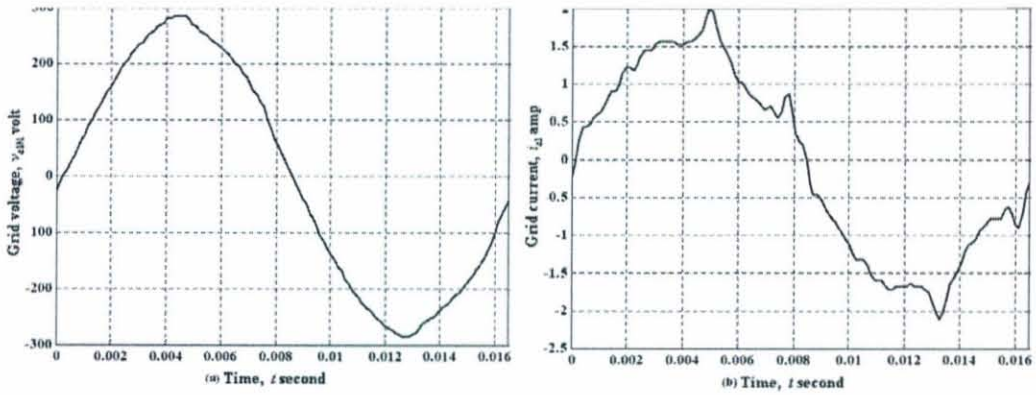

Fig. 5.25 a) Instantaneous grid a) Line-to-line voltage v_{a1b1}, b) Line current i_{a1}

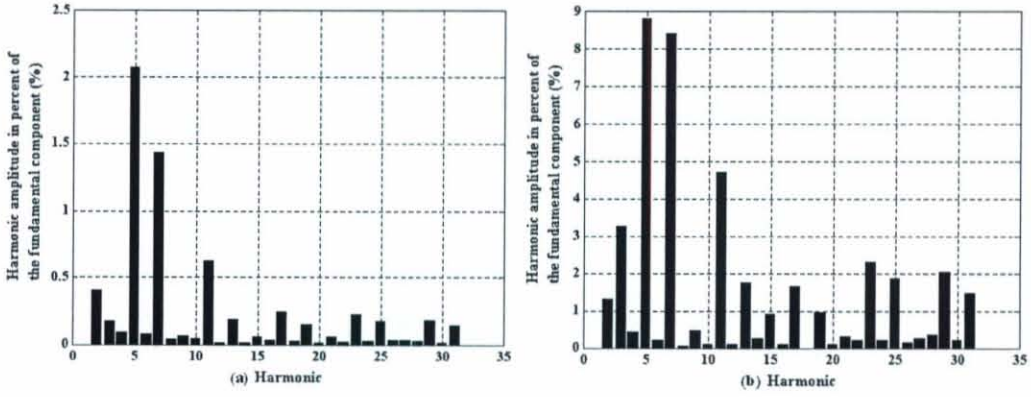

Fig. 5.26 Harmonic content of the grid output a) Voltage, b) Current

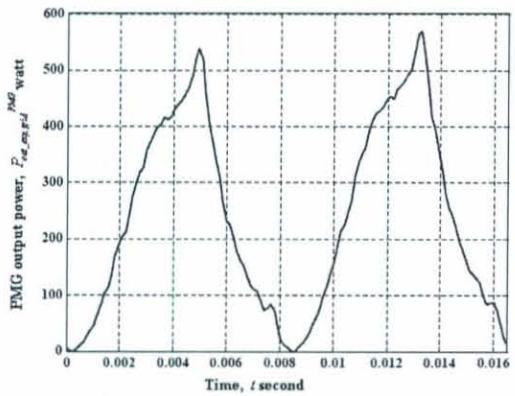

Fig. 5.27 Instantaneous power injection to the grid

addition, regulation of the harmonics will increase the cost of the system to a great extent. The calculated instantaneous power, $P_{out,gen}^{PMG}$ (Fig. 5.24) corresponding to the PMG output voltage and current is averaged as 335W, while the rectified DC power, $P_{out,rec}^{PMG}$ at the output of the 3-phase bridge rectifier is found as 326 W using (5.15). As a result, the 3-phase bridge rectifier power loss, $P_{l,rec}^{PMG}$ is calculated as 9 W by (5.16). The grid voltage, v_{a1b1} current, i_{a1} and power are shown in Fig. 5.25a and Fig. 5.25b. A frequency of 60.5 Hz is observed. The harmonic content for the voltage and current is presented in Fig. 5.26a and Fig. 5.26b respectively. It can be seen that the 5th, 7th, 11th, 17th, and 23rd harmonic content of the voltage is significant, while the 5th, 7th, 11th, 13th, 17th, 23rd, 25th, 29th and 31st is significant for the current. The THD for the voltage and current is 2.68% and 14.3% respectively. The high THD of the current is because of the operation of the BCI unit at a low power level. The average power, $P_{out\_exp,grid}^{PMG}$ flowing into the grid is calculated as 238 W from the instantaneous power curve given in Fig. 5.27, which is quite

close to the rated maximum power of 254 W at 6 m/s wind speed. However, the commercial value of the grid power, $P_{out\_com,grid}^{PMG}$ from the BCI unit is found to be 242 W, which is slightly higher than the value found by the experimentation. The experimental, P_{t_exp,BCI_unit}^{PMG} and commercial, P_{t_com,BCI_unit}^{PMG} power losses of the BCI unit are 89 W and 85 W respectively. The experimental and commercial values of grid power are less than the generator power due to the system losses.

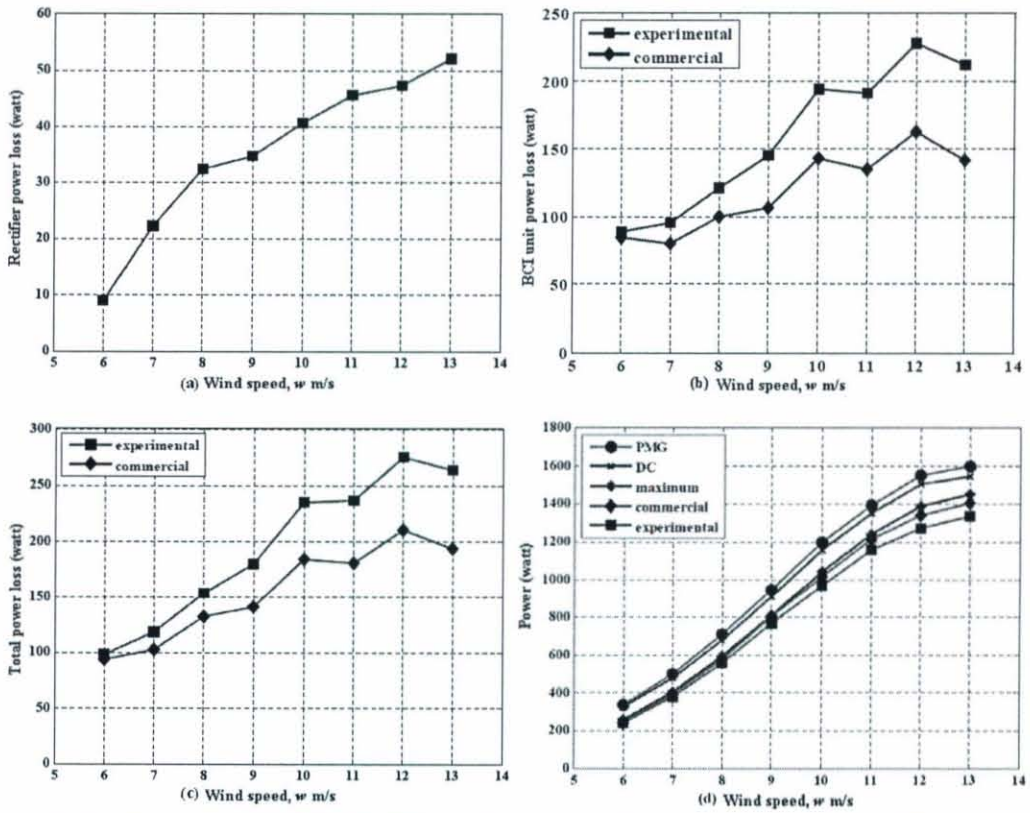

Fig. 5.28 Characteristic of the PMG-based system a) Rectifier power loss, b) BCI unit power loss, c) Total power loss, d) Power at different stages

The calculation procedures described above based on the experimental voltage and current waveform is applied to all wind speeds and power losses for each component are determined. Fig. 5.28a depicts the power losses of the rectifier when the system is subjected to the same wind speed profile that was applied to the emulator. The wind speed of 6 m/s is included in the presentation of the results for convenience of observing the behavior of system. It can be seen that the rectifier power loss increases with increasing wind speed and reaches a maximum of 52 W at a wind speed of 13 m/s. The BCI unit power losses are depicted in Fig. 5.28b. A significant difference between the experimental and commercial power values is observed. This is because the commercial BCI unit never mentions the accuracy of their internal instrumentation that usually used for data collection. As a result, with a lower accuracy on the commercially available BCI unit, it is expected to provide a high value, while it differs a lot in absolute terms when experimentation carried out with the same instruments. This is also a reason why people mislead when calculating the expected outcome from a small wind turbine system using the manufacturers' data sheet values. Moreover, the circumstances become more severe when the BCI unit operates at high wind speed. At high wind speed, the BCI unit operates with higher values of voltage and current and consequently power losses increase and so does the difference between experimental and commercial loss. The sum of the losses of the rectifier and BCI unit provides the total power losses (commercial and experimental) of the PCS as illustrated in Fig. 5.28c, while Fig. 5.28d incorporates power values at several stages of the system. The PMG output power has the highest value as expected. The theoretical maximum power of the system is presented and can be seen that the experimental and commercial power nearly follows the maximum power values for

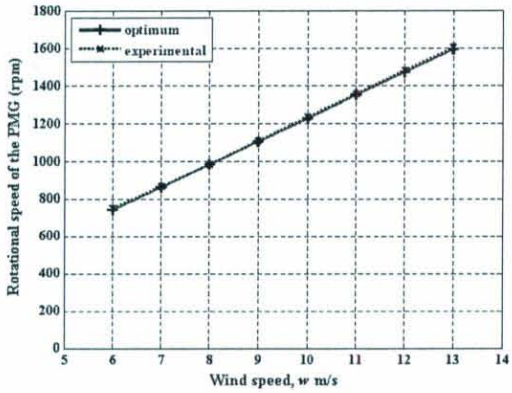

Fig. 5.29 Variation of the speed of the PMG with wind speed

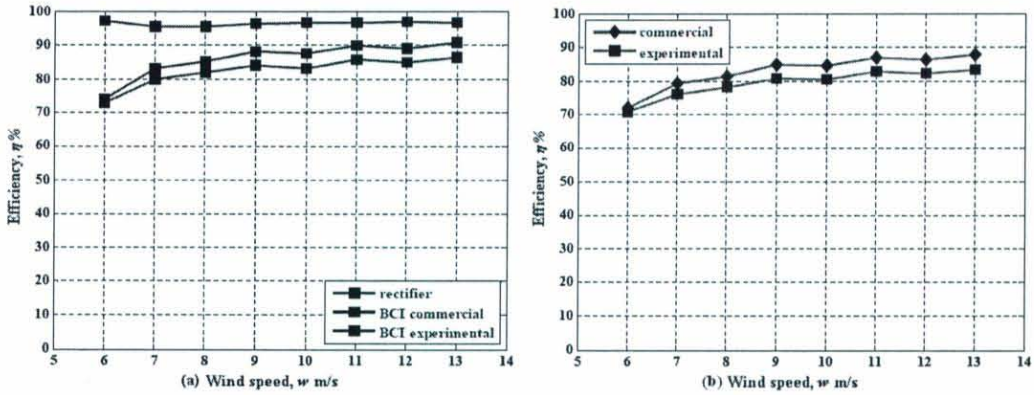

Fig. 5.30 Variation of the efficiency a) Component, b) Composite

each wind speed and the corresponding rotational speed is presented in Fig. 5.29. It can be seen that for each wind speed, the system is able to produce maximum power, while maintaining the optimum speed and ensuring the MPPT control strategy. It should be mentioned that the experimental and commercial power values are not exactly the same as the theoretical maximum power values; however, they behave logically. Fig. 5.30a shows the efficiency characteristics of the rectifier and BCI unit in the case where the wind speed is changed from low to high under the condition of maximum power transfer to the grid. The measured efficiency of the rectifier η_{rec} is at least 97%, while the

experimental efficiency, η_{exp,BCI_unit} and commercial efficiency, η_{com,BCI_unit} for the BCI unit is 86% and 91% respectively. A lower experimental value is observed which is expected as the power losses of the BCI unit from the experimental is higher than the

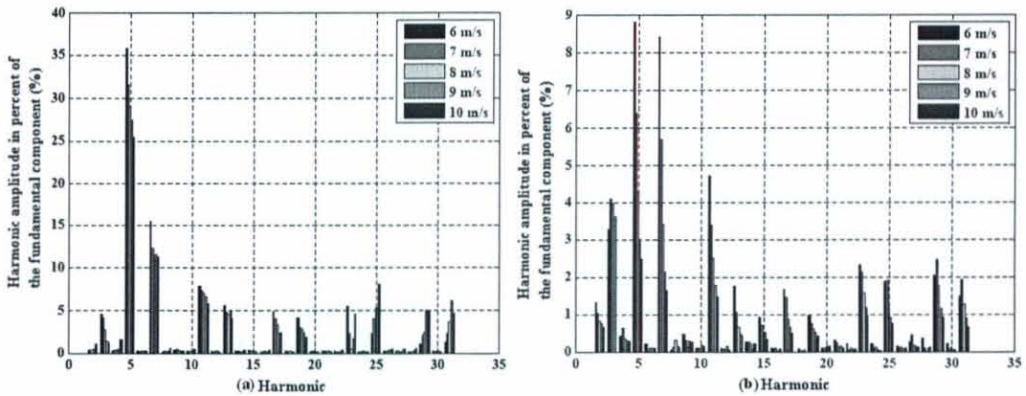

Fig. 5.31 Harmonic content of the a) PMG output current, b) Grid output current

commercial. The composite efficiency is the product of rectifier and BCI unit efficiencies and illustrated in Fig. 5.30b. Both experimental, $\eta_{exp,composite}$ and commercial, $\eta_{com,composite}$ efficiency is more than 80% at high wind speed situation. Indeed the experimental efficiency is lower in value than the commercial efficiency, and the results suggest that the manufacturer's stated efficiency may not be reliable. The generalized claim of the manufacturers rarely mentions the operating condition of a system. From the composite efficiency, it is observed that the efficiency drops at low wind speed, i.e., light load; a typical challenge in variable speed wind generation system. Another point worthy of note is that at full load, the generated current harmonic content will be minimized due to the influence of machine stator equivalent inductance and resistance, while the grid current harmonic content will be minimized because the BCI unit will operate at a high power

level. Fortunately, this effect was noticeable when the wind speed increases and therefore, the maximal output power increases and the THD decreases as presented by Fig. 5.31a and Fig. 5.31b with a wind speed variation of 6 m/s to 10 m/s.

5.3.2.2 Power Loss of the WRIG-based System

Figures 5.32 a-d show the observed instantaneous waveforms of the line-to-line stator voltages v_{a3c3}, v_{b3c3} and line current i_{a3}, i_{b3} respectively when the system is operating at 60.5 Hz in steady state. From the measurement result of the stator voltage and current, the instantaneous values of the power are calculated and presented in Fig. 5.32e and Fig. 5.32f. The sum of the average value of the generated stator electric power, $P_{out\_exp,grid}^{WRIG}$ is 243 W, which is quite close to the rated maximum power of 254 W at 6 m/s wind speed. In addition, the stator voltage and current is essentially sinusoidal, which is a desirable feature because harmonics in the supply may produce adverse effects on the supply system. The experimental instantaneous waveforms for the rotor voltage and current are presented in Fig. 5.33a and Fig. 5.33b respectively when the generator is operating at 17.5 Hz, i.e., 527 rpm at super synchronous speed. The rotor voltage is sinusoidal and is rich in harmonics, which is easily notable from the harmonic of rotor voltage as presented in Fig. 5.34a. It can be seen that the high as well as low-order harmonic contents are present; however, the amplitude as well as the THD (11.9%) are low. In contrast to the voltage, the effect of commutation overlap is evident from the waveform of the rotor current and is not sinusoidal. The associated harmonic content is presented in Fig. 5.34b, and it can be seen that the 5^{th} and 7^{th} harmonics have the dominant effect on the rotor current and the THD was found to be 23.7%. The THD for

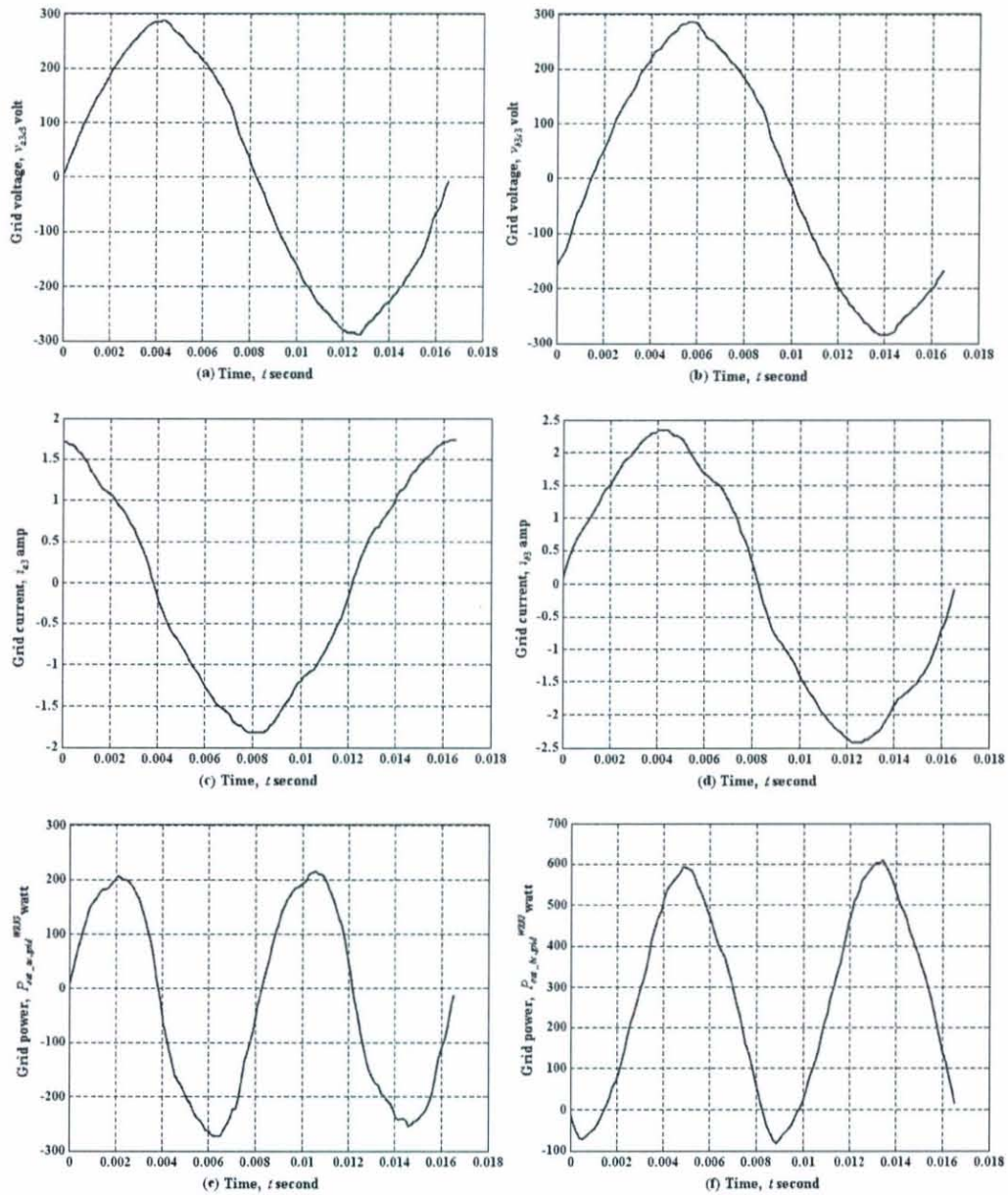

Fig. 5.32 Instantaneous value of stator a) Line-to-line voltage v_{a3c3}, (b) Line-to-line voltage v_{b3c3}, c) Line current i_{a3}, d) Line current i_{b3}, e) Line power $P_{out\_ac,grid}^{WRIG}$, f) Line power $P_{out\_bc,grid}^{WRIG}$

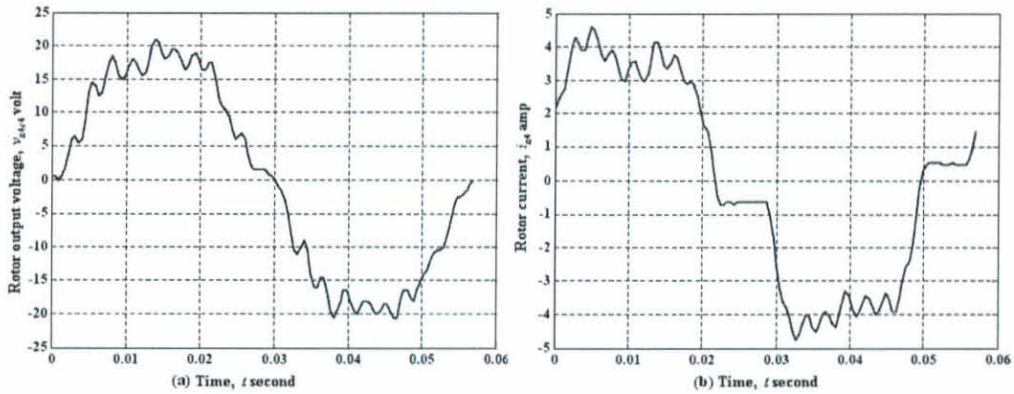

Fig. 5.33 Instantaneous rotor output a) Line-to-line voltage v_{a4c4}, b) Line current i_{a4}

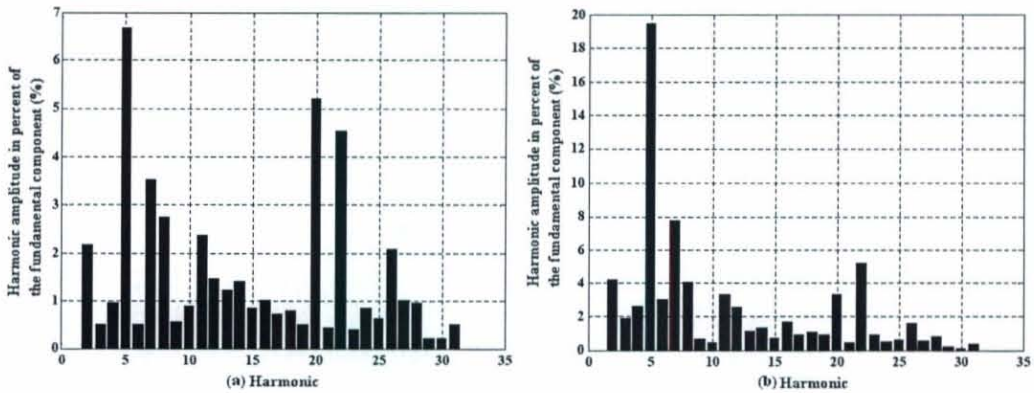

Fig. 5.34 Harmonic content of the rotor output a) Voltage, b) Current

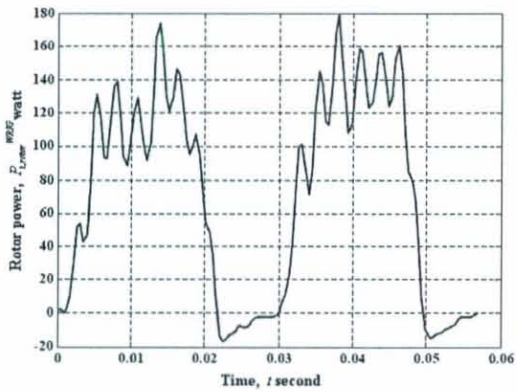

Fig. 5.35 Instantaneous power output from the rotor

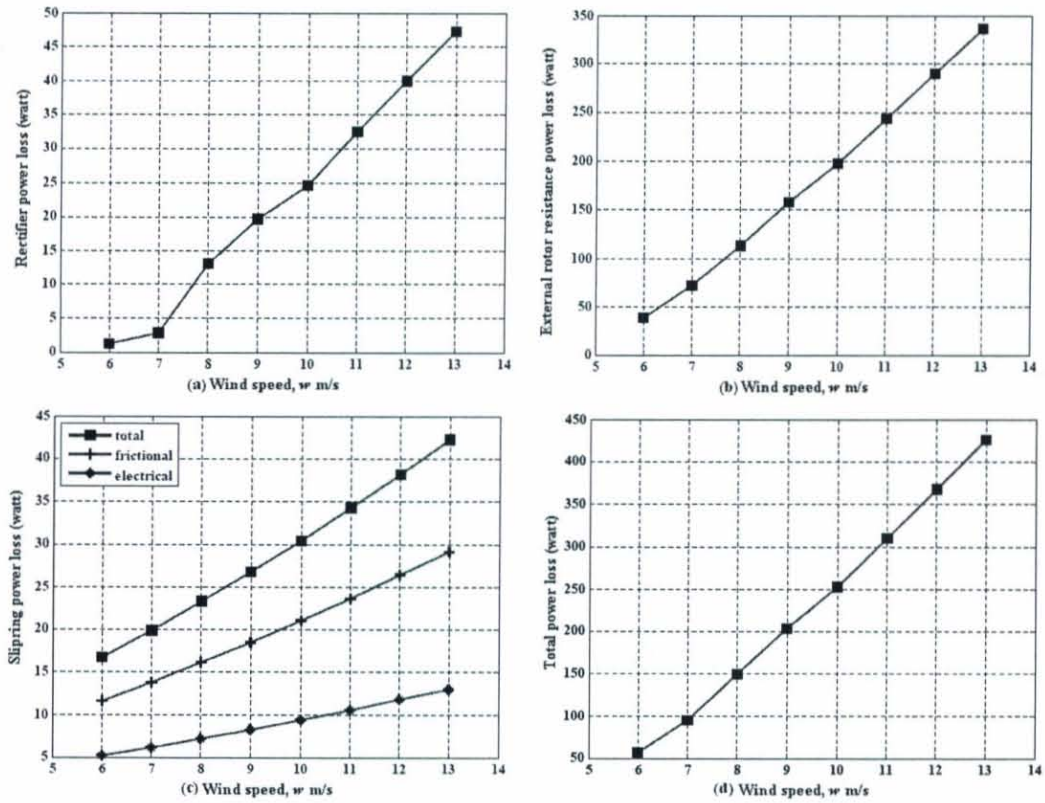

Fig. 5.36 Characteristic of the losses of the WRIG-based system a) Rectifier, b) External rotor resistance, c) Slip ring, d) Total power loss

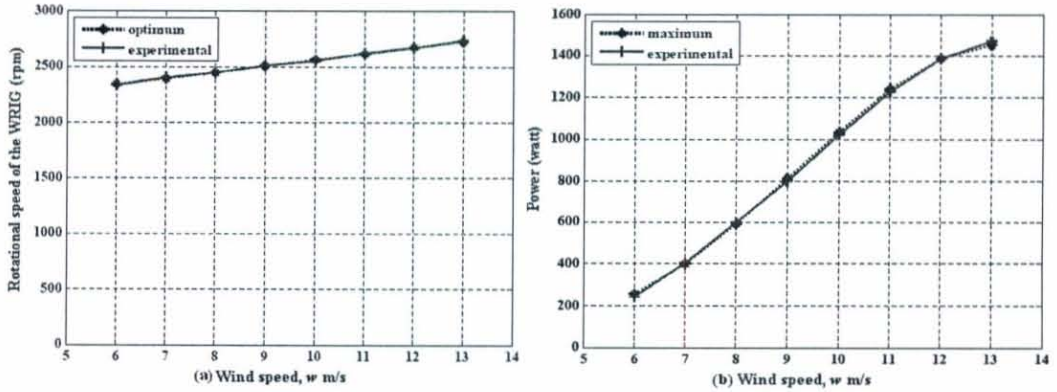

Fig. 5.37 Variation with the wind speed a) Shaft speed, b) Power to the grid

both voltage and current is quite high. The power graph (Fig. 5.35) produces an average instantaneous power loss, $P_{t,rotor}^{WRIG}$ into the rotor circuit which was amended to the corresponding slip as 40 W. The power loss in the external rotor resistance $P_{t,ext}^{WRIG}$ was found to be 38 W and after calculation, the rectifier power loss, $P_{t,rec}^{WRIG}$ was found to be 2W. The slip-ring electrical, $P_{elec\_slipring}^{WRIG}$ and frictional, $P_{fric\_slipring}^{WRIG}$ losses were calculated based on the speed of the generator and were found to be 5 W and 12 W respectively. The same procedure was repeated for the same wind profile applied to the emulator. The results of the losses of the rectifier are presented in Fig. 5.36a. The external rotor resistance losses are presented in Fig. 5.36b, while the electrical, frictional and total losses of the slip ring are presented in Fig. 5.36c. The summation of all the losses is the total power losses of the system and is depicted in Fig. 5.36d. Power losses increase with increase in wind speed, which is an expected behavior from the system. In order to verify the MPPT control strategy, the speed of the system (optimum and experimental) is recorded and presented in Fig. 5.37a, followed by the corresponding power injection to the grid (maximum and experimental) by the stator, in Fig. 5.37b. It is evident from this figure that the experimental grid power and speed maintains a high agreement with the theoretical maximum power and speed for each wind speed, which consequently ensures the MPPT control strategy.

5.3.3. Performance Characteristic of the Systems

One of the basic objectives of this research is to compare the losses over a period of a year, i.e., overall efficiency for the two systems in a number of wind conditions. As presented in Chapter 4, eight sites were selected and compared for a wind speed range of

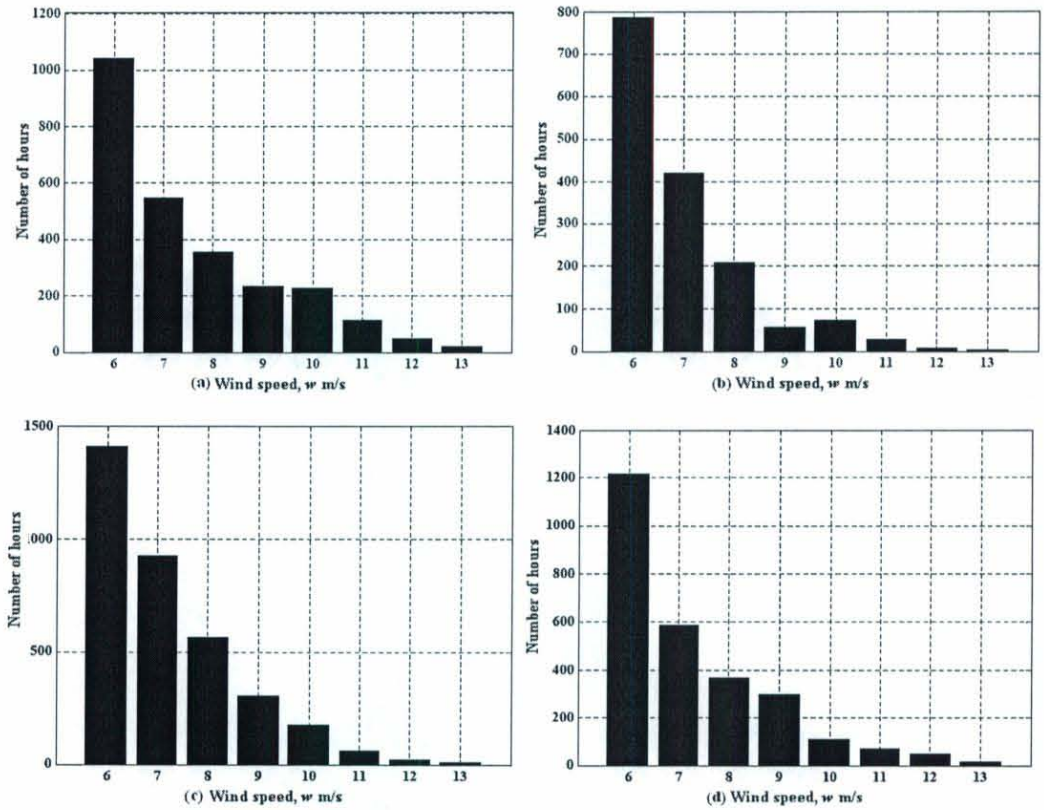

Fig. 5.38 Wind speed distribution for a) Battle Harbour (BH), b) Cartwright (CW), c) Little Bay Island (LB), d) Mary's Harbour (MH)

2 m/s to 17 m/s and conclusions were drawn. However, as far as the experimentation is concerned, the same eight sites were considered and the respective wind speed distributions are presented in Fig. 5.38 and Fig. 5.39, which can be reproduced from the wind speed distribution presented in Chapter 4. The annual energy capture of the PMG and WRIG-based system was calculated as presented in Section 4.3 in Chapter 4. The power loss for the PMG and WRIG-based system for the wind speeds are presented above used to calculate the AEL of each system, as described in Section 4.3. It should be mentioned that due to the introduction of commercial power loss of the PCS, the annual

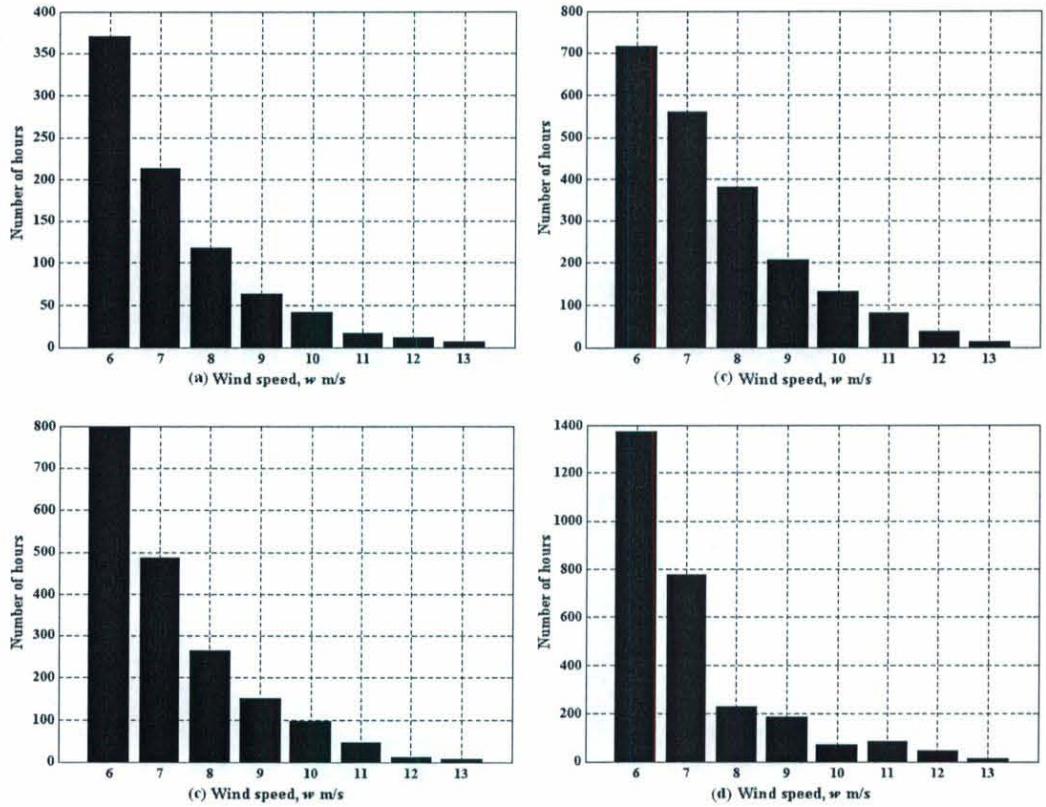

Fig. 5.39 Wind speed distribution for a) Nain (NA), b) Ramea (RA), c) St. Brendan's (SB), d) St. John's (SJ)

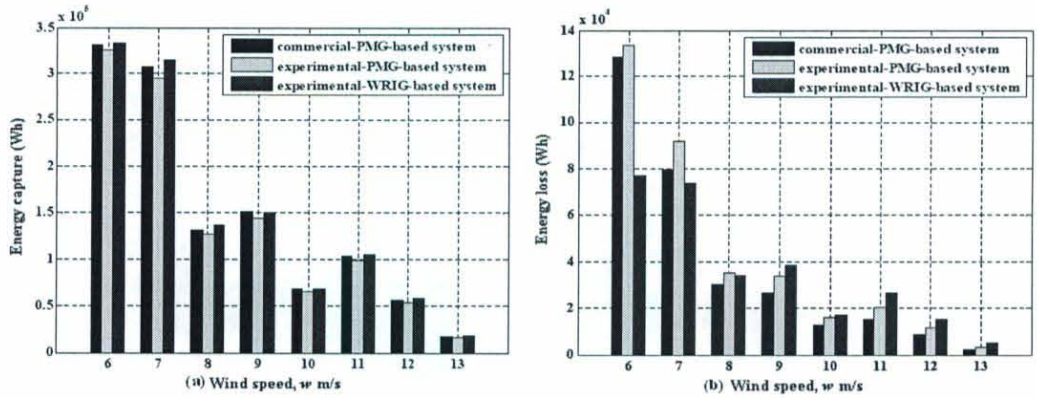

Fig. 5.40 Variation of energy for St. John's, a) Energy capture, b) Energy loss

energy capture, annual energy loss and efficiency will be different for the PMG-based system, while the WRIG-based system is not subjected to such situation. In order to observe the effect of low wind speed regime for of the 8 sites considered, an example using St. John's is presented because other regions behaved more or less the same. The resulting energy capture, energy loss is presented in Fig. 5.40a and Fig. 5.40b respectively. It is notable that the WRIG-based system is more efficient for the low wind speed regime though higher energy losses occur at the high wind regime. However, the high frequency of occurrence of low wind speed would diminish the effect of high energy loss on the system efficiency and will make the WRIG-based system more efficient than the PMG-based system.

Fig. 5.41a depicts the annual energy capture by the PMG-based system (experimental and commercial) and WRIG-based system. It is evident that the commercial energy production of the PMG-based system always shows a higher value than the experimental, which is because low power values were observed in all experiments. Although the maximum power is supposed to be the same for both systems, a slight variation in values was observed for the maximum power for both systems and reflected on the annual energy capture values. This deviation is not unusual as it is very difficult to inject the same power to the grid. However, it should not affect the calculation as more (less) power injection to the grid will produce more (less) power losses on the required power electronics for each system. Fig. 5.41b shows the AEL for both systems and several interesting points can be noticed. The AEL for the WRIG-based system is lower for all sites than the calculated AEL of the PMG-based system. But the commercial AEL of the PMG-based system is lower than the WRIG-based system at Battle Harbour and Ramea,

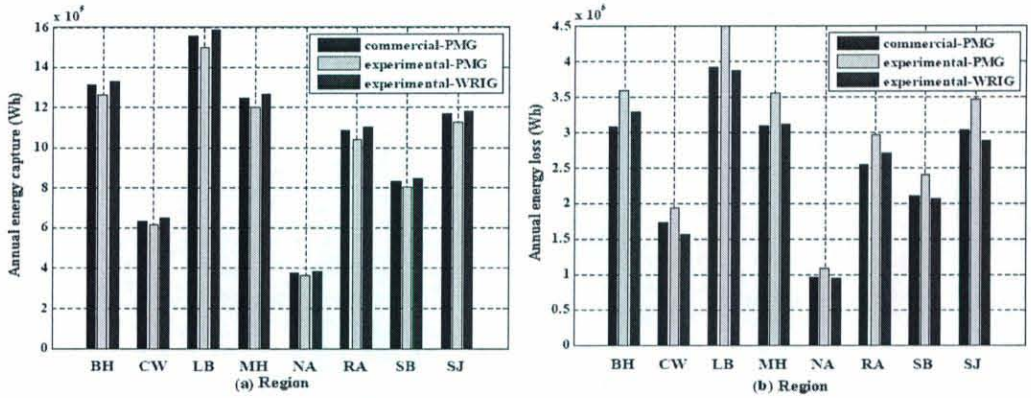

Fig. 5.41 a) Annual energy capture for the PMG and WRIG-based system, b) Annual energy loss for the PMG and WRIG-based system

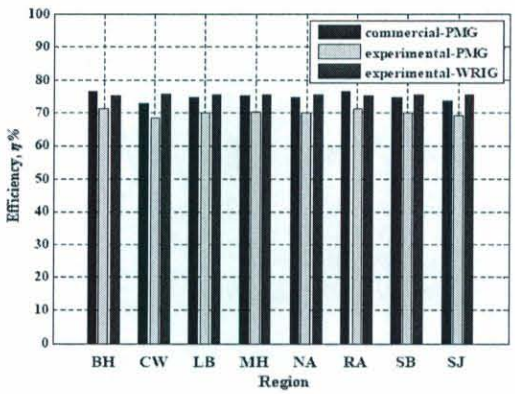

Fig. 5.42 Variation in efficiency for the PMG and WRIG-based system

while the AEL remains almost the same for Mary's Harbour and Nain. This is a very important point to consider as relying on the manufacturer values could lead to a miscalculation of the annual energy loss of a system and could discourage the possible penetration of a specific system. However, it should be observed from the total power losses figures that the total power loss of the WRIG-based system remains low for wind speeds up to 7 m/s, but starts to increase above 7 m/s. Therefore, from cut-in wind speed to 7 m/s wind speed, the total power losses are less than the PMG-based system. In

Table 5.1 Performance characteristics of the PMG-based SWT system

Region	Annual energy capture [Wh]		Annual energy loss as a percentage of the annual energy capture				Efficiency, η [%]	
	Com	Exp	Diode bridge rectifier [%]		BCI unit [%]			
			Com	Exp	Com	Exp	Com	Exp
BH	1311280	1260084	4.43	4.61	19.03	23.87	76.52	71.50
CW	635363	613573	4.62	4.79	22.37	26.71	73	68.49
LB	1556458	1499049	4.66	4.84	20.49	25.11	74.83	70.04
MH	1247259	1200958	4.50	4.67	20.22	24.86	75.26	70.45
NA	377700	363818	4.57	4.74	20.59	25.19	74.83	70.06
RA	1081526	1039260	4.60	4.78	18.81	23.64	76.58	71.56
SB	831915	801319	4.60	4.78	20.58	25.19	74.80	70.02
SJ	1165376	1124061	4.50	4.66	21.54	26.01	73.94	69.31

Table 5.2 Performance characteristics of the WRIG-based SWT system

Region	Annual energy capture [Wh]	Annual energy loss as a percentage of the annual energy capture				Efficiency, η [%]
		Slip ring electrical [%]	Slip ring frictional [%]	Diode bridge rectifier [%]	Switch and external rotor resistance [%]	
BH	1331215	1.29	2.91	1.80	18.61	75.36
CW	645811	1.49	3.35	1.38	17.90	75.86
LB	1581484	1.39	3.13	1.58	18.26	75.61
MH	1266039	1.37	3.08	1.67	18.40	75.45
NA	383953	1.39	3.13	1.60	18.32	75.53
RA	1100044	1.30	2.91	1.78	18.62	75.36
SB	844841	1.40	3.14	1.58	18.25	75.62
SJ	1183171	1.45	3.27	1.46	18.12	75.68

addition, the wind speed distribution shows that the systems face low wind speed most of the time of the year, which suggests higher power loss in the PMG based system rather than the WRIG-based system. So even if the commercial AEL of the PMG-system is same or lower, it will eventually be higher if a full scale testing is performed. The efficiency for the PMG-based system (experimental and commercial) and WRIG-based system is presented in Fig. 5.42, which shows that the WRIG-based system maintains a high efficiency for most of the system. Table 5.1 and Table 5.2 show the comparison of the performance characteristics for the PMG and WRIG-based system respectively from 7 m/s to 13 m/s wind speeds for all eight sites. The tables include the annual energy capture as well as the energy loss as a percentage of the annual energy capture for both systems. It is notable that the difference between the commercial and experimental AEC is certainly a large amount and results in a difference of efficiency of around 4% - 5% for all sites. Moreover, considering the experimental efficiency of the PMG-based system, the efficiency of the WRIG-based system is around 5% higher for all eight sites. As a result it is concluded that the WRIG-based system could be an optimum surrogate in the small wind energy conversion area.

5.4 Summary

The experimental test bench results that have been presented in this Chapter reveal several important observations which validate the conclusions from the numerical simulation presented in Chapter 4. The synopses of the investigation are presented below:

- A furling control and resulting dynamics based wind turbine emulator was developed that emulates the behavior of a wind turbine in the laboratory. The criteria imposed on the emulator performance were satisfied;
- A complete development and implementation of the PMG and WRIG-based system was undertaken and the required maximum power point control strategy was defined for each system. It was found that both of the systems were able to sustain the maximum power point control strategy, thus ensuring the variable speed operation;
- A procedure to calculate the power losses for each system was described and it was found that the WRIG-based system provides less power loss at low wind speed regime than the PMG-based system;
- Efficiency of the systems was calculated for eight sites in Newfoundland and Labrador. A significant difference was observed between the commercial and experimental AEC for a PMG-based system. This difference reflected on the efficiency values and it was found that the experimental efficiency was 5% lower than the commercial efficiency for a PMG-based system;
- It was found that a WRIG-based system could provide 5% higher efficiency than a PMG-based system when considering the experimental efficiency values for both systems and consequently, can be considered to be a better option for high penetration of wind energy in future.

Chapter 6

Reliability Comparison

The purpose of this chapter is to investigate the reliability of the power conditioning system of a Permanent Magnet Generator (PMG) and Wound Rotor Induction Generator (WRIG)-based system. This chapter focuses on 1) development of the mathematical model for the reliability of the power conditioning system; 2) the identification of the least reliable subsystem within the power conditioning system; and 3) calculation of the reliability of the systems. A comparative study is also performed in order to investigate an optimum system for the small wind power generation.

6.1 Failure Rate and Reliability of a Device

The failure rate of a device can be described by the Bathtub curve (Fig. 6.1), which represents the failure rate over the lifetime of a component or system [110,111]. There are two areas of high failure rate, early and wear out failures. Early failures are most often due to manufacturing defects of the device. Wear out failures are due to the natural aging of the device. The failure rate of the device is constant in the middle where the failure is random. This region is used to model the expected life time of the system. The

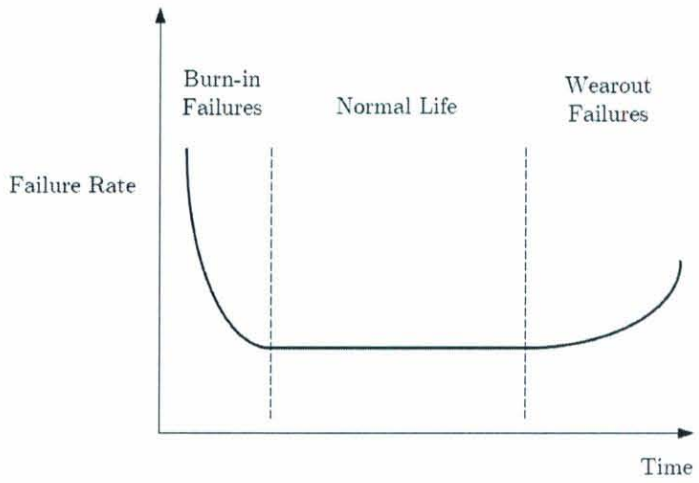

Fig. 6.1 Failure rate curve

reliability of a system can be determined from the failure rates of the devices that comprise the system. It is important to note that the reliability of a system is related to the operating conditions and parameters, known as covariates. The covariates represent the stress on the device, which can include, but are not limited to, current, voltage, and temperature. The failure rate of a system can be described by [110, 111].

$$\delta(t,z)=\delta_0(t)\exp\left(z\overline{\beta}\right) \tag{6.1}$$

where, δ_0 is the base line failure rate, z is a vector containing covariates, and $\overline{\beta}$ is a vector of regression coefficients.

Under rated conditions, the reliability of a system is a constant function of time, $R_0(t)$, the base line reliability. The reliability of the system including the covariates is given by [112].

$$R(t,z)=R_0(t)\exp\left(-z\overline{\beta}\right) \tag{6.2}$$

Under different operating parameters, there are de-rating factors associated with the current, voltage, and temperature that are outside of the normal operating ranges. These de-rating factors negatively affect the reliability. As a result, the system reliability can be modeled as a constant base reliability plus an additional factor for each rating above the normal ranges. An example of such rating would be operating a device at a higher temperature than it is rated value or at a higher power level. According to Reliasoft Incorporation, this is a common practice for accelerated life testing [69, 113]. By applying an increased stress over a short time interval, it is possible to simulate a lesser stress over a longer time period.

6.2 Arrhenius Life Model

Accelerated life testing employs a variety of high stress test methods that shorten the life of a device or quicken the degradation of the product's performance. The goal of such testing is to efficiently obtain performance data that, when properly analyzed, yields reasonable estimates of the devices's life or performance under normal conditions. A variety of high stress test methods can be employed to shorten the life of a device and/or quicken the degradation of product performance. This induces early failures that would sometimes manifest themselves in the early years of a devices life, and also allows issues related to design tolerances to be discovered before commercial manufacturing. Both the type of stressor and the time under test are used to determine the normal lifetime. There are various stressors including, but not limited to, heat, humidity, temperature, vibration, voltage, current and load. The effect of these stressors on the devices's life can be mathematically determined. However, when it is necessary to calculate or predict the reliability of some electronic equipment, the Arrhenius life-stress model (or relationship)

is probably the most common life-stress relationship utilized in life prediction of the material [67]. It has been widely used when the stimulus or acceleration variable (or stress) is thermal (*i.e.* temperature). It is derived from the Arrhenius reaction rate equation proposed by the Swedish physical chemist Svandte Arrhenius in 1887. The Arrhenius reaction rate equation is given by [112, 113]

$$R(T_r) = A\exp\left(\frac{-E_A}{KT_r}\right) \tag{6.3}$$

where R is the speed of reaction or failure rate, T_r is the absolute temperature in Kelvin, K is the Boltzman's constant, E_A is the activation energy of the semiconductor, and A is the model parameter.

The reaction represents the rate of decay and is useful for representing the life of a device when temperature is a stress variable. As the temperature increases, the energy available to initiate a reaction increases. The activation energy denoted by E_A is the amount of energy required for a molecule to take part in the reaction. As the temperature increases, the reaction increases, reducing the life of the component. The Arrhenius life-stress model is derived from the reaction rate equation by assuming life time is proportional to the inverse reaction rate of the process. The life time of the device can be expressed as

$$L(V) = C\exp\left(\frac{E_A}{KT_r}\right) \tag{6.4}$$

where L is the quantitative life measurement (hours), C is the model parameter and V is the stress (based on temperature in Kelvin)

6.3 Reliability Calculation

Reliability is the probability that a component will satisfactorily perform its intended

function under given operating conditions. The average time of satisfactory operation of a system is the Mean Time Between Failures (MTBF) and a higher value of MTBF refers to a system of higher reliability and vice versa. As a result, engineers and designers always strive to achieve higher MTBF of the power electronic components for a reliable design of the power electronic systems. The MTBF calculated in this chapter is carried out at the component level and is based on the life time relationship where the failure rate is constant over time in a bathtub curve [111]. In addition, the system is considered repairable. It is assumed that the system components are connected in series from the reliability standpoint. The lifetime of a power semiconductor is calculated by considering junction temperature as a covariate for the expected reliability model. The junction temperature for a semiconductor device can be calculated as [114].

$$T_J = T_A + P_{loss} R_{JA} \tag{6.5}$$

P_{loss} is the power loss (switching and conduction loss) generated within a semiconductor device and can be found by replacing the P_{loss} from the loss analysis described in Section 4.2 of Chapter 4 for each component.

The life time, $L(T_J)$ of a semiconductor is then described as

$$L(T_J) = L_0 \exp(-B\Delta T_J) \tag{6.6}$$

where

L_0 is the quantitative normal life measurement (hours) assumed to be 1×10^6

$B = \frac{E_A}{K}$, K is Boltzmann's constant which has a value of 8.6×10^{-5} eV/K, E_A is the activation energy, which is assumed to be .2 eV, a typical value for semiconductors

[116], T_A and ΔT_J are the ambient temperature and variation of junction temperature respectively and can be expressed as

$$\Delta T_J = \frac{1}{T_A} - \frac{1}{T_J} \tag{6.7}$$

The failure rate is described by

$$\gamma = \frac{1}{L(T_J)} \tag{6.8}$$

The global failure rate, γ_{system} is then obtained as the summation of the local failure rates, γ_i as:

$$\gamma_{system} = \sum_{i=1}^{N} \gamma_i \tag{6.9}$$

The Mean Time Between Failures, $MTBF_{system}$ and reliability, R_{system} of the system are given respectively by

$$MTBF_{system} = \frac{1}{\gamma_{system}} \tag{6.10}$$

$$R_{system} = e^{-\gamma_{system} t} \tag{6.11}$$

6.3.1 Reliability Calculation of the PMG-based System

The reliability analysis for the PCS of the PMG based configuration is performed by the formulation described in Section 6.3. A Matlab program is developed which computes the component junction temperature using the conduction and switching loss formulations described in Chapter 4, Section 4.2.1. After the determination of the failure rate for each component using (6.8), the program sums up the failure rates to evaluate the

total system failure rates (6.9). The reliability of the system is obtainable once the system MTBF

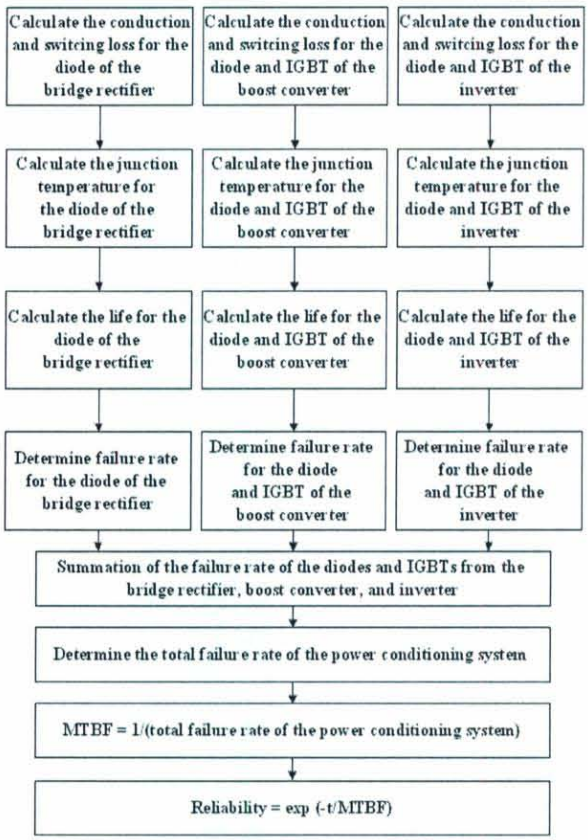

Fig. 6.2 Determining system reliability through component reliability for a PMG-based system

(6.10) is known. A brief schematic of the program and its operating procedure is given in Fig. 6.2.

6.3.2 Reliability Calculation of the WRIG-based System

The procedure described in Section 6.2 is used to calculate the reliability of the rectifier and chopper for the WRIG based system. In addition to the above mentioned method, a partial stress prediction method is used to calculate the reliability of the external rotor

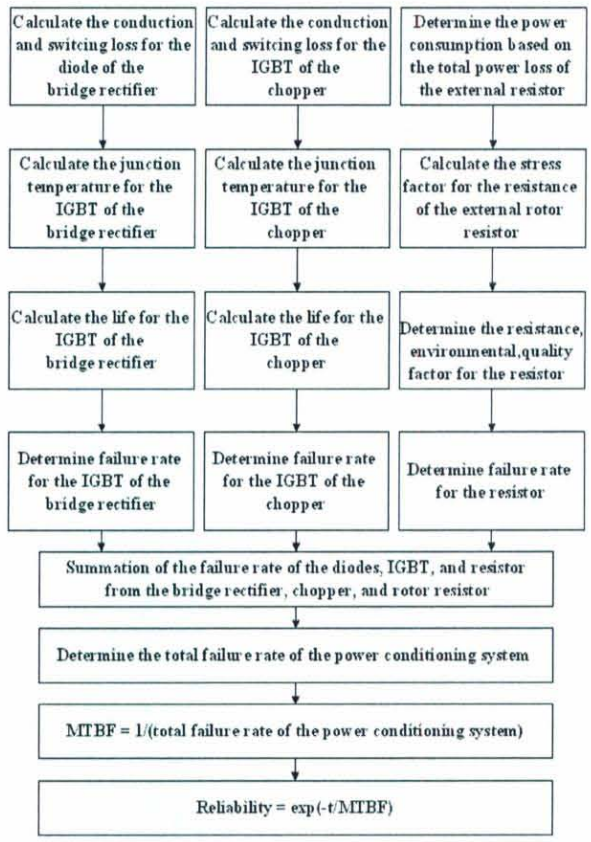

Fig. 6.3 Determining system reliability through component reliability for a WRIG-based SWT

resistor. The method calculates the failure rate of any component by multiplying a base failure rate with operational and environmental stress factors (electrical, thermal etc). It is assumed that the chopper carries a predetermined duty cycle variation. The power loss in the external resistor can be found by simply subtracting the power losses of the chopper from the total power loss produced by $V_D I_D$. Based on this assumption, a commercially available resistor is selected and the stress ratio, S is calculated as the ratio of the

operating power to the rated power of the resistor. The base failure rate, γ_b is than calculated as [76]

$$\gamma_b = 4.5\times10^{-9}\exp\left(12\left(\frac{T_v+273}{343}\right)\right)\exp\left(\frac{S}{.6}\left(\frac{T_v+273}{273}\right)\right) \tag{6.13}$$

where T_v is the ambient temperature (^{0}C) and S is the stress factor.

The failure rate for a wire wound resistor is given by [76]

$$\gamma_R = \gamma_b\pi_R\pi_E\pi_Q\times1\times10^{-6} \text{ failure/ hour.} \tag{6.14}$$

where the resistance factor, π_R is 1 as the external resistance is less than 1 $M\Omega$. The environmental factor, π_E is 1 due to the fact that a harsh environment is not considered, and the quality factor, π_Q is considered to be 15 due to the use of a commercial resistor. A detailed schematic of the calculation procedure is depicted in Fig. 5.3.

6.4 Simulation Results

The analytical calculations illustrated in the preceding Section are carried out to determine the MTBF and consequently the reliability of the systems for a predetermined wind speed condition. The rated power for the wind turbine is assumed to be 1.5 kW. The expected operating condition of the wind turbine is 6 m/s. It is assumed that the generator speed is proportional to the output voltage of the 3-phase rectifier for the PMG-based system. The switching frequency of the boost converter, inverter and chopper is considered as 20 kHz. In order to investigate the worst case scenario of the power loss in the numerical simulation study, the modulation index is assumed to be unity and the load current is assumed to be in phase with the output for the PMG-based system. The analytical calculation is based on the data sheet on the EUPEC IGBT module

Table 6.1 Component reliability for the PMG-based system

Quantity	Rectifier	Boost Converter		Inverter	
	Diode	Diode	IGBT	Diode	IGBT
Power loss [W]	.5587	4.2581	22.3313	2.05459	7.9621
Junction temperature [^{0}K]	298.8101	304.1742	321.4478	303.5238	314.7205
Life expectancy [hr]	9.895×10^5	9.24×10^5	7.5273×10^5	9.3158×10^5	8.1311×10^5
Failure rate [hr^{-1}]	1.0106×10^{-6}	1.0823×10^{-6}	1.3285×10^{-6}	1.0734×10^{-6}	1.2298×10^{-6}

Table 6.2 Component reliability for the WRIG-based system

Quantity	Rectifier	Chopper	External resistor
	Diode	IGBT	
Power loss [W]	.9028	2.0602	31.5280
Junction temperature [^{0}K]	299.3091	302.3264	---
Life expectancy [hr]	9.8311×10^5	9.458×10^5	7.2464×10^6
Failure rate [hr^{-1}]	1.0172×10^{-6}	1.0573×10^{-6}	1.38×10^{-7}

FP15R12W1T4_B3 [99]. The results of the analysis following the procedure outlined are presented in Table 6.1 and Table 6.2 respectively.

The calculation reveals that the PCS failure rate for the PMG-based system is 1.7688×10^{-5} and the MTBF is 5.6537×10^4 hours (6.5 years). The corresponding figures for the WRIG-based system are 7.2984×10^{-6} and 1.3702×10^5 hours (15.8 years). It is

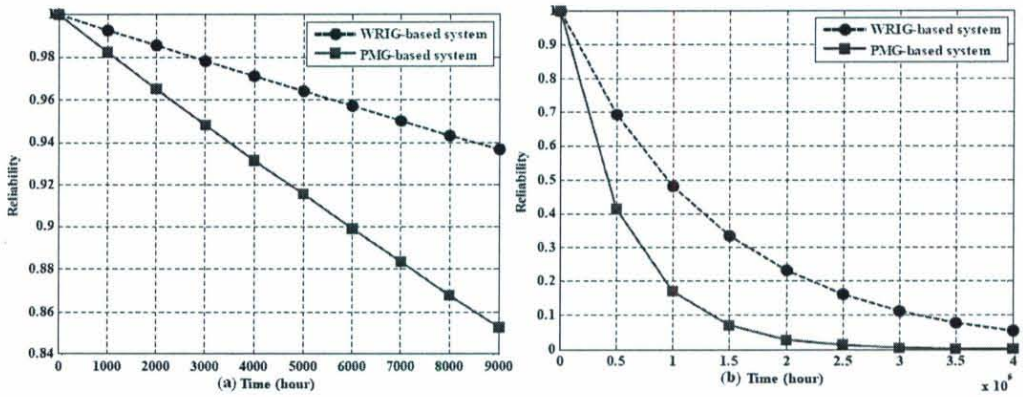

Fig. 6.4 Reliability of the power conditioning system a) Over a year, b) Over time

well understood that the small wind turbine and the PCSs need to be affordable, reliable and most importantly, almost maintenance free for the average person to consider installing one. As can be seen, the need to replace the PCS for the PMG-based system corresponds to the MTBF value of 6.5 years. This leads to a more vulnerable system as compared to the lifespan of the wind turbine system, which is usually 15 to 20 years. Also from the financial standpoint, replacement of such a complex PCS is expensive and needs a highly skilled repair professional. In contrast to the PMG-based system, the WRIG-based system exhibits longer lifetime and remains in a good agreement with the lifespan of the wind turbine, which is 15.8 years.

Fig. 6.4a shows the reliability of the PCS for a period of one year (8760 hours) for the PMG and WRIG-based system. The result reveals that the reliability of the PCS for the PMG-based system drops to 85.28% after one year, while the reliability of the PCS for the WRIG-based system drops to 93.64% after one year. The reliability of the PMG and WRIG-based system with time is presented in Fig. 6.4a and Fig. 6.4b respectively. It is easily noted that the reliability of the PCS for the PMG-based system reaches less than

50% at 40000 hours (4.5 years), this is obviously unacceptable for high penetration of any specific system. In contrast to the PMG-based system, the reliability of the PCS for the WRIG-based system remains more than 70% at 40000 hours (4.5 years), which certainly could save cost of repair for the system. In both scenarios, the PCS of the WRIG-based system illustrates higher reliability than the PMG-based system. The higher reliability value of the WRIG-based system is certainly advantageous in terms of maintenance and replacement costs.

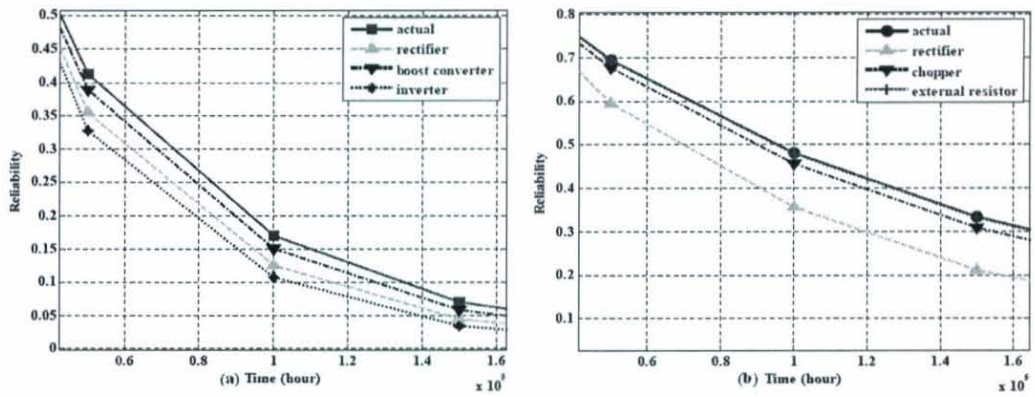

Fig. 6.5 Effect of reliability variation of the components for a) PMG-based system, b) WRIG-based system

Following the calculation of the reliability of the systems, an attempt is made to identify the subsystems in the PCS that are the least reliable. To achieve this objective for the PMG-based system, the MTBF of the rectifier is decreased by 50% while the MTBFs of the boost converter and inverter are unchanged. In the same way, the effect of changes in the MTBFs for each of the boost converter and inverter on the system reliability has been calculated and is presented in Fig. 6.5a. It is observed that the inverter has the most dominant influence on the system reliability, while the boost converter has less

significant effect than the rectifier. It has been found in the literature that the inverter is the least reliable subsystem [67, 72, 116-118]. This study confirms the results through quantitative analysis. In a similar manner, the effect of the rectifier, chopper and external resistor of the WRIG-based system is investigated with a reduction in MTBF of 50% for each, and presented in Fig. 6.5b. It has been found that the rectifier is the least reliable component in the PCS of such a system. From the financial standpoint, a rectifier is easily replaceable while replacement of an inverter is expensive and needs a highly skilled repair professional. The PCS of the WRIG-based system is composed of fewer parts as well as a lower failure rate. Maintenance and replacement costs of the WRIG-based system will be lower and thus favourable for the small wind turbine industry. As a whole, this research suggests that one should aim for a WRIG-based system that will have a lower failure rate as well as less complex architecture and consequently will be more reliable and less costly during operation.

6.5 Summary

Summarizing the formulations and results presented in this chapter, it can be stated that the proposed reliability analysis

- is focused on the component level that ensures an in-depth analysis rather than considering the system level reliability data provided by the manufacturer;
- is easy to extend for other power conditioning systems of the wind power systems, provided that the system configuration is known;
- confirms the least reliable component through quantitative analysis for both topologies, thus enhancing the design criteria of the power conditioning system for the small wind power generation;

- supports recent research that for a grid connected wind turbine system, a PMG-based system is not the best option from the reliability standpoint and research should be focused on a WRIG-based system due to higher reliability, less maintainable.

Chapter 7

Conclusions

As the demand for electricity energy increases, the development and utilization of wind energy gain growing interest. The efficiency and reliability of grid connected small wind turbine systems equipped with Wound Rotor Induction Generator (WRIG) in comparison to Permanent Magnet Generator (PMG) has been investigated. It has been concluded from perspective of efficiency and reliability that a WRIG-based system performs better than a PMG-based system under similar operating conditions. Concerning wind energy technology for small-scale electricity generation, the grid connected WRIG-based small wind turbine system is ideally suited for grid connected applications than the PMG-based system and the former is expected to keep an optimum position for electricity generation in future.

Furthermore, the continuing need for an optimum system for low wind speeds also makes the WRIG-based system an attractive option for higher efficiency than the PMG-based system.

7.1 Concluding Summary

In Chapter 3, the market potential of a PMG and WRIG-based system was discussed as well as their power conditioning systems. It was shown that despite the ambiguous specification asserted by manufacturers, users more often preferred to use the PMG-based system due to the large number of manufacturers' advertisements and their availability in market. However, reliability is often ignored, which is an important criterion for a successful penetration of a specific system. In consideration of these facts, it was concluded that the WRIG-based system could be an optimum surrogate for wind power generation as the system requires less power electronics, control complexity as well as being easily maintainable. The research thus starts investigating the PMG and WRIG-based system in detail in order to compare the actual system performance from the point of view of losses, efficiency, and reliability.

In Chapter 4, the power loss calculations of the power conditioning system for the grid connected PMG and WRIG-based system were described. The mathematical expressions for the losses in the rectifier, boost converter, and inverter of a power conditioning system for the PMG-based system, as well as the losses in the rectifier, switch, external rotor resistance, and slip ring for the WRIG-based system were presented for the same operating conditions of the wind turbine. The requirement for low loss in low wind speed regimes is a unique challenge to the small wind power field and the WRIG-based system appears to be an optimum option in the low wind speed regime than the PMG-based

system. The comparison was further explored in terms of annual energy capture, annual energy loss and efficiency based on the wind information for eight different sites in Newfoundland and Labrador, Canada. The results showed that the annual energy loss is lower and efficiency is higher for the WRIG-based system than the PMG-based system. The proposed analysis aimed to show that the surrogate WRIG-based system would achieve low power loss and higher performance characteristics during operation than the mainstream PMG-based system.

In Chapter 5, an experimental verification was performed in order to verify the conclusion reached in Chapter 4. The development of a wind turbine emulator for small wind turbine system with furling control and resulting dynamics was presented in this Chapter. Several implementation issues were identified and resolved. Afterwards, the grid connected PMG and WRIG-based system along with the required power conditioning systems and control schemes were designed, implemented and tested in the laboratory. Maximum power extraction was ensured by operating the systems at an optimum tip-speed ratio. A procedure to calculate the power losses for the power conditioning systems was developed and applied on the system. Test results showed acceptable performance of the systems in terms of wind turbine power loss and maximum power point tracking characteristics. Finally, the efficiency of the systems was calculated and it was found that the WRIG-based system maintains higher efficiency than the PMG-based system, thus validating the theoretical conclusion.

In Chapter 6, the reliability analysis of the power conditioning system for the grid connected PMG and WRIG-based system was presented. Temperature was used as a stress factor for the reliability analysis and it was found that the power conditioning

system of the PMG-based system suffers from low reliability as compared to the WRIG-based system. The least reliable component of the power conditioning system was identified quantitatively as the inverter and rectifier for the PMG and WRIG-based system respectively. It was shown that the WRIG-based system with a simple power conditioning system could be surrogate for future research in the small wind turbine system area.

7.2 Thesis Contributions

The main scientific contributions of this research may be summarized as follows:

- An investigation of the existing grid connected small wind turbine systems was described. This investigation assisted to select the mainstream grid connected system and a possible surrogate system along with the power conditioning system to ensure variable speed operation. Furthermore, the reliability of the small wind turbine systems was analyzed and as a result of the evaluation, the most vulnerable sub systems of a wind energy conversion system were identified. The major contribution of this work was to narrow down the research to a specific direction for further investigation.
- The comprehensive power loss calculation for the power conditioning system of the grid connected PMG and WRIG-based system was documented in Chapter 4. The calculation was further extended to determine the annual energy capture/loss and finally, the efficiency for eight different sites in Newfoundland and Labrador, Canada. By itself, a simple calculation of power losses for the PMG and WRIG based system is not new, neither is the calculation of efficiency for the PMG and WRIG based system. The combination of both in a comprehensive manner and

the performance of a comparison study, however, are unique. A unique approach leads to a unique result. Furthermore, a laboratory examination based on a novel small wind turbine emulator was neither explored nor evaluated in previous research. Two contributions follow from these:

1. The derived analytical model for power loss calculation of the PMG and WRIG-based system provided a clear demonstration of the power loss of the systems. Moreover, the investigation in the low wind regime was expected to enhance the high penetration of the WRIG-based system compared to the PMG-based system. A global conclusion was reached in favor of the WRIG-based system after applying the calculation to eight different sites in Newfoundland and Labrador, Canada. The typical obstacle of the variable speed system can be overcome using the WRIG-based system. This is considered to be a major contribution of this research.
2. Investigations on wind turbine emulator are not new on their own. However, the furling control and resulting dynamics based small wind turbine emulator were not found in previous literature. Furthermore, comparison of performance on the basis of experimentation of the PMG and WRIG-based system was also not available in previous research.

The following publications arose from the contributions described above:

Journals:

- **Md. Arifujjaman,** M.T. Iqbal, J.E. Quaicoe, "Experimental Verification of Performances of Grid Connected Small Wind Energy Conversion

Systems," Under review with the Wind Engineering Journal, 2010.

- **Md. Arifujjaman,** M.T. Iqbal, J.E. Quaicoe, "Performance Comparison of Grid Connected Small Wind Energy Conversion Systems," Wind Engineering, vol. 33, no. 1, pp. 1–18, 2009.
- **Md. Arifujjaman,** M.T. Iqbal, J.E. Quaicoe, "Analysis of Conversion Losses in Grid Connected Small Wind Turbine Systems," The Open Renewable Energy Journal, ISSN 1876-3871, vol. 2, pp. 59–69, 2009.
- **Md. Arifujjaman,** M.T. Iqbal, J.E. Quaicoe, "Emulation of a Small Wind Turbine System with a Separately-Excited DC Machine," Journal of Electrical and Electronic Engineering, Istanbul University, vol. 1, Issue 15, no. 1, pp. 569–579, 2008.

Conferences:

- **Md. Arifujjaman,** M.T. Iqbal, J.E. Quaicoe, "Testing of Grid Connected Small Wind Energy Conversion Systems," Submitted to the IEEE Electrical Power and Energy, (EPEC), Halifax, Nova Scotia, Canada, August 23 – 25, 2010.
- **Md. Arifujjaman,** M.T. Iqbal, J.E. Quaicoe, "A Comparative Study of Conversion Losses in Grid Connected Small Wind Turbine Systems," Canadian Wind Energy Association (CanWEA), Vancouver, BC, Canada, October 19–22, 2008.
- **Md. Arifujjaman,** M.T. Iqbal, J.E. Quaicoe, "Loss Calculation in Grid Connected PMG based Small Wind Turbine Systems," The 18th IEEE

Newfoundland Electrical and Computer Engineering Conference (NECEC), St. Johns, NL, Canada, November 8, 2008.

- **Md. Arifujjaman,** M.T. Iqbal, J.E. Quaicoe, "Conversion Losses in Utility Interfaced Small Wind Turbine Systems," Aldrich Conference, St. John's, NL, Canada, February 8–10, 2008.

❒ The use of temperature as a covariate to calculate the reliability of the power electronic components is not new. What has been done in this research, however, forms a contribution, as a use of the reaction rate equation was related to the power electronic component reliability evaluation and used to calculate the reliability of the power conditioning system of the PMG and WRIG-based system. The analytical model of the reliability can be used to calculate the reliability of any power conditioning system as long as the configuration is known in advance. Such a tool is also a contribution. Furthermore, the reliability was quantified for both power conditioning systems and considered an innovative approach in the wind energy area for calculating reliability of power electronics.

The following publications arose from the contributions described above:

Journals:

- **Md. Arifujjaman,** M.T. Iqbal, J.E. Quaicoe, "Reliability Analysis of Grid Connected Small Wind Turbine Power Electronics," Applied Energy Journal, vol. 86, Issue 9, pp. 1617–1623, 2009.

Conferences:

- **Md. Arifujjaman,** M.T. Iqbal, J.E. Quaicoe, "A Comparative Study of Power Electronics Reliability in Grid Connected Small Wind Turbine

Systems," IEEE Canadian Conference on Electrical and Computer Engineering (CCECE), St. John's, NL, Canada, May 3–6, 2009.

In addition to the major contributions described above, related and complementary investigation of the analysis of the grid connected small wind turbine systems resulted in the following publications

Journals:

- **Md. Arifujjaman,** M.T. Iqbal, J.E. Quaicoe, "Vector Control of a DFIG based Wind Turbine," Journal of Electrical and Electronic Engineering, Istanbul University, vol. 9, Issue 18, no. 2, pp. 1057–1066, 2009.

Conferences:

- **Md. Arifujjaman,** M.T. Iqbal, J.E. Quaicoe, "Simulation and Control of a DIFG based Wind Turbine," The 17th IEEE Newfoundland Electrical and Computer Engineering Conference (NECEC), St. Johns, NL, Canada, November 8, 2007.

7.3 Recommendations for Future Research

It is important to understand this study not as one which has produced final results, but rather as a starting point for further investigations. Based on this work, the following have been identified as key considerations for any discussions on the direction of future research efforts in this area.

- ❒ The power loss calculation for the PMG-based system may be improved by investigating ways to include different modulation schemes. While this may not yield significant improvement in power loss, it may lead to an optimized modulation scheme that result in minimal power loss. Such an effort is

worthwhile as valuable information on a preferred modulation scheme can be identified;

- Some work may be done on generalizing a conclusion reached by this research so that the conclusion remains valid for other grid connected small wind turbine systems. One attempt that must certainly be made is to use other power conditioning systems for both PMG and WRIG-based systems and recalculate the power losses and subsequently, evaluate the performances of both systems;
- The collection of reliability field data over a certain period of time for different components of the power conditioning system of the PMG and WRIG-based system is an important endeavor because in such a scenario, it would be possible to compare the expected results with the actual. Moreover, inclusion of different power conditioning systems for both the PMG and WRIG-based systems will produce different reliability values. A comparison of these will certainly be an interesting and worthwhile venture.

References

1. Ahmet Duran Şahin "Progress and recent trends in wind energy," Progress in Energy and Combustion Science, vol. 30, Issue 5, pp.501–543, 2004.
2. International Energy Agency (IEA) [http://www.iea.org/]
3. http://www.btm.dk/
4. Herbert, J.G.M., Iniyan, S., Sreevalsan, E. and Rajapandian, S., "A Review of wind energy technologies," Renewable and Sustainable Energy Reviews, vol. 11, Issue 6, pp. 1117–1145, 2007.
5. World Wind Energy Association (WWEA) [http://www.indea.org/]
6. Canadian Wind Energy Association (CanWEA) [http://www.canwea.ca/]
7. American Wind Energy Association (AWEA) [http://www.awae.org/]
8. European Wind Energy Association (EWEA) [http://www.ewea.org/]
9. British Wind Energy Association (BWEA) [http://www.bwea.com/]
10. M.T. Iqbal, "Modeling and simulation of a small wind turbine," In Newfoundland Electrical and Computer Engineering Conference (NECEC), St. John's, NL, Canada, Nov. 2003.
11. Md. Arifujjaman, M.T. Iqbal, and J.E. Quaicoe, "Energy capture comparison of a small wind energy conversion system," Applied Energy Journal, vol. 85, Issue 1, pp. 41–51, 2008.

12. T. Forsyth, and P. Tu, "Economics of grid-connected Small Wind Turbines in the domestic Market" In AWEA Wind Power Conference, Burlington, Vermont, USA, Jun. 1999.

13. J. Marques, H. Pinheiro, H. Grundling, J. Pinheiro, and H. Hey, "A survey on variable-speed wind turbine system," In Brazilian Power Electronics Conference (COBEP), Fortaleza, Brazil, Sep. 2003, vol. 1, pp. 732–738.

14. www.sma.de

15. S. Soter, and R. Wegener, "Development of induction machines in wind power technology," In International Electric Machines & Drives Conference (IEMDC), Antalya, Turkey, May 2007, vol. 2, pp. 1490 – 1495

16. Paul Kühn. "Big Experience with small wind turbines –235 Small Wind Turbines and 15 Years of Operational Results," In European Wind Energy Conference & Exhibition (EWEC), Milan, Italy, 2007.

17. J. Ribrant, and L.M. Bertling, "Survey of failures in wind power systems with focus on Swedish wind power plants during 1997–2005," IEEE Transaction on Energy Conversion, vol. 22, Issue 1, pp.167 – 173, 2007.

18. P.J. Tavnet, G.J.W. Van Bussel, and F. Spinato, "Machine and converter reliabilities in wind turbines," In International Conference on Power Electronics Machines and Drives (PEMD), Dublin, Ireland , Apr. 2006

19. G.J.W. Van Bussel, and M.B. Van Zaaijer, "Reliability, availability and maintenance aspects of large scale offshore wind farms, a concept study," In Marine Renewable Energy Conference (MAREC), Newcastle, UK, Mar. 2001.

20. P. Bauer, "Offshore wind farms electrical systems configuration - A case

study," In Power Conversion Intelligent Motion Conference (PCIM), Nurnberg, Germany, May 2003.

21. L. Cano, L. Arribas, I. Cruz, and L. Hernández, "Analysis and testing of the connection of small wind turbines to weak and autonomous grids," In European Wind Energy Conference & Exhibition (EWEC) Athens, Greece, Mar. 2006
22. J. Birk, and B. Andresen, "Parallel-connected converters for optimizing efficiency, reliability and grid harmonics in a wind turbine," In European Conference on Power Electronics and Applications (EPEA), Aalborg, Denmark, Sep. 2007, pp. 1 – 7.
23. A.D. Hansen, L.H. Hansen, "Wind turbine concept market penetration over 10 years (1995-2004)," Wind Energy, vol. 10, Issue 1, pp. 81–97, 2006.
24. O. Carlson, J.K. Hylander, and Thorborg, "Survey of variable speed operation of wind turbines," In European Union Wind Energy Conference (EUWEC), Goteborg, Sweden, May 1996, pp. 406–409.
25. D.S. Zinger, E. Muljadi, "Annualized wind energy improvement using variable speeds," IEEE Transaction on Industrial Applications., vol. 33, no. 6, pp. 1444–1447, 1997.
26. H. Vihriala, R. Perala, L. Soderlund, and J.T. Eriksson, "Reducing costs of wind power with a gearless permanent magnet generator," In EWEA Special Topic Conference, Helsinki, Finland, Sep. 1995, vol.1, pp. 225–229.
27. Z.M. Salameh, and L.F. Kazda, "Analysis of the double-output induction generator using direct three-phase model. Part II - Harmonic Analysis," IEEE Transaction on Energy Conversion, vol.-2, no.2, pp. 182–188, 1987.

28. O. Carlson, and J. Hylander, "Electrical system with frequency converters for variable speed operation of wind turbines," In European Wind Energy Conference (EWEC), Glasgow, Scotland, Jul. 1989.

29. R. Hoffmann, and P. Mutschler, "The influence of control strategies on the energy capture of wind turbines," In Industry Applications Conference, Barcelona, Spain, Oct. 2000, vol. 2, pp. 886 – 893.

30. H. Polinder, F.F.A. Van der Pijl, G.J. De Vilder, and P.J. Tavner, "Comparison of direct-drive and geared generator concepts for wind turbines," IEEE Transaction on Energy Conversion, vol. 21, Issue 3, pp. 725 – 733, 2006.

31. F. Abrahamsen, F. Blaabjerg, J.K. Pedersen, and P.B. Thoegersen, "Efficiency-optimized control of medium-size induction motor drives," IEEE Transactions on Industry Applications, vol. 37, Issue 6, pp. 1761–1767, 2001.

32. H. Li, Z. Chen, "Design optimization and site matching of direct-drive permanent magnet wind power generator systems," Renewable Energy, vol. 34, Issue 4, pp. 1175–1184, 2001.

33. W. Qiao, W. Zhou, M. Aller, José, and G.R. Harley, "Wind speed estimation based sensorless output maximization control for a wind turbine driving a DFIG," IEEE Transaction on Power Electronics, vol. 23, Issue 3, pp. 1156–1169, 2008.

34. L. Aarniovuori, L. Laurila, M. Niemela, and J. Pyrhonen, "Loss calculation of a frequency converter with a fixed-step circuit simulator," In European Conference on Power Electronics and Applications (EPE), Aalborg, Denmark, Sep. 2007, pp.1 – 9.

35. C. Whitaker, J. Newmiller, and W. Bower, "Converter Performance Certification:

Results from the Sandia Test Protocol," In Photovoltaic Energy Conversion, Waikoloa, Hawaii, May 2006, vol. 2, pp. 2219 – 2222.

36. F. Soltani, and N. Debbache, "Integration of converter losses in the modeling of hybrid photovolatic-wind generating system," European Journal of Scientific Research, ISSN 1450-216X, vol. 21, no. 4, pp. 707–718, 2008.
37. J. Hurng-Liahng, W. Kuen-Der, W. Jinn-Chang, and S. Jia-Min, "Simplified maximum power point tracking method for the grid-connected wind power generation system ," Electric Power Components and Systems, vol. 36, Issue 11 pp. 1208 – 1217, 2008.
38. X. Zeng , Z. Chen, and F. Blaabjerg, "Design and comparison of full-size converters for large variable-speed wind turbines," In European Conference on Power Electronics and Applications, Aalborg, Denmark, Sep. 2007.
39. Z. Chen, and E. Spooner, "Wind turbine power converters: A comparative study," In International Conference on Power Electronics and Variable Speed Drives, London, UK, Sep. 1998.
40. F. Blaabjerg, U. Jaeger, and S. Munk-Nielsen, "Power losses in PWM-VSI inverter using NPT or PT IGBT devices," IEEE Transactions on Power Electronics, vol. 10, Issue 3, pp. 358–367, 1995.
41. L. Helle, and S. Munk-Nielsen, "Comparison of converter efficiency in large variable speed wind turbines," In IEEE Applied Power Electronics Conference and Exposition (APEC), California, USA, Mar. 2001.
42. F. Blaabjerg, J.K. Pedersen, and U. Jaeger, "Evaluation of modern IGBT-modules for hard-switched AC/DC/AC converters," In IEEE Industry Applications

Conference, Orlando, Florida, USA, Oct. 1995.

43. R. Kraus, P. Turkes, and J. Sigg, "Physics-based models of power semiconductor devices for the circuit simulator SPICE," In IEEE Power Electronic Specialist Conference (PESC), Fukuoka, Japan, may 1998, vol. 2, pp.1726 – 1731.
44. R. Azar, F. Udrea, M. De Silva, G. Amaratunga, N. Wai Tung, F. Dawson,, W. Findlay, and P. Waind, "Advanced SPICE modeling of large power IGBT modules," IEEE Transaction on Industry Applications, vol. 40, no. 3, pp. 710–716, 2004.
45. S. Miaosen, A. Joseph, J. Wang, F.Z. Peng, and D.J. Adams, "Comparison of traditional inverters and Z-source inverter for fuel cell vehicles," IEEE Transactions on Power Electronics, vol. 22, Issue 4, pp. 1453 – 1463, 2007.
46. J.W. Kimball, T.L. Flowers, and P.L. Chapman, "Low-input-voltage, low-power boost converter design issues," IEEE Power Electronics Letter, vol. 2, Issue 3, pp. 96 – 99, 2004.
47. M.G.H. Aghdam, and G.B. Gharehpetian, "Modeling of switching and conduction losses in three-phase SPWM VSC using switching function concept," In IEEE Power Tech, St. Petersburg, Russia, Jun. 2005
48. C. Rivas, and A. Rufer, "P.W.M current converter for electric energy production systems from fuel-cells," In European Conference on Power Electronics and Applications, Graz, Austria, Sep. 2001.
49. A. Grauers, "Efficiency of three wind energy generator systems," IEEE Transaction on Energy Conversion, vol. 11, Issue 3, pp.650 – 657, 1996.
50. A. Inoue, M. Hasan Ali, R. Takahashi, T. Murata, J. Tamura, M. Kimura, M.

Futami, M. Ichinose, and I. Kazumasa, "A calculation method of the total efficiency of wind generators," In International Conference on Power Electronics and Drives Systems (PEDS), Kualamlumpur, Malaysia, No. 2005, vol. 2, pp.1595 – 1600.

51. N.A. Orlando, M. Liserre, V.G. Monopoli, R.A. Mastromauro, and A. Dell'Aquila, "Comparison of power converter topologies for permanent magnet small wind turbine system," In International Symposium on Industrial Electronics (ISIE), Cambridge, UK, Jun. –Jul. 2008, pp.2359– 2364
52. R.W. Erickson, "A Novel Power Electronics System for Wind Generation Applications," National Renewable Energy Laboratory (NREL), October 2004, NREL/SR-500-33396
53. O. Al-Naseem, R.W. Erickson, and P. Carlin, "Prediction of switching loss variations by averaged switch modeling," In Applied Power Electronics Conference and Exposition (APEC),New Orleans, Louisiana, USA, Feb. 2000, vol. 1, pp.242 – 248.
54. H. Huang, and L. Chang; "Energy flow principles of IGBT inverters in wind energy conversion systems," In Canadian Conference on Electrical and Computer Engineering (CCECE), Halifax, Canada, May 2000, vol. 1, pp. 545 – 549.
55. L. Chang, R. Doraiswami, T. Boutot, and H. Kojabadi, "Development of a wind turbine simulator for wind energy conversion systems," In Canadian Conference on Electrical and Computer Engineering (CCECE), Halifax, Canada, May 2000, vol. 1, pp. 550 – 554
56. H.M. Kojabadi, L. Chang, and T. Boutot, "Development of a novel wind turbine

simulator for wind energy conversion systems using an inverter-controlled induction motor," IEEE Transactions on Energy Conversions, vol. 19, no. 3, pp. 547 – 552, 2004.

57. H.M. Kojabadi, and L. Chang, "A novel steady state wind turbine simulator using an inverter controlled induction motor," Wind Engineering, vol. 28, no. 4, pp. 433–446, 2004.
58. C. Nichita, D. Diop, A. Belhache, J. Jean, B. Dakyo, and L. Protin, "Control Structure Analysis for a Real Time Wind System Simulator," Wind Engineering, vol. 22, no. 6, 1998.
59. B. Rabelo, W. Hofmann, and M. Gluck, "Emulation of the static and dynamic behaviour of a wind-turbine with a DC- machine drive," In IEEE Power Electronics Specialists Conference (PESC), Aachen, Germany, Jun. 2004, vol. 3, pp. 2107 – 2112
60. J.F. Manwell, J.G. McGowan, A. Rogers, and W. Stein, "Developments in Experimental Simulation of Wind/Diesel Systems," In European Wind Energy Conference (EWEC), Glasgow, Scotland, Jul. 1989.
61. J.T.G. Pierik, M.J. Hoeijmakers, J.M. Vleeshouwers, T.G. V. Engelen, C.W.A. Baltus, A.T. Veltman, and A. Warmenhoven, "A variable speed system with integral control for wind turbines (IRFLET): Design of the test-rig," In Wind Energy: Technology and Implementation Conference, Amsterdam, Netherland, Oct. 1991, pp. 90–93.
62. F. Barrero, J.L. Mora, M. Perales, A. Marchante, E. Galvàn, J.M. Carrasco, A. Torralba, and L.G. Franquelo, "A Test-Rig to evaluate a wind turbine generation

control system based on DSP," In European Conference on Power Electronics and Applications (EPE), Trondheim, Norway, Sep. 1997.

63. P.E. Battaiotto, R.J. Mantz, and P.F. Puleston, "A wind turbine emulator based on a dual DSP processor system," Control Engineering Practice, vol 4, no. 5, pp. 1261–1266, 1996.
64. D. Diop, C. Nichita, J.J. Belhache, B. Dakyo, and E. Ceanga, "Error evaluation for models of real time wind turbine simulators," Wind Engineering , vol. 24, no. 3, pp. 203-221, 2000.
65. N.H. Teng, and W.J. Kolaik "On/off Cycling Under Multiple Stresses," IEEE Transactions on Reliability, vol. 38, Issue 4, pp. 494 – 498, 1989.
66. D. Hirschmann, D. Tissen, S. Schroder, and R.W. De Doncker, "Reliability Prediction for Inverters in Hybrid Electrical Vehicles," IEEE Transactions on Power Electronics, vol. 22, Issue 6, pp. 2511 – 2517, 2007.
67. M.B. Pregelj, and A. Rohatgi, "Impact of Inverter Configuration on PV system Reliability and Energy Production," In IEEE Photovoltaic Specialists Conference, New Orleans, Louisiana, USA, May 2002.
68. A.L. Julian, and G. Oriti, "A Comparison of Redundant Inverter Topologies to Improve Voltage Source Inverter Reliability," IEEE Transactions on Industry Applications, vol. 43, Issue 5, pp. 1371 – 1378, 2007.
69. R.H. Bonn "Developing a "Next Generation" PV Inverter," In IEEE Photovoltaic Specialists Conference, New Orleans, Louisiana, USA, May 2002.
70. S. Daher, J. Schmid, and F.L.M. Antunes, "Multilevel Inverter Topologies for Stand-Alone PV Systems," IEEE Transactions on Industrial Electronics, vol. 55,

Issue 7, pp. 2703 – 2712, 2007.

71. H. Oldenkamp, I.J. de Jong, C.W.A. Baltus, S.A.M. Verhoeven, and S. Elstgeest, "Reliability and Accelerated Life Tests of the AC Module Mounted OKE4 Inverter," In IEEE Photovoltaic Specialists Conference, Washington, DC, USA, May 1996.
72. A. Ristow, M. Begovic, A. Pregelj, and A. Rohatgi,. "Development of a Methodology for Improving Photovoltaic Inverter Reliability," IEEE Transactions on Industrial Electronics, vol. 55, Issue 7, pp. 2581 – 2592, 2008.
73. M. Aten, G. Towers, C. Whitley, P. Wheeler, J. Clare, and K. Bradley, "Reliability Comparison of Matrix and Other Converter Topologies," IEEE Transactions on Aerospace and Electronic Systems, vol. 42, Issue 3, pp. 867 – 875, 2006.
74. W.M. Rohouma, I.M. Molokhia, and A.H. Esuri, "Comparative Study of Different PV Modules Configuration Reliability," In Arab International Conference on Solar Energy (AICSE), Kingdom of Bahrain, Apr. 2007.
75. V. Sameer, and T. Michel, "Performance and Reliability Analysis of Wind Turbines Using Monte Carlo Methods Based on System Transport Theory," In AIAA Structural Dynamics and Materials Conference, Austin, Texas, USA, Apr. 2005.
76. Military Handbook MIL-HDBK-217F, Reliability Prediction of Electronic Equipment, U.S. Dept. Defense, Washington, DC, Dec. 2, 1991.
77. H. Calleja, F. Chan, and I. Uribe, "Reliability-Oriented Assessment of a DC/DC Converter for Photovoltaic Applications," In IEEE Power Electronics Specialists

Conference (PESC), Orlando, Florida, USA, Jul. 2007.

78. J.M. Carrasco, L.G. Franquelo, J.T. Bialasiewicz, E. Galvan, R.C. PortilloGuisado, M.A.M. Prats, J.I. Leon, and N. Moreno-Alfonso, "Power Electronic Systems for the Grid Integration of Renewable Energy Sources: A Survey," IEEE Transactions on Industrial Electronics, vol. 53, Issue 4, pp. 1002 – 1016, 2006.
79. "Guidelines to understanding reliability prediction," In European Power Supply Manufacturers Association (EPSMA), Edition 24, Jun. 2005.
80. E. Muljadi, T. Forsyuth, and C.P. Butterfield, "Soft–stall control versus furling control for small wind turbine power regulation," In Windpower Conference, Bakersfield, California, USA, Apr. May. 1998, pp. 5–14.
81. D. Corbus, and D. Prascher, "Analysis and comparison of test results from the small wind research turbine test project," In AIAA Aerospace Sciences Meeting and Exhibit, Reno, Nevada, Jan. 2005.
82. A.J. Jr. Eggers, K. Chaney, W.E. Holley, H. Ashley, J. Green, and J. Sencenbaugh, "Modeling of Yawing and furling behavior of small wind turbines," In AIAA and the American Society of Mechanical Engineers , Orlando, Florida, USA, Nov. 2000, pp. 1–11.
83. J.T. Bialasiewicz, "Furling control for small wind turbine power regulation," ISIE, RioDe Jeneiro, Brazil, Jun. 2003, vol. 2, pp. 804 – 809,
84. F. Casanellas, "Losses in PWM inverters using IGBTs," In IEE Electric Power Application., vol. 141. Issue 5, 1994, pp. 235 – 239.
85. L.K. Mestha, and P.D. Evans, "Analysis of On-State Losses in PWM Inverters," IEE Proceedings, vol. 136, Pt. B, No. 4, 1989

86. A.M. Massoud, S.J. Finney, and B.W. Williams, "Conduction loss calculation for multilevel inverter: a generalized approach for carrier-based PWM technique," In International Conference on Power Electronics, Machines and Drives (PEMD), SanAntonio, Texas, USA, Mar. Apr. 2004, vol. 1, pp. 226 – 230

87. M.H. Rashid, "Power electronics Circuits, Devices, and Applications" Second Edition, Prentice-Hll, Inc., Englewood Cliffs, N.J., U.S.A., ISBN-81-203-0869-7

88. M.S. Chinthavali, L.M. Tolbert, and B. Ozpineci, "4H-SiC GTO thyristor and p-n diode loss models for HVDC converter," IEEE IAC 04, vol. 2, 2004, pp.1238 – 1243.

89. O. Al-Naseem, R.W. Erickson, and P. Carlin, "Prediction of switching loss variations by averaged switch modeling," In IEEE Application Power Engineering Conference (APEC), New Orleans, Louisinia, USA, Feb. 2000, vol. 1, pp.242–248.

90. N. Mohan, T.M. Undeland, and W.P. Robbins, "Power Electronics: Converters, Applications and Design," John Wiley and Sons INC., Third edition, 2003.

91. K. Kretschmar, and H..P. Nee, "Analysis of the Efficiency and Suitability of Different Converter Topologies for PM Integral Motors," In Australian Universities Power Engineering Conference (AUPEC), Kish Island, Iran, May 2001, pp. 519–525

92. D.W. Chung, S.K. Sul "Minimum-loss strategy for three-phase PWM rectifier," IEEE Transactions on Industrial Electronics, vol. 46, Issue 3, pp.517 – 526, 1999.

93. J.W. Kolar, H. Ertl, and F.C. Zach, "Influence of the modulation method on the conduction and switching losses of a PWM converter system," IEEE Transactions

on Industry Applications, vol. 27, Issue 6, pp.1063 – 1075, 1991.

94. P.J.P. Perruchoud, and P.J. Pinewski, "Power losses for space vector modulation techniques," In Conference on Power Electronics in Transportation, Oct. 1996, pp.167 – 173

95. M.H. Bierhoff, and F.W. Fuchs, "Semiconductor losses in voltage source and current source IGBT converters based on analytical derivation," In Power Electronics Specialist Conference (PESC), Aachen, Germany, Jun. vol. 4, pp. 2836–2842.

96. K. Mishra, and A.K. Wahi, "Performance Analysis and Simulation of Inverter-fed Slip-power Recovery Drive," Journal- Institutions of Engineers In India Part El Electrical Engineering Division, vol. 85, pp. 89–95, 2004.

97. E. Nordlund, F. Magnussen, G. Bassilious, and P. Thelin, "Testing of Silver-Copper- and Electro-Graphite Brush Materials for Slip Ring Units," In Nordic Workshop on Power and Industrial Electronics (NORPIE), Trondheim, Norway, Jun. 2004

98. www.infineon.com

99. V.D. Jeroen, and M. Meadors. "Power Performance Test Report for the Bergey Excel-S/60 Wind Turbine with SH3052 Airfoil Blades," National Renewable research laboratory (NREL), April 2003, NREL/EL-500-33452

100. "Safety and Function Test Report for the Bergey Excel-S with Gridtek Inverter," National Renewable research laboratory (NREL), May 2003, NREL/EL-500-33963

101. I. Tsagas "Laboratory Evaluation of DC/AC Inverters for Stand-Alone &

Grid-Connected Photovoltaic Systems," MSc's Dissertation, Energy Systems Research Unit, University of Strathclyde, 2002

102. A. Woyte, S. Islam, R. Belmans, and J. Nijs, "Undersizing the inverter for grid-connection—where is the optimum?," In Photovoltaische Solar Energie, Bad Staffelstein, Germany, Mar. 2003, pp. 414–419.

103. www.beygey.com

104. K. Ogata, "Modern control engineering," 3rd edition.@1997 by Prentice-Hall, Inc., Upper Saddle River, New Jersey 07458, U.S.A.

105. A.M.O. El Zawawi, and H.A. Ashour, "A fast acting current limit for a PC based DC drive," In Mediterranean Electrotechnical Conference (MELECON), Jun. 1996, Biry, Italy, May 1996, vol. 1, pp.332 – 336

106. E. Zawawi, "A PC controlled DC drive using parallel port interfacing," Alexanderia Eng. Journal, vol. 34, no. 1, pp. 1–9, 1995.

107. K.R. Zelenka, and T.H. Barton, "A fast acting current limit for DC motor drive," IEEE Transaction on Industrial Applications, vol. 22, no. 5, pp. 798–804, 1986.

108. M. Minkova, D. Minkov, J.L. Rodgerson, and R.G. Harley, "Current limitation in the adaptive neural speed control of a DC motor," In African Electrical Technology Conference (AFRICON), South Africa, Sep. 1996, vol. 2, pp. 837 – 842

109. Md. Arifujjaman, M.T. Iqbal, J.E. Quaicoe, "Emulation of a Small Wind Turbine System with a Separately-Excited DC Machine," Journal of Electrical

and Electronic Engineering, Istanbul University, vol. 1, Issue 15, no. 1, pp. 569–579, 2008

110. National Semiconductor Corporation. Reliability Programs. Nov 2004. http://www.national.com/quality/reliability programs.html.

111. E.E. Lewis, and H.C. Chen, "Load-capacity Interference and the Bathtub Curve," IEEE Transactions on Reliability, vol. 43, Issue 4, pp. 470 – 475, 1994.

112. P.V.N. Prasad, and K.R.M. Rao, "Reliability Models of Repairable Systems Considering the Effect of Operating Conditions," In IEEE International Reliability and Maintainability Symposium, Seatle, Washington, Jan. 2002, pp. 503–510.

113. Reliasoft Corporation. Arrjenius Relationship Introduction. Sept 2004. http://www.weibull.com/AccelTestWeb/arrhenius relationship introduction.htm.

114. F.F. Oettinger, D.L. Blackburn, and S. Rubin, "Thermal Characterization of Power Transistors," IEEE Transactions on Reliability, vol. 23, Issue 8, pp. 831 – 838, 1976.s

115. www.siliconfareast.com

116. R. Tirumala, P. Imbertson, N. Mohan, C. Henze, and R. Bonn, "An Efficient, Low Cost DC-AC Inverter for Photovoltaic Systems with Increased Reliability," In Proceedings of the Industrial Electronics Conference (IECON), Sevilla, Spain, Nov. 2002.

117. B. Maish, C. Atcitty, S. Hester, D. Greenberg, D. Osborn, and D. Collier, "Photovoltaic System Reliability," In IEEE Photovolatic Specialist Conference (PVSC), Anaheim, CA, USA, Sep. Oct. 1997, pp.1049–1054

118. W. Bower, "Inverters- Critical Photovoltaic Balance-of-system Components :Status, Issues and New-Millennium Opportunities," Progress in Photovoltaics: Research and Applications, vol. 8, Issue 1, 2000, pp. 113–126

Appendix A

Wind Turbine Technical Specifications

This appendix provides the technical specifications for the wind turbine used during simulation studies throughout the proposal.

Type	3 Blade Upwind
Rated Power	1500 Watts
Rotor Diameter	2.4 m
Cut-in Wind Speed	2 m/s
Rated Wind Speed	13 m/s
Cut-Out Wind Speed	17 m/s
Furling Wind Speed	13 m/s
Blade Pitch Control	None
Over speed Protection	Furl

Gearbox	None, Direct Drive
Temperature Range	-40 to +60 Deg. C
Generator	Permanent Magnet Generator (PMG), Wound Rotor
Induction Generator (WRIG)	
Output Form	Grid Connected
Control System	Personnel Computer (PC)-based

Appendix B

Parameters of the IGBT-Module

This appendix provides the parameter specifications for the IGBT-Module EUPEC FP15R12W1T4_B3 used during simulation studies throughout the thesis

Housing Type	EASY PIM1B
$I_{c,nom}$ [A]	15
V_{ce0} [V]	2.15
r_{ce} [Ω]	0.0833
E_{ON} [mJ]	1.75
E_{OFF} [mJ]	1.20
V_{fo} [V]	0.7
r_d [Ω]	0.07
E_{SR} [mJ]	0.68

Diode R_{JA} [K/W]	1.05
IGBT R_{JA} [K/W]	1.75

Appendix C

Nameplate Information of the DC Motor

This appendix provides the name plate information for the separately-excited DC motor used for the wind turbine emulator

Model No	M253AS-DBZ
Serial No	370-117-301
Type	M-1670
Enclosure	OPEN
Rated Power	2 kW
Full Load RPM	1750
Full Load Amps.	16
Volts	125
Field Amps.	0.85

Field Volts	125
Ambient ^{0}C	40
^{0}C Rise	60
Company	Canron Limited
Country	Canada

Appendix D

Nameplate Information of the Permanent Magnet Generator (PMG)

This appendix provides the name plate information for the permanent magnet generator used to implement PMG-based small wind turbine system

Serial No	260-007-302
Type	PMG-1480
Enclosure	OPEN
Rated Power	1.6 kW
RPM	1800
Amps.	5.5
Phase	3
Volts	120/208
Hertz	60

Ambient ^{0}C	40
^{0}C Rise	60
Company	Canron Limited
Country	Canada

Appendix E

Nameplate Information of the Wound Rotor Induction Generator (WRIG)

This appendix provides the name plate information for the wound rotor induction generator used to implement the WRIG-based small wind turbine system

Model No	215-DBWD
Serial No	322-093-210
Type	WR-1066-A
Enclosure	D.P.
Rated Power	1.8 kW
RPM	1725
Amps.	19
Phase	3

Volts	120/208
Hertz	60
Rotor Volts	10.5
Rotor Amps.	11
Ambient ^{0}C	40
^{0}C Rise	90
Company	Canron Limited
Country	Canada

Appendix F

Component List

This appendix provides the component list for the Permanent Magnet Generator (PMG) and Wound Rotor Induction Generator (WRIG)-based small wind turbine system

Component List for the PMG-based Small Wind Turbine System

3-phase Bridge Rectifier	PVI-7200
Ammeter	M-52-0055-6
BCI unit	PVI-3600-OUTD-US-F-W
Circuit Breaker	CAT EB3015
Diversion Load	5P00041-2767
Power harmonics Analyzer	FLUKE-41B
Voltmeter	M-3800

Component List for the WRIG-based Small Wind Turbine System

3-phase Bridge Rectifier	26MT40
AC/DC Current Probe	80i-110s

Ammeter	M-52-0055-6
Circuit Breaker	CAT EB3015
External Variable Resistance	EC-609-65
Power harmonics Analyzer	FLUKE-41B
Voltmeter	M-3800